

SINGLE-ENDED ANTENNA MATRIX DESIGN GUIDE

1. Introduction

This application note describes the design challenges, difficulties, and conclusions regarding single-ended Antenna Matrix design. It also discusses the effects of human hand proximity on these antennas.

The single-ended antennas used in the Antenna Matrix are mostly specialized monopole antennas. Most of the antennas are printed, but there are also helical wire examples and chip antennas. Unfortunately, the internal structures of the chip antennas are unknown, so the tuning possibilities are limited.

2. Antenna Basics

This section describes the essential antenna definitions and principles required to understand subsequent sections in this application note. Many books and papers discuss this field in detail ([1], [2], [3], [4], [5]). Proceed to the next section if already familiar with the terms and concepts below.

An antenna transforms conducted RF power to radiated RF power. DC current or static charge does not radiate. Only accelerating electrical charges create radiation, so alternating currents or pulses with discontinuities (wire ends, bending, etc.) in the conductor are required.

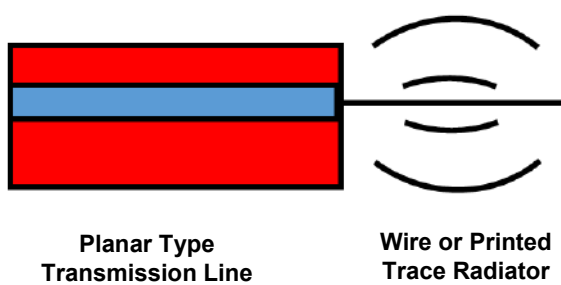


Figure 1. Transmission Line and Antenna

2.1. Near Field and Far Field

The space around the antenna can be divided into near field and far field regions.

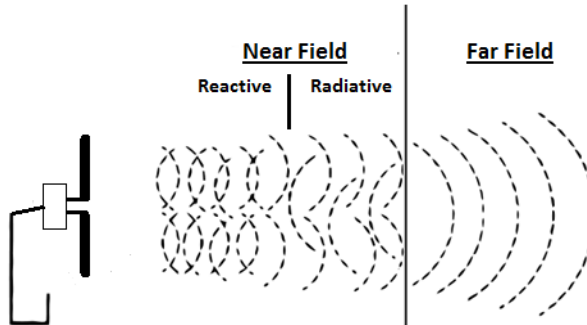


Figure 2. Near Field and Far Field Regions

The main property of the far field region is that the radiation pattern does not change with the distance. However, in the near field region, the radiation pattern strongly depends on the distance from the antenna.

As shown in Figure 2, the near field region can be divided into a reactive and radiative near field. The reactive near field boundary is well defined as $\lambda/2\pi$ and does not depend on the antenna size. Thus, for small antennas ($D < \lambda/2$, where D is the largest dimension of the antenna) the reactive near field boundary extends further, relative to the antenna size.

There are many definitions for the radiative near field and far field boundaries, the most popular being the following equation: $d_{ff} = 2D^2/\lambda$ (where D , again, is the largest dimension of the antenna).

In the case of small antennas ($D < \lambda/2$), this far field boundary equation yields less than $\lambda/2$ distance. But, in practice, the far field should be measured from at least two wavelengths distance, even if the antenna is small.

2.2. Antenna Impedance

The reactive (static) near field of the antenna mainly determines the reactive portion of antenna impedance.

The radiated loss and ohmic loss determine the real part of the impedance and thus the Q. The aim is to minimize ohmic resistance relative to radiation resistance in order to radiate rather than dissipate the RF energy applied to the antenna.

2.3. Minimum Antenna Q

The antenna Q is determined by the ohmic loss and radiated loss. In an ideal ohmic-loss-free case, all the RF energy is radiated, and the Q is determined purely by the radiation loss. According to the theory, this purely radiated Q of an ideal antenna has a theoretical minimum, which depends only on the antenna size relative to the wavelength. In the case of small antennas, the Q is inversely proportional to the third power of the antenna size [6]:

$$Q_{min} = \frac{1 + 3(2\pi)^2 \left(\frac{a}{\lambda}\right)^2}{(2\pi)^3 \left(\frac{a}{\lambda}\right)^3 (1 + (2\pi)^2 \left(\frac{a}{\lambda}\right)^2)} \approx \left(\frac{\lambda}{a}\right)^3$$

where 'a' is the radius of the smallest sphere that can surround the antenna.

As the radiation resistance is inversely proportional to the Q in the ohmic-loss-free ideal cases, the higher the antenna, the higher the radiation resistance. So a larger antenna will have better radiation.

2.4. Antenna Efficiency

In a real antenna, both ohmic losses and radiation losses are present. The ohmic loss dissipates while the radiation loss radiates the RF energy. The aim is to maximize the radiated loss/ohmic loss ratio. Based on this, the antenna radiation efficiency is defined as:

$$\eta = \frac{R_R}{R_R + R_L}$$

Where “ R_L ” is the ohmic loss and “ R_R ” is the radiation loss, as shown in Figure 3.

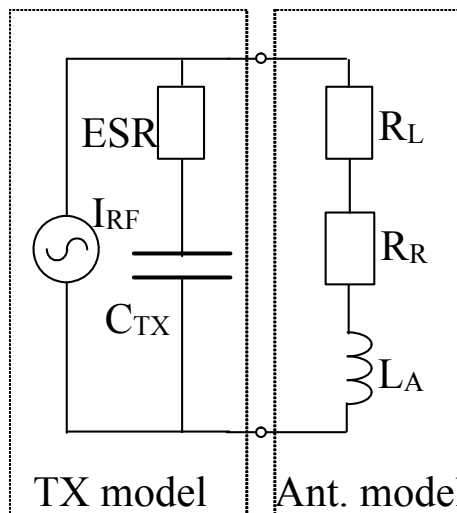


Figure 3. Ohmic and Radiation Losses

Increase of ohmic loss decreases efficiency and Q. Here, the decrease of Q is not advantageous as only the dissipated RF energy increases (the radiated energy will also decrease in most cases).

Unfortunately, a high Q antenna is a very narrowband antenna and thus more sensitive to detuning (due to technological spreading, hand effect, etc.). Moreover, a high Q antenna is also difficult to match and tune. For low matching network loss, the Q of the matching/tuning elements should be significantly higher than the Q of the antenna. In the case of a higher Q antenna with typical SMD external matching elements, the matching loss can be significant.

So in many ways a lower Q antenna is more advantageous, but only if the Q decrease originates from increased radiation and not from higher ohmic losses.

2.5. Antenna Pattern and Gain

An antenna works as a spatial filter for the radiation, which is directly influenced by the antenna size and the voltage/current distribution on it. The radiation pattern describes the far field radiation, the region where the pattern does not change shape with distance. A typical dipole radiation pattern is shown in Figure 4.

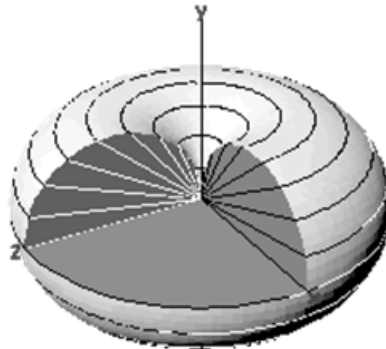


Figure 4. Typical Dipole Radiation Pattern, Antenna Axe Coinciding with Y-Axe

The direction of maximum radiation and the maximum gain are related. The maximum radiation can be described by the directivity and gain. These quantities describe how much energy the antenna can concentrate in a given direction.

The definition of the antenna directivity (D_A):

$$D_A = \frac{\text{Radiation in the direction of maximum}}{\text{Ideal isotropic radiation with same total radiated Rf power}}$$

The directivity does not comprise the antenna non-radiating (ohmic, dielectric stb.) losses.

The definition of the Antenna Gain (G_A) is as follows:

$$G_A = \frac{\text{Radiation in the direction of maximum}}{\text{Ideal isotropic radiation with the same input Rf power}}$$

The Gain comprises the antenna non-radiating losses.

The Antenna Efficiency can also be defined by the Gain and Directivity:

$$\eta = \frac{G_A}{D_A} = \frac{P_{RAD}}{P_{IN}}$$

Neither the Directivity nor the Gain comprise the input mismatch, so a perfect input match is assumed.

2.6. Maximum Gain

It is already shown that an antenna with larger dimensions has a lower Q and better radiation efficiency. A logical assumption is that a larger antenna can also concentrate the radiation better in one direction and, thus, has higher directivity and gain.

This rule can be shown in an intuitive way on an aperture antenna. A general rule is that the received power is proportional to the effective aperture of the antenna (in case of incoming plane waves i.e. far field):

$$P_{\text{rec}} = S * A_{\text{eff}}$$

where S is the RF power density in W/m^2 at the receiver antenna position.

In the case of aperture antennas, the effective area and the physical area are also related to each other:

$$A_{\text{eff}} = \rho_A \times A_{\text{phy}}$$

where ρ_A is a constant that describes the equivalent fraction of the antenna aperture, which is fully illuminated by the RF plane wave. This constant is usually lower than 0.8.

From the reciprocity theorem:

$$\frac{G_A}{A_{\text{eff}}} = \frac{4\pi}{\lambda^2}$$

And thus, the antenna gain is related to the physical antenna area:

$$G_A = \frac{4\pi}{\lambda^2} A_{\text{phy}} \rho \leq \frac{4\pi}{\lambda^2} A_{\text{phy}} 0.8$$

For a parabolic dish, the physical area is:

$$A_{\text{phy}} = \frac{d^2}{4} \pi$$

where d is the diameter of the dish.

So, the gain is proportional to the square of the diameter:

$$G_A = \frac{\pi^2 d^2}{\lambda^2} \rho$$

Interestingly, this rule is valid for small ($l < \lambda/2$) wire antennas as well, where the gain is proportional to the square of the length of the antenna.

In any case, the practical achievable gain (to the direction of maximum radiation) of a nearly half-wave wire monopole antenna is in the 0 to 3 dB range. However, due to secondary effects (nearby large metal object, hand etc.) it can be significantly lower (-5 to -10 dB).

2.7. Ground Plane as an Electrical Mirror

Since the electrical field must be perpendicular to the plane of a perfect conductor, if one places an electrical charge above the conductor plane, an equal virtual mirror charge with opposite sign appears on the other side of the conductor. In other words, above the perfect conductor, the electric field distribution is the same as it would be between two equal charges of opposite sign, as shown in Figure 5.

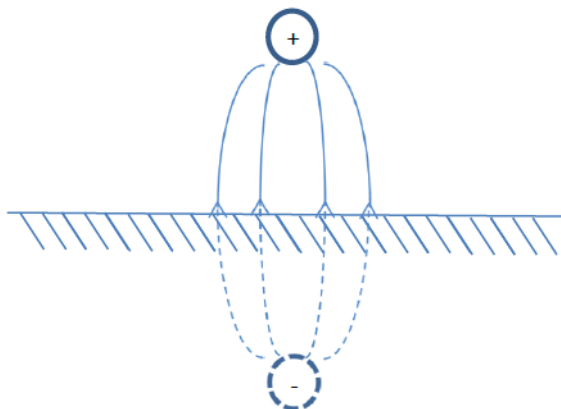


Figure 5. Image Effect on a Single Charge

If a current exists between two non-equipotential charges above the conductor, the image charges and thus, the image current vector appears as well. As shown in Figure 6, the tangential components are opposite each other, while the normal components flow in the same direction.

So if the wire is parallel with the ground surface, the image antenna current and field adds in a destructive manner to the real antenna.

However, if the antenna wire is perpendicular to the ground, the image antenna current and field adds in a positive manner to the real antenna. These effects are illustrated in Figure 7.

Since a large ground plane behaves like an electromagnetic mirror, a simple monopole behaves like a half dipole with identical generated electric field above the ground conductor. This is shown in Figure 8.

As the input voltage swing is half that of the dipole, the input impedance of the monopole is also half that of the dipole. However, the monopole gain is double (or 3 dB higher) than that of the dipole. This is because in the case of the monopole, all the RF energy is radiated above the ground plane, i.e., to the upper half hemisphere.

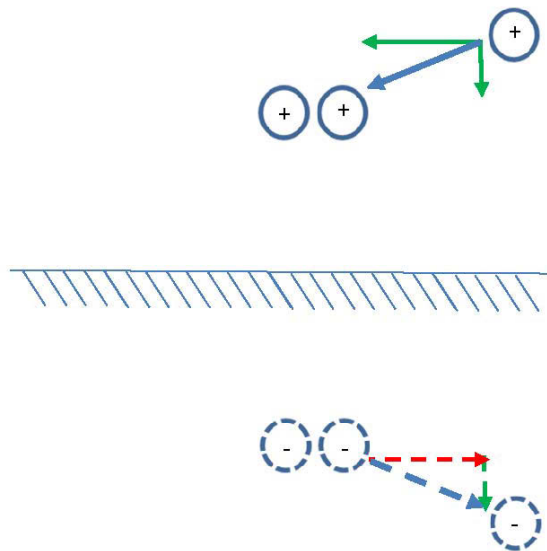


Figure 6. Image Effect on Currents Induced by Potential Differences

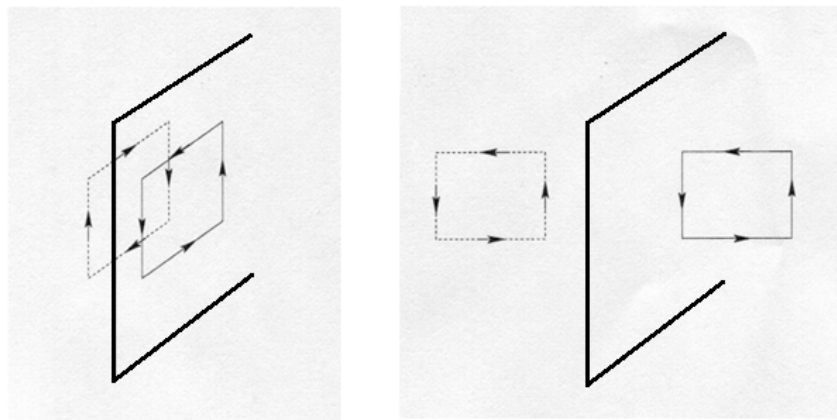


Figure 7. Image of Loop Antenna and the Current with Parallel and Perpendicular Position to the Large Ground Plane

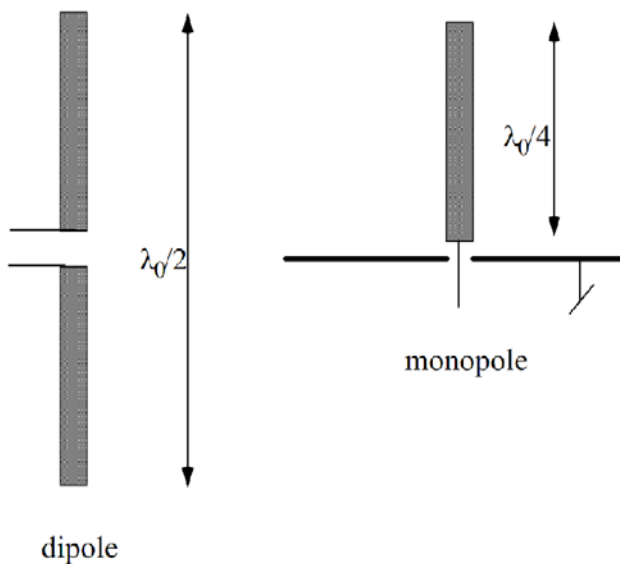


Figure 8. Monopole as Half Counterpart of the Dipole

2.8. Polar Coordinate System for Antenna Patterns

The polar coordinate system usually applied for antenna pattern is shown in Figure 9. Usually, three planar cuts (XY, YZ, XZ) are shown with both horizontal and vertical polarization.

In the XY cut, the azimuth ϕ angle runs, while in the YZ, XZ cut the elevation Θ angle runs.

Typically:

- In the XY cut, the ϕ runs anticlockwise and starts from the X-axis.
- In the YZ cut, the Θ runs clockwise and starts from the Z-axis.
- In the XZ cut, the Θ runs anticlockwise and starts from the Z-axis.

2.8.1. Measurement Coordinate System

In the antenna matrix measurement application notes (AN848, AN850, and AN782), the antenna PCB is in the XY plane, and the Z-axis is perpendicular to the PCB plane. Typical PCB positions at the XY, XZ, and YZ cuts are shown in Figure 10. In the measured pattern plots, the angle rotation is clockwise. In the XY cut, the rotation starts from the X-axis while, in the XZ and YZ cuts, it starts from the Z-axis. For a clearer understanding, a picture of the DUT in the right cut is always put in the middle of the pattern plots.

2.8.2. Simulation Coordinate System

Unfortunately, the applied measurement coordinate system cannot be fully synchronized with the EM simulators used (Sonnet, AWR Axiem).

The AWR Axiem simulator editor window, together with the coordinate system, is shown in Figure 11. Sonnet uses the same coordinate system. If the antenna is facing to the right side of the screen (i.e. towards the X-axis) as in Figure 11, then the following transformation has to be used on the simulated pattern plots to be comparable with the measured patterns (see Figure 11):

1. In the XY cut, the simulated angle rotates counterclockwise and starts from the X-axis; so, the simulated pattern has to be mirrored to the X-axis to be compatible with the measured pattern. The simulated phi polarization corresponds to the measured horizontal polarization, while the theta polarization corresponds to the measured vertical polarization.

2. In the XZ cut (Phi=0 deg and Theta runs in the simulator), the simulated angle rotates counterclockwise and starts from the Z-axis; so the simulated pattern has to be mirrored to the Z-axis to be compatible with the measured pattern. The simulated phi polarization corresponds to the measured vertical polarization while the theta polarization corresponds to the measured horizontal polarization.
3. In the YZ cut (Phi=90 deg and Theta runs in the simulator), the simulated angle rotates clockwise and starts from the Z-axis; so the simulated pattern is the same as the measured one. The simulated phi polarization corresponds to the measured vertical polarization while the theta polarization corresponds to the measured horizontal polarization.

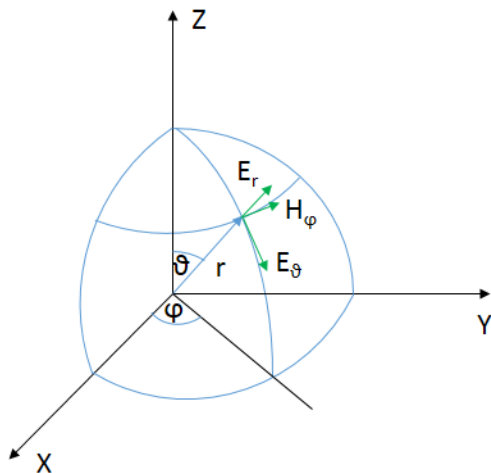


Figure 9. General Coordinate System for Antenna Pattern Measurements

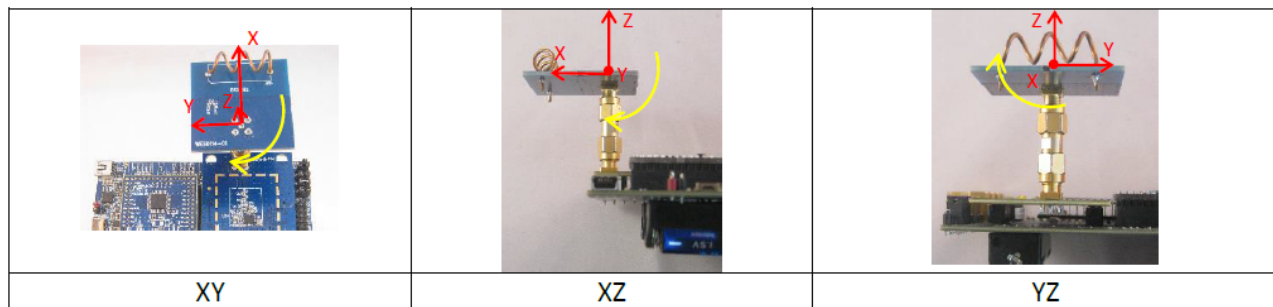


Figure 10. XY, XZ, and YZ Cuts in the Antenna Pattern Measurements

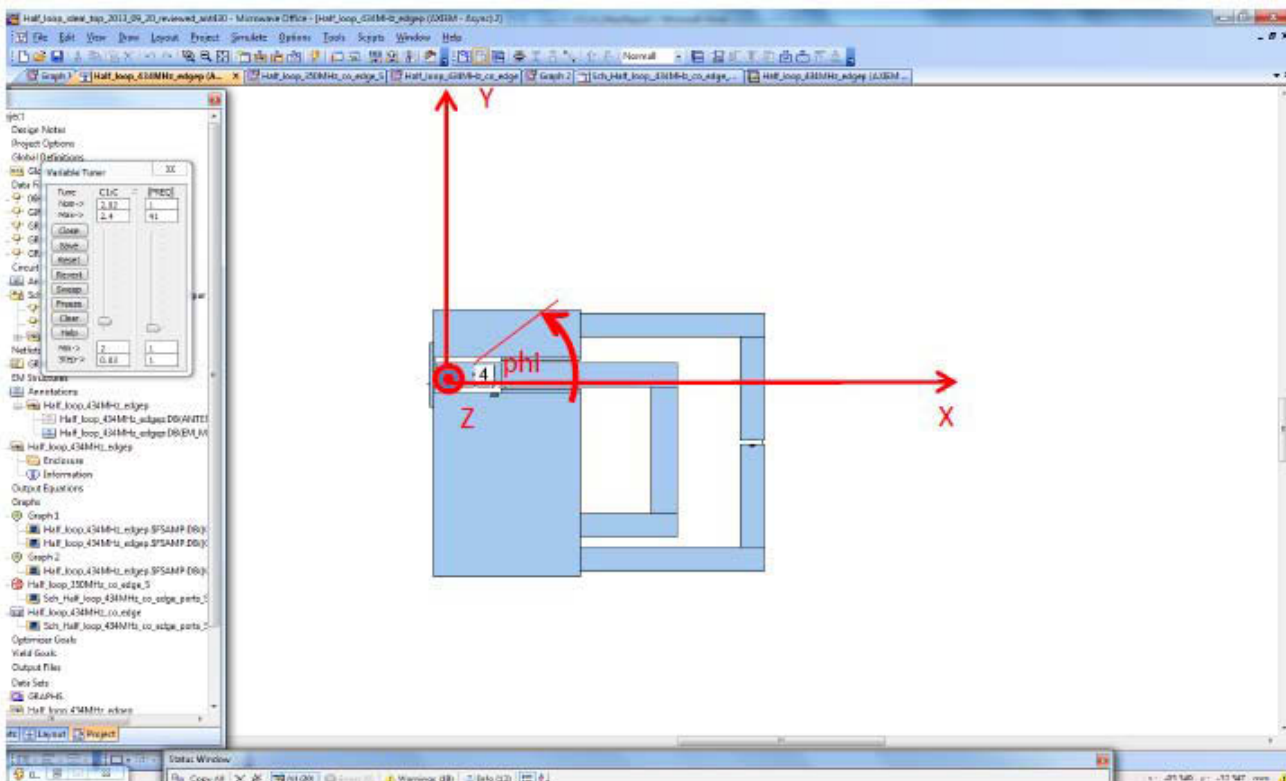


Figure 11. AWR and Sonnet Editor Display Coordinate System

2.9. Small Antenna Types

The small antenna types can be grouped in several ways:

- A small antenna can be a differential (e.g., dipole, loop) or single-ended (e.g., monopole, half loop).
- A small antenna can be a wire type (e.g., dipole, monopole) or aperture type (e.g., patch).
- A small antenna can be an E field type (e.g., dipole, monopole) or an H field type (e.g., loop).

3. Monopole Antennas—Theoretical Background

Since most single-ended antennas are basically monopoles, a basic understanding of traditional dipole and monopole antenna theory is important. The monopole antenna is a half dipole if a large perpendicular ground plane is applied at the feeding point, so the dipole antenna description can be applied to monopole antennas as well.

Dipole antenna theory is well known and is widely available in print ([1], [2], [3], [4], [5]) and e-literature, so readers already familiar with monopole and dipole theory can skip this section.

The results of some sections are derived through complicated mathematical calculations. Most of these calculations are presented in detail in “Appendix A—Dipole Antenna Radiation Calculations”.

The monopole impedance is half that of a dipole. The radiation pattern is the same, and the gain of the monopole is 3 dB higher.

3.1. Hertz Dipole

The dipole radiation can be originated from the radiation of a very small dipole radiator called the Hertz dipole. The most important property of the Hertz dipole is the constant current along the antenna arms due to its very short dimensions. The length is very small compared to the wavelength and is denoted by ‘dz’.

3.1.1. Radiated Far Field of the Hertz Dipole

The Hertz dipole in the coordinate system is shown in Figure 12.

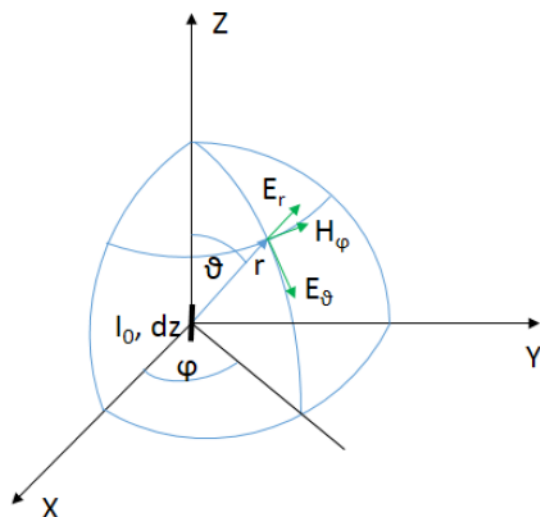


Figure 12. Hertz Dipole in the Coordinate System

The calculation of a Hertz dipole radiation field is extremely complicated. The generated field contains both near field (vanish with the second and third power of the distance) and far field components. Here, only the resulting far field components are given. The generated far field comprises only Theta (E_θ) E field and Phi (H_ϕ) H field components:

$$E_\theta = \frac{I_0 dz}{4\pi} \sqrt{\frac{\mu_0}{\epsilon_0}} \frac{j\beta}{r} e^{-j\beta r} \sin \theta = j \frac{60\pi I_0 dz}{\lambda r} e^{-j\beta r} \sin \theta$$

$$H_\theta = \frac{I_0 dz}{4\pi} \frac{j\beta}{r} e^{-j\beta r} \sin \theta = j \frac{I_0 dz}{2\lambda r} e^{-j\beta r} \sin \theta$$

There are some main properties of the generated field:

- The field is symmetrical around the antenna axis, so it is dependent only on the elevation (ϑ).
- The field decrease linearly with the distance.
- The E and H field are perpendicular to each other and are in phase.
- The E and H field is parallel with the spherical surface around the antenna.
- At a given distance, the fields are dependent only on the antenna length and RF current.

According to the Poynting Theorem, the electromagnetic wave propagates perpendicular both to $E\vartheta$ and to $H\phi$. This is the normal direction to the spherical wave front, i.e., the RF wave propagates away from the antenna to the direction of E_r .

The spherical wavefront can be considered as a plane wave when the observer is far enough from the antenna and if only a small fraction of space is investigated.

The characteristic impedance of the propagation is the E field to H field ratio:

$$\frac{E_\vartheta}{H_\phi} = \sqrt{\frac{\mu_0}{\epsilon_0}} = 120\pi$$

which is identical to the inherent free space characteristic impedance.

3.1.2. Total Radiated Power and Radiation Resistance of the Herz Dipole

From the Poynting theory, the generated power density at r distance can be calculated:

$$Re \frac{1}{2} \langle \bar{E} \times \bar{H}^* \rangle = \frac{1}{2} |E_\vartheta| |H_\phi| \Rightarrow S(\vartheta) = \frac{15\pi I_o^2 dz^2}{\lambda^2 r^2} \sin^2 \vartheta \text{ [watt/m}^2\text{]}$$

At a given distance, this depends on the square of the elevation, antenna length, and RF current. Also, the power density decreases with the square of the distance.

The total radiated power can be calculated by integrating the power density to the whole space (the spherical surface around the antenna). These calculations are detailed in "Appendix A—Dipole Antenna Radiation Calculations" on page 88. The resulting formula of the total radiated power is:

$$P_S = 40\pi^2 I_o^2 \langle \frac{dz}{\lambda} \rangle^2$$

From the total radiated power, the radiation resistance can be calculated:

$$R_S = \frac{2P_S}{I_o^2} = 80\pi^2 \langle \frac{dz}{\lambda} \rangle^2$$

Note: The radiation resistance and thus the radiation efficiency increases with the square of the antenna length.

3.1.3. Herz Dipole Antenna Gain and Pattern

As has been shown, the generated fields and power density depend only on the elevation. They are at maximum if $\theta = 90^\circ$ as $\sin(\theta)$ is maximum (1) there.

By definition, the antenna directivity is:

$$D_A = \frac{\text{Radiation in the direction of maximum}}{\text{Ideal isotropic radiation with same total radiated Rf power}}$$

The Herz dipole directivity pattern is shown in Figure 14A. The gain maximum is 1.5 (or +1.76 dB) in the XY plane ($\theta = 90$ deg). The calculation of the maximum gain is detailed in Appendix A on page 89.

If there are no other losses (e.g., ohmic, dielectric, or matching network losses) in the antenna, the gain is identical to the directivity.

3.2. Normal Dipole (Monopole) Field

In the case of a normal (real) dipole/monopole, the current along the antenna is no longer constant due to the greater length, and the current distribution is sinusoidal.

The large antenna can be divided into small dipoles with constant current distribution. The field of each small dipole can be described by the Herz dipole results. The weighted sum (with the current distribution) of the radiation patterns of these small dipoles yields the radiated field of the larger dipole. This calculation is detailed in Appendix A on page 89. Assuming a sinusoidal current distribution, the total radiated field of the dipole at distance r is as follows:

$$E_\theta = j60I_m \frac{e^{-j\beta r}}{r} \frac{\cos(\beta l \cos \theta) - \cos(\beta l)}{\sin \theta}$$

where I_m is the maximum of the sinusoidal current distribution. **As can be seen, the electric field has only θ polarized component and, besides the elevation, is also dependent upon the antenna length in a complex fashion.**

In the case of a long dipole antenna ($L=2l > \lambda/2$), the current maximum falls somewhere on the antenna depending on the length. Whereas, for short antennas ($L=2l \leq \lambda/2$), the current has a local maximum at the feed point, however, that is lower than the possible sinusoidal maximum (I_m). So, in the case of a short antenna, the I_m has to be calculated from the input current value and from the antenna length. More detail is given in Appendix A on page 91.

The H field is calculated from the E field by dividing it with the intrinsic free space characteristic impedance. The H field is phi polarized and its formula is similar to that of the E field.

$$H_\phi = \frac{E_\theta}{120\pi}$$

3.2.1. Total Radiated Power and Radiation Resistance of a Normal Dipole (Monopole)

The total radiated power can be calculated by integrating the power density over the whole spherical surface surrounding the antenna. The power density can be calculated from the field formulas of the previous chapter. From the total radiated power, the radiation resistance can be calculated as well. All of these calculations are presented in Appendix A on page 91.

The numerical curve of the radiation resistance of a dipole ($L = 2l$) is shown in Figure 13. The monopole has half this value.

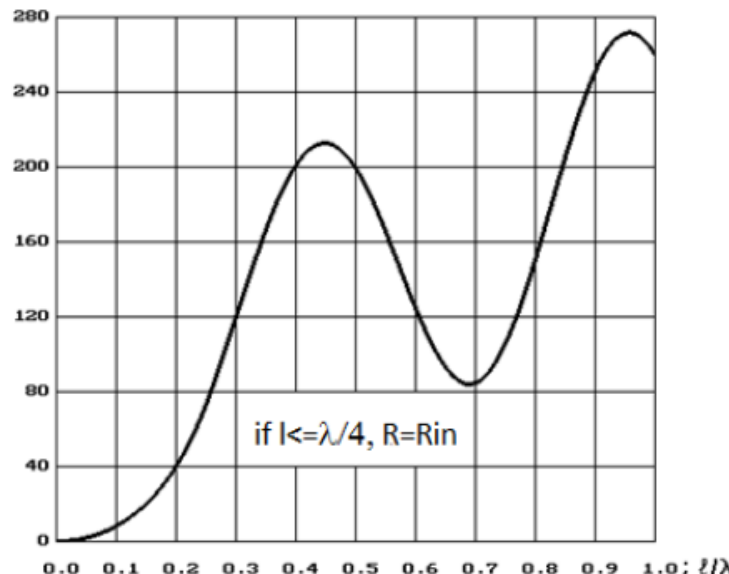


Figure 13. Radiation Resistance vs. Antenna Length in Wavelengths

Properties of the dipole's radiation resistance are as follows:

- Monotonically increases up to $l = 0.45 \lambda$ (i.e. when the total length of the dipole is $L = 2l = 0.9 \lambda$).
- If the antenna is short (i.e. the total dipole length $2l \leq \lambda/2$ or, in the case of a monopole, lower than a quarter wave), the radiation resistance is nearly proportional to the square of the length as with the very small Herz dipole antennas.
- The radiation resistance of a half-wave dipole ($l = 0.25 \lambda$) is $\sim 72 \Omega$. A quarter wavelength monopole has $\sim 36 \Omega$.

3.2.2. Dipole (Monopole) Radiation Pattern and Gain

A detailed calculation of the E field dipole pattern and directivity is presented in Appendix A on page 91. The dipole radiation characteristic for different l/λ ratios is shown in Figure 14. As can be seen, the directivity is minimum if the antenna is very short (Herz dipole case with a D of 1.5) and increases with longer lengths. The maximum is at $l = 0.625\lambda$. Unfortunately, at this length, side lobes appear, and, by further increasing the length, the side lobe level monotonically increases as well, and the main lobe diminishes.

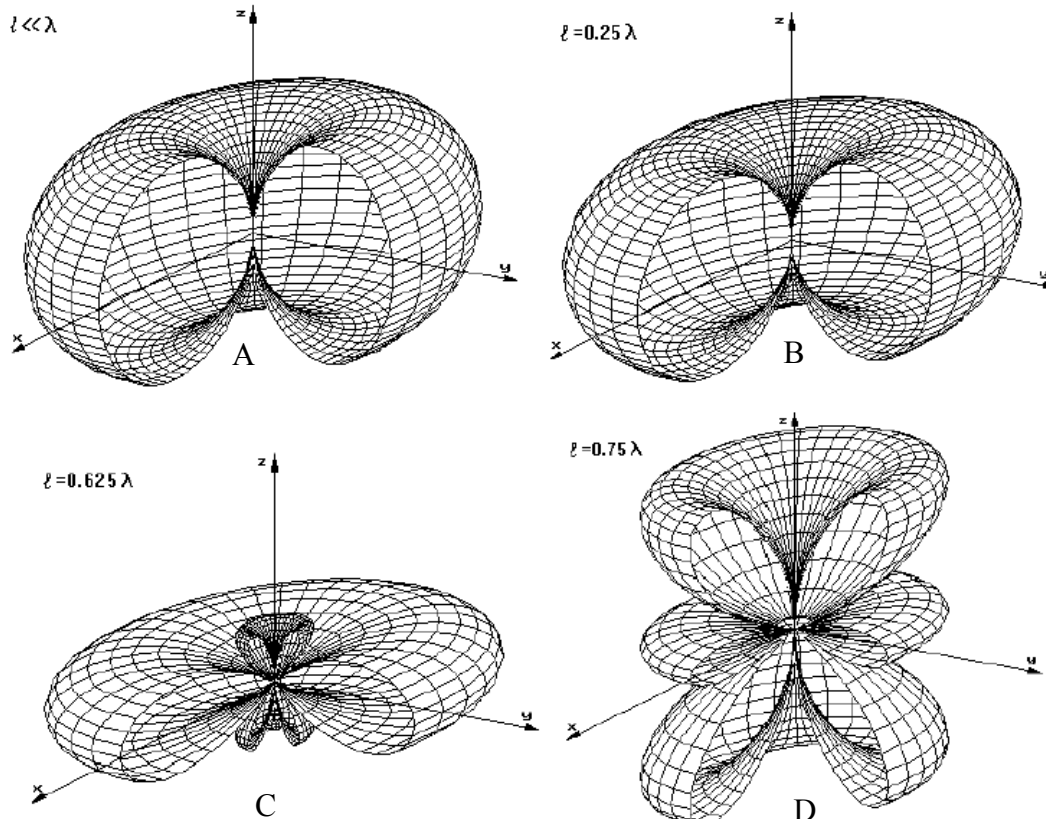


Figure 14. Dipole Radiation Patterns with Different Antenna Lengths

The directivity (identical to the gain if there is no additional loss) curve of the dipole vs. antenna length in lambda is shown in Figure 15. **The gain of a monopole is 3 dB higher** because it radiates the total power to the upper hemisphere only (but only if an infinitely large perpendicular ground plane presents at the feeding point). The gain of a loss-free half-wave dipole is 1.64, i.e. 2.14 dB. The 1.25 lambda dipole ($l/\lambda = 0.625$) has the highest gain of ~3.26, i.e. ~5.14 dB. Unfortunately, the 1.25 lambda dipole has high side lobe levels, and the impedance is far from the desired 72Ω , so it is not popular in practice.

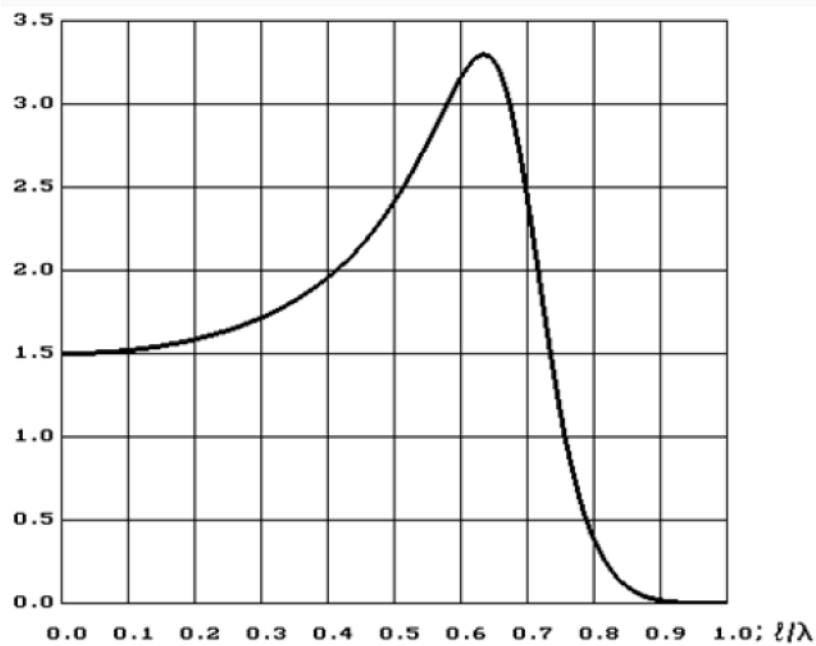


Figure 15. Dipole Directivity vs. Antenna Length

3.2.3. Dipole (Monopole) Impedance

The dipole complex impedance vs. electrical length (βl) is shown in Figure 16. The ohm is the wire thickness factor:

$$\Omega = 2 \ln \frac{2l}{a}$$

where a is the diameter of the wire.

The dashed lines shows the equal electrical length regions. The inflection point is at $\beta l = \pi/2 = 1.57$. The impedance at the inflection point (i.e. the impedance of an ideal half-wave dipole) is $\sim 73 + j42 \Omega$. The impedance of a quarter wave monopole (with very large ground metal) is half of this: $\sim 36 + j21 \Omega$.

The first series resonance (the so-called resonance point) has a slightly lower electrical length than this. In this electrical length region, the impedance does not depend significantly on the wire diameter. The impedance at the resonant point is pure real and lower ($\sim 60 \Omega$ for dipole and $\sim 30 \Omega$ for monopole).

However, at longer electrical lengths, the dependency become strong. At the first parallel resonance point (known as the “antiresonance” point), both the impedance value and the resonant electrical length depend strongly on the wire diameter.

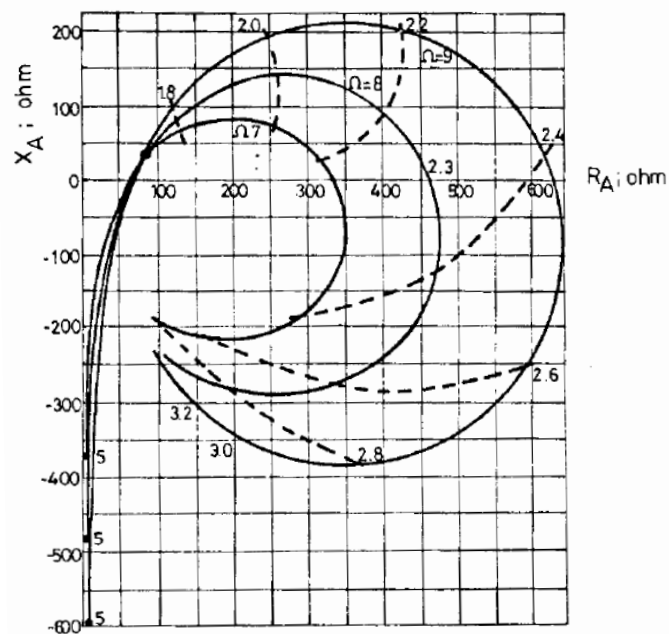


Figure 16. Ideal, Loss Free Dipole Complex Impedance Change at Various Electrical Lengths and Wire Diameters

4. Real Properties of Small Monopoles

The main effects that degrade the properties of a real dipole or monopole from an ideal one are:

- Dissipative losses: dielectric loss, ohmic, and skin effect loss.
- Proximity of conductors or human hands.
- Non-ideal differential excitation or asymmetrical antenna (only with dipoles).
- Matching network loss (if required).

In the case of monopoles, there is another effect, which is the most frequent one. This is the effect of small (not very large compared to the wavelength) ground metal at the antenna feed point.

Only single-ended monopole type solutions are detailed in this application note. The non-ideal differential excitation case of dipoles is not discussed.

4.1. Sonnet EM Simulator Coordinate System

Before discussing the properties of non-ideal monopoles, we will examine the coordinate system of the far-field solver of the applied Sonnet EM simulator.

The simulation of antenna radiation in Sonnet has many limitations:

- The applied box is a waveguide in which the PCB is a cross-sectional plane board.
- The top and bottom terminations of the waveguide should be free space.
- The cross sectional size of the box should be higher than lambda.
- No box self-resonance should occur at the simulated frequency.
- Simulated radiation is not valid at the plane of the PCB.
- Effect of PCB cutting edge close to the antenna trace cannot be simulated as the PCB substrate extends to the whole cross section of the applied box.
- Effect of connected external ground metals, such as SMAs, PicoBoards and/or baseboard, cannot be simulated accurately. Only the influence of a large parallel metal can be modeled.
- Hand effect cannot be taken into account in a precise way. Again, the impact of a parallel layer with typical human body tissue properties can be investigated.

Thus, only a rough estimate of the antenna radiation can be done by Sonnet. Also, only rough estimates of the effect of large nearby conductors or human body proximity can be made.

The applied coordinate system in Sonnet is shown in Figure 17. This is basically identical to what is shown in Figure 9, only the Sonnet's editor screen orientation is also shown.

In our plots, usually, the Theta (elevation) is running from 0 to 360°, and these vertical cuts are plotted at several azimuth (Phi) degree values. Rarely, the azimuth (Phi) is running from 0° to 360°, and the azimuth cuts are plotted at several Theta values.

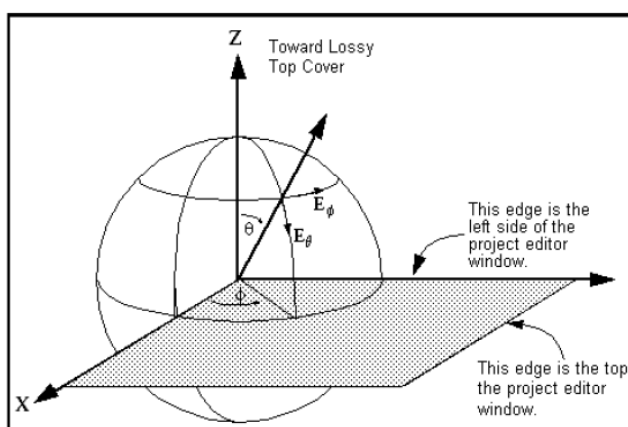


Figure 17. Applied Coordinate System in Sonnet

4.2. Effect of Dissipative Losses (Dielectric, Ohmic and Skin Effect)

The impedance curves of the ideal dipole presented previously are valid for ideal loss free case only where the real part is identical to the radiation resistance.

In real antennas the dielectric and ohmic loss exists as well. Moreover, both losses increase at high frequencies. The ohmic loss increase is caused by the skin effect. As the radiated loss varies with the square of the dipole length at short antenna sizes ($L = 2l < \lambda/2$ or $l < \lambda/4$ in monopoles) its value can be comparable or even lower than the sum of the dielectric and ohmic loss value. In these cases, the antenna efficiency drastically drops as the RF energy is dissipated rather than radiated.

4.2.1. Effect of Ohmic Loss with Skin Effect

Many formulas for excess ohmic loss and skin effect increase can be found in the literature or on the internet. In the critical small-antenna cases, the sinusoidal current distribution can be approximated by a linear one to simplify the calculation. With this assumption, the excess ohmic loss formula, including skin effect, is:

$$R_{\text{loss}} = \frac{L}{6\pi a} \sqrt{\frac{\pi f \mu}{\sigma}}$$

Where “ σ ” is the conductivity of the wire; “ L ” is the total length of the dipole, and “ a ” is the wire diameter. For monopoles, the ohmic loss value is half of the dipole value.

In the case of half-wave dipoles or quarter wave monopoles, the ohmic (loss + skin effect) loss is usually not significant compared to the radiated loss. To demonstrate this, the real impedance of a 915 M printed ILA antenna (bended monopole shown in Figure 18) is simulated both with ideal loss-free conductor and with 35 μm thick (1 oz) copper in Figures 19 and 20. In both cases, a 1.55 mm thick substrate is used with 4.5 epsilon without any dielectric loss (tangent delta (Tangd) = 0).

In Figures 19 and 20, the low value (~3 Ω) of the real antenna impedance is surprising. This is basically due to the very small ground metal, which is not perpendicular to the antenna axis in this real-life example. In addition, the bending reduces the effective radiation length of the monopole antenna (but the impedance is tuned). All of these effects will be detailed later. From a radiation point of view, this antenna is equivalent to a significantly shorter one with reduced radiation resistance. Despite this, as can be seen in Figures 19 and 20, the ohmic loss and skin effect together increase the real part impedance by only 10 to 15%, which is practically negligible. In the case of a straight quarter-wave monopole with large ground, the radiation resistance is many times higher, and, thus, the real part impedance increase caused by the ohmic loss would be only 2 to 3%.

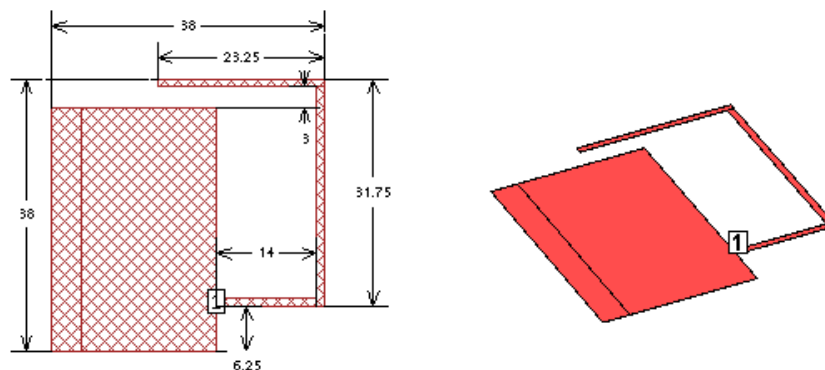


Figure 18. Simulated Printed ILA Antenna

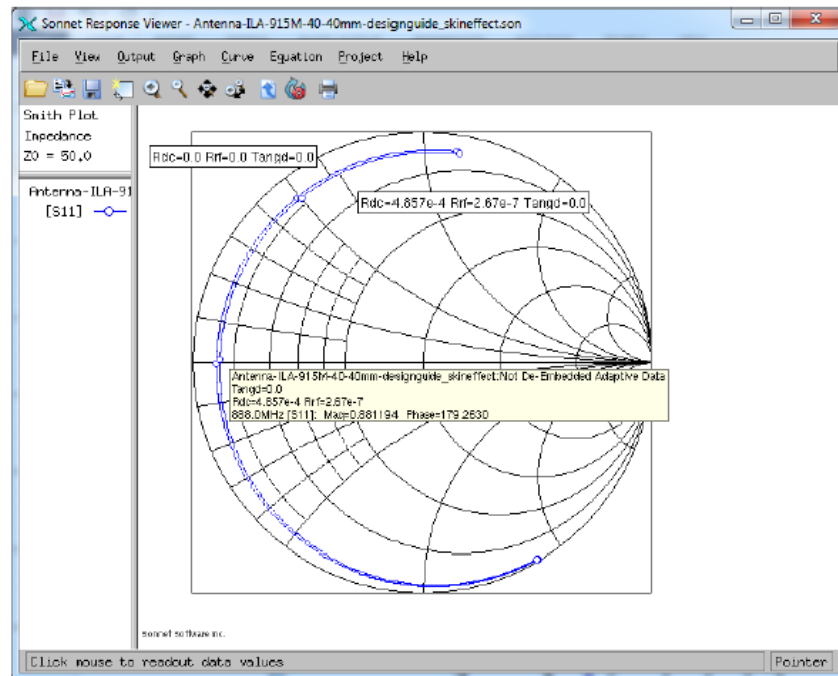


Figure 19. ILA Antenna Impedance (700 to 1000 MHz) Showing With and Without Ohmic and Skin Effect Losses. This Example Antenna Resonates at 888 MHz.

Note: For Figure 19 and 20, 1 oz copper and 1.55 mm substrate with an Epsilon of 4.5 is assumed. Here the dielectric loss is neglected (i.e. the tangent delta [denoted by Tangd] is zero).

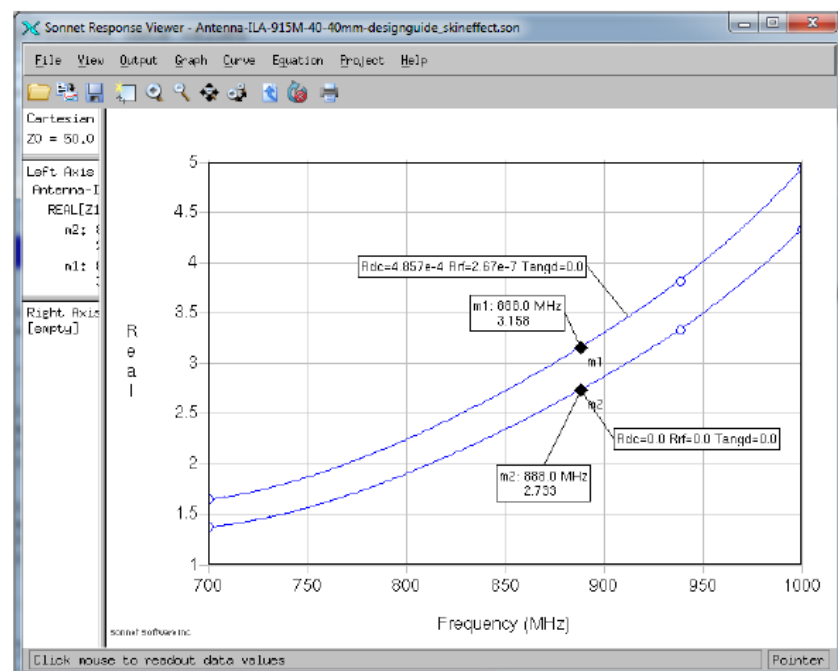


Figure 20. ILA Antenna Impedance Real Part (700 to 1000 MHz) Showing with and without Ohmic and Skin Effect Losses. This Example Antenna Resonates at 888 MHz.

4.2.2. Effect of Dielectric Loss

The dielectric loss has a much stronger effect than the ohmic loss. Figures 21 (in Smith) and 22 (in real_imaginary format) show the curves with and without dielectric loss. In Figure 21, two curves are shown, one with ($\text{Tangd}=0.02$) and another without ($\text{Tangd}=0$) dielectric loss. In both cases the Ohmic and skin effect loss is neglected ($\text{Rdc} = 0$ and $\text{Rrf} = 0$). In Figure 22, a third curve with both dielectric and ohmic (also with skin effect) loss is shown as well.

In the simulations, the assumed epsilon is 4.5, and the tangent delta (Tangd) is 0.02. These are the typical values of an FR4 substrate.

As one can see, the dielectric loss is the main loss mechanism. It increases the real part impedance by 80 to 90% in the case of this small bended ILA antenna. Here, the radiation resistance is inherently small (in the range of 2 to 4Ω) due to the lack of large perpendicular ground metal. As it is shown by the third curve (with Ohmic losses, i.e. where Rdc and Rrf is not zero) of Figure 22, the effect of the ohmic loss is very small compared to the dielectric loss. This behavior is typical for small monopole type antennas like the ILA example in Figure 21. In the case of a larger straight quarter lambda monopole with a large ground, the radiation resistance is many times higher, and, thus, the real impedance increase caused by the losses is less significant: it is around 10 to 20% in practical cases, caused mainly by the dielectric loss.

If a lower tangent delta substrate is used or the antenna is a wire type without lossy substrate in the vicinity, the dissipative losses are usually significantly lower than the radiation losses.

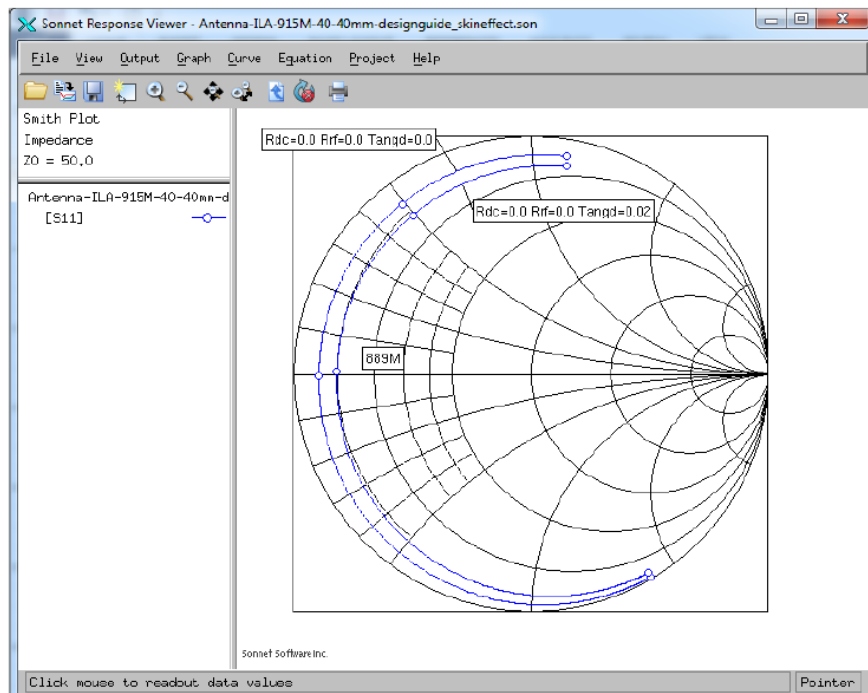


Figure 21. ILA Antenna Impedance (700 to 1000 MHz) with ($\text{Tangd}=0.02$)and without ($\text{Tangd}=0$) Dielectric Losses, Ohmic Loss is Neglected ($\text{Rdc}=0$, $\text{Rrf}=0$). Assumed FR4 Substrate: Epsilon=4.5, 1 oz Copper, 1.55 mm Thickness

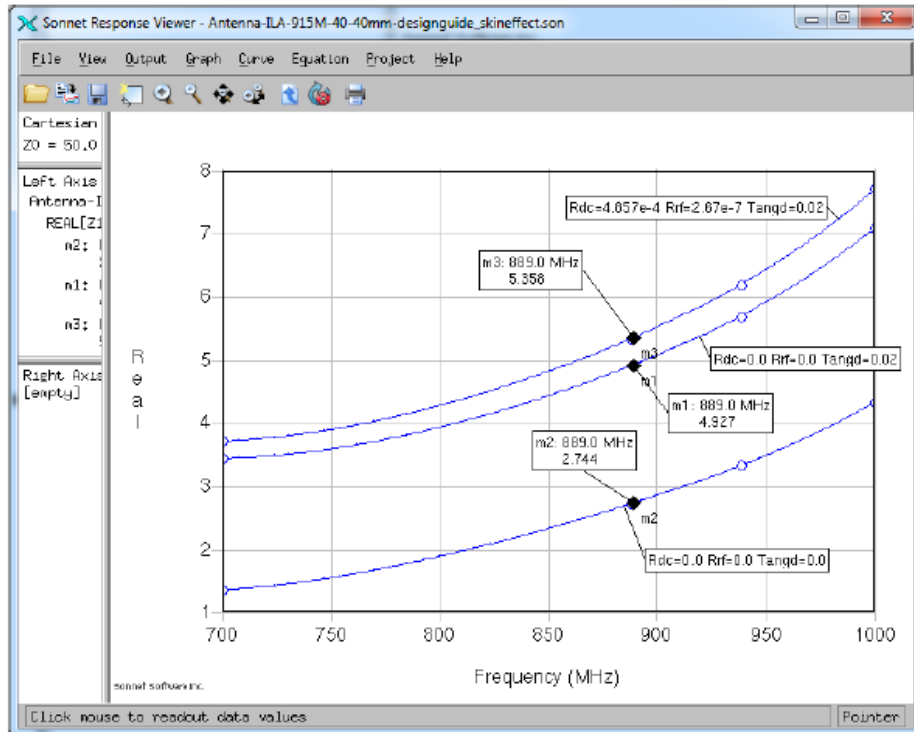


Figure 22. ILA Antenna Impedance (700 to 1000 MHz) with ($\text{Tangd}=0.02$) and without ($\text{Tangd}=0$) Dielectric Losses. Highest Curve Introduces the Ohmic Loss (i.e. Rdc and Rrf are Not Zero) as well. Same Substrate in Figure 21.

4.3. Effect of Nearby Metal on Monopole Type Antennas

As described in Section “2.7. Ground Plane as an Electrical Mirror”, the proximity of a large conductor to a monopole antenna has a strong effect on the antenna’s properties.

The effect basically depends on the size, orientation, and distance of the ground metal. If the metal is at the antenna feeding point and perpendicular to the antenna axis, then it behaves as an electrical mirror and has a positive effect on the radiation. This case is shown in Figure 23.

If the conductor overlaps the antenna and is parallel with the antenna axis, it degrades the antenna performance. A typical destructive configuration is shown in Figure 24.

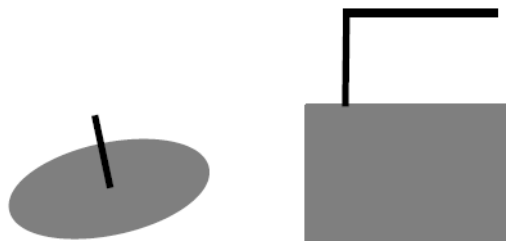


Figure 23. Useful Ground Positions for Monopole Type Antennas



Figure 24. Destructive Ground Position for Monopole Type Antennas

To better see the negative effect of a nearby large conductor, the ILA antenna of Figure 18 is simulated with a large parallel metal plane (320x320 mm) situated close to the antenna. Here, the distance between the antenna and the large metal is varied. Figure 25 shows the EM simulation setup (in the 2.5D planar Sonnet Em simulator). The “dist_bot” variable sets the distance between the antenna and the large metal plane (represented by the large pink square in Figure 25). The antenna is simulated in a 1000x1000 mm large box. The top and bottom sides of the box are open (free space) and placed 100 mm away from the simulated structure to calculate the radiated far field from the steady state waveguide modes (the simulated antenna is in a cross sectional substrate in a waveguide with metal walls as detailed earlier).

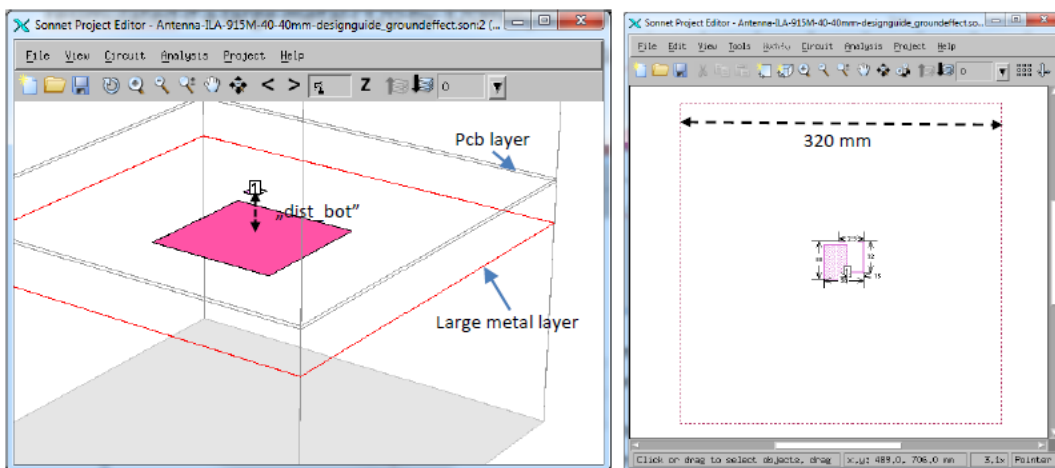


Figure 25. Simulation Setup with Large Parallel Bottom Metal.

The Substrate is a 1.55 mm thick FR4 with an Epsilon of 4.5 and a Tangent Delta of 0.02

Figures 26 (in Smith) and 27 (in real-imaginary format) show the variation of the antenna impedance if the distance (denoted by “dist_bot” variable) between the antenna board and the large bottom metal plane is varied. Due to the proximity of the parallel metal plane, the real part of the ILA antenna impedance decreases (the antenna Q increases). This is because the antenna radiation efficiency and, thus, the radiation resistance drops as the large metal plane gets closer.

It is also interesting to see the resonant frequency (i.e. where the imaginary part of the impedance crosses the zero line in Figure 27) of the antenna does not change except when the metal plane gets very close (dist_{bot}=1 and 5 mm curves) to the antenna board. The antenna resonance is set by the antenna reactance, which is mainly determined by the reactive near-field close to the antenna. If the large metal plane disturbs the reactive near-field, then it detunes the antenna as well. The reactive near field boundary is at ~5 to 6 mm at 880 to 900 MHz (see “2.1. Near Field and Far Field”), and, thus, significant impact can be seen if the metal is closer. According to this, the detuning effect starts at 5 mm distance and is very strong with 1 mm distance as shown in Figure 27.

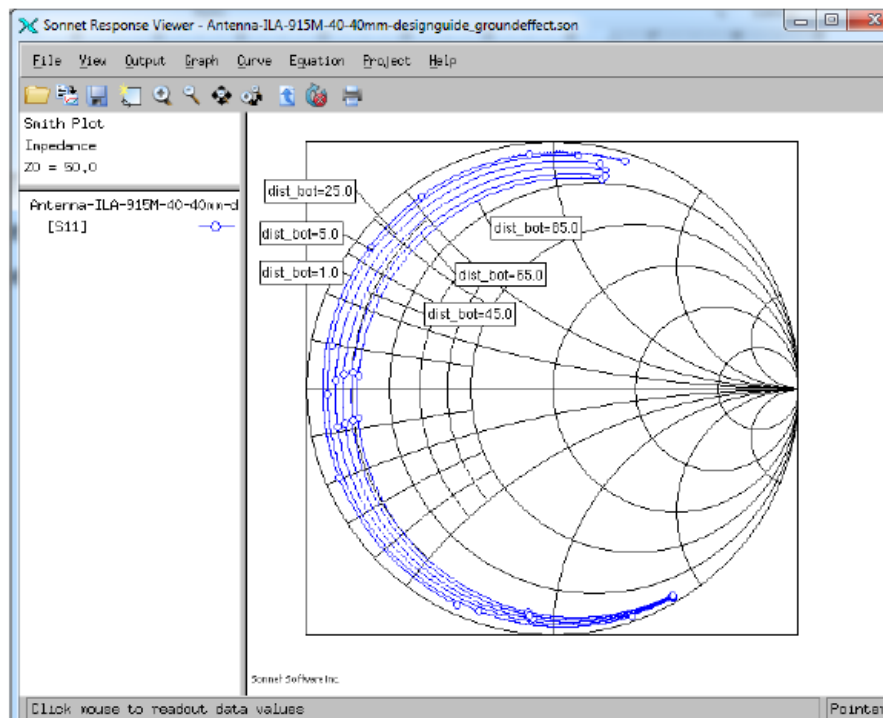


Figure 26. Simulated ILA Impedance with Large Parallel Bottom Metal. The Parameter (“dist_{bot}”) of the Curves is the Distance Between the Antenna Board and the Bottom Metal in mm.

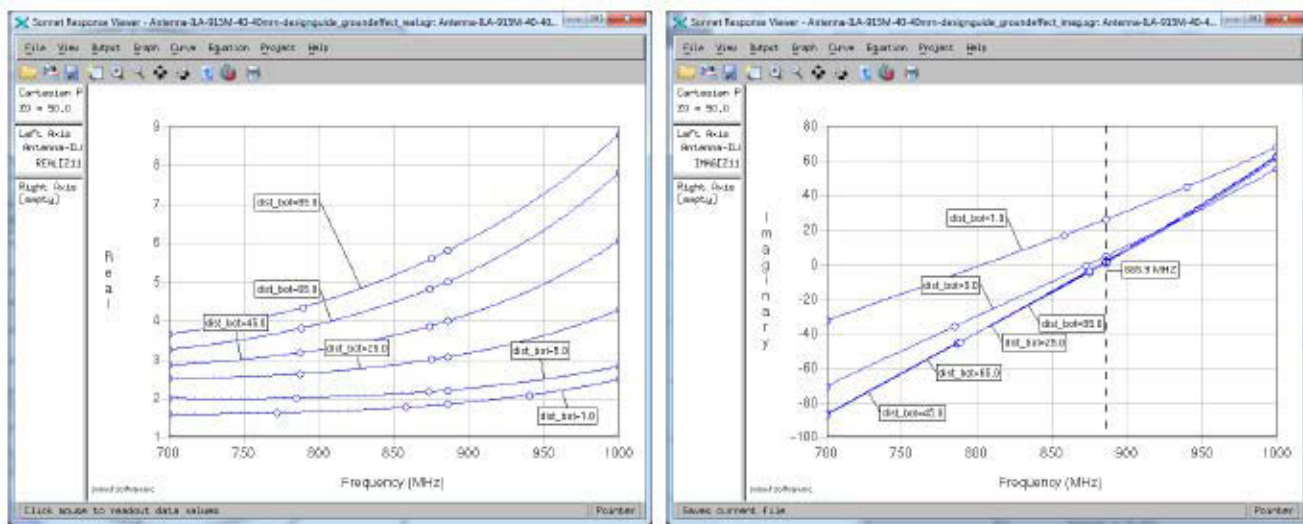


Figure 27. Simulated Real and Imaginary Impedance with Large Bottom Conductor. The Parameter (“dist_bot”) of the Curves is the Distance between the Antenna Board and the Bottom Metal in mm

The radiation efficiency (i.e., the antenna gain) drops significantly if a large parallel metal object appears in the vicinity of the antenna. This effect is shown in Figure 28, where the ILA antenna gain is shown with different large metal plane distances (i.e. with different “dist_bot” values). In each plot, the vertical cuts (the Theta elevation degree is running in 5° step) are shown at different azimuth (Phi) degrees as parameter (Phi varies between 0 and 350 ° in 10 ° steps). A detailed description of the coordinate system and the radiation pattern simulation limitations (e.g., the gain not being valid at the PCB plane, i.e., at a theta of 90 and -90 deg) can be found in Section "4.1. Sonnet EM Simulator Coordinate System" on page 18. In these investigations the antennas are perfectly matched to the feeding generator, i.e., the input mismatch loss is eliminated.

As can be seen, the gain is maximum at Theta = 0° (perpendicular to the PCB plane) where the Phi value has no effect. At close (< 25 mm) distances, the gain practically collapses to any direction (i.e., to the direction of maximum: from the original +1 dBi to -10 dBi). The main direction gain decrease is less than 2 dB if the large metal object is not closer than ~50 mm, which is ~0.15 lambda. Of course, it depends on the antenna type and size as well, but for practical applications, a general rule is to keep all large metal objects at least a quarter lambda away from the antenna.

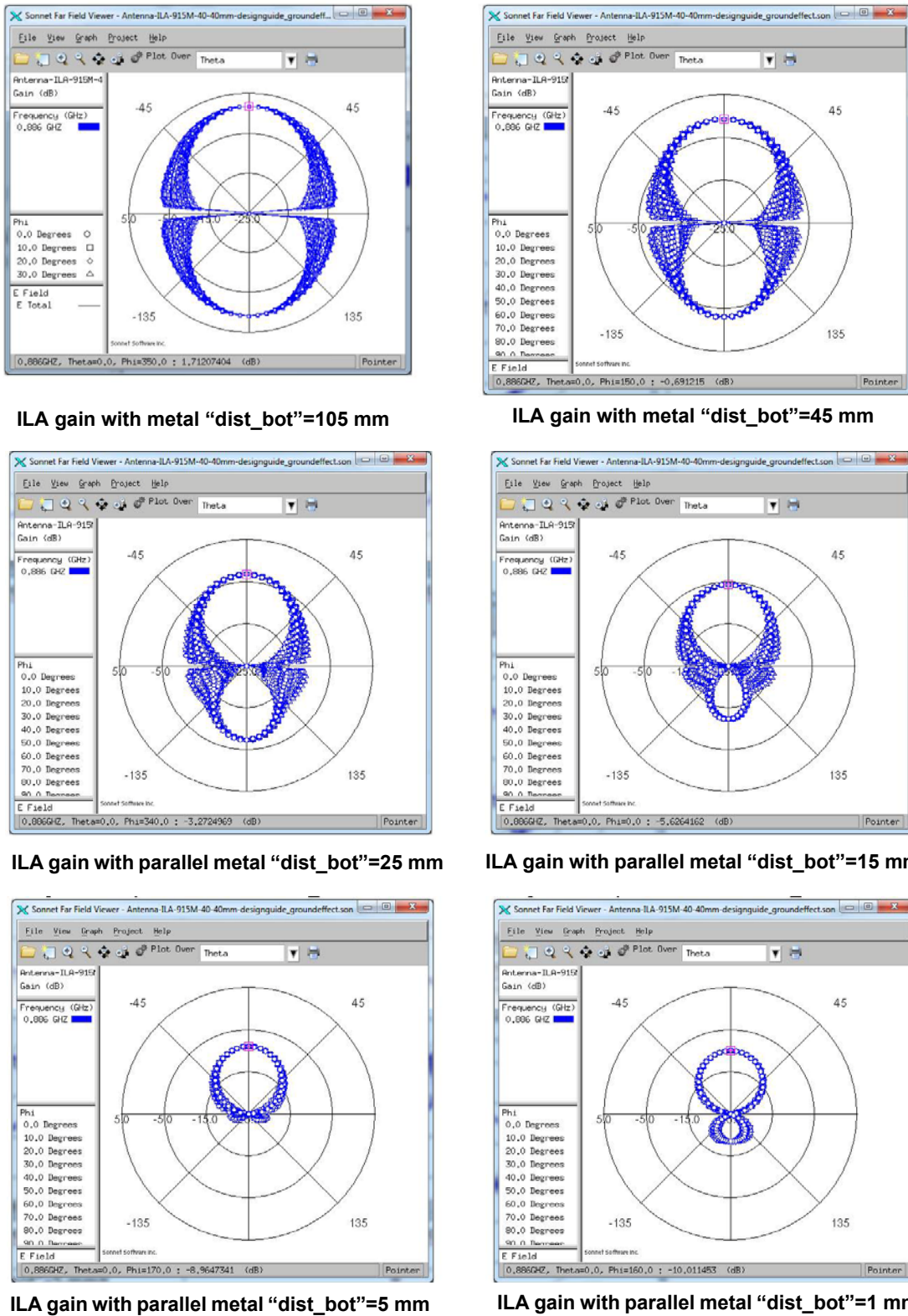


Figure 28. Simulated ILA Antenna Gain Variation at Different Large Metal Distances ("dist_bot" Variable)

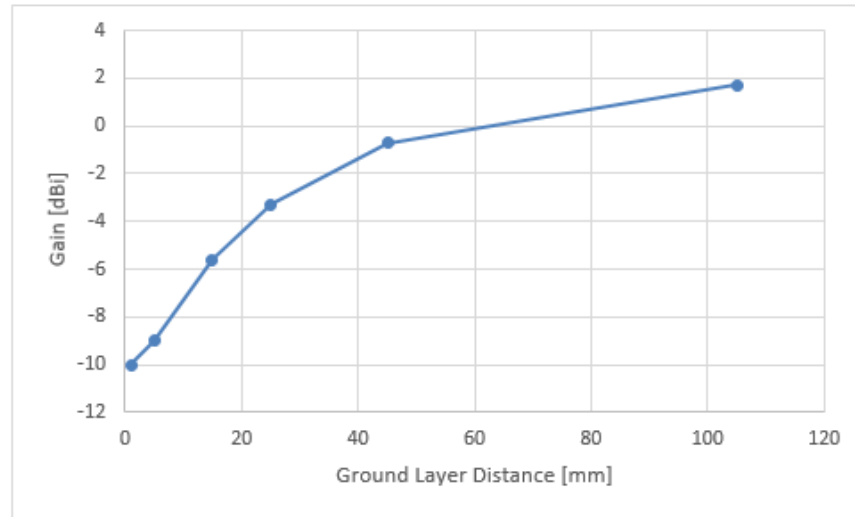


Figure 29. Printed ILA with Parallel Large Ground Layer. Gain vs. Ground Plane Distance

4.4. Effect of the Human Body or Hand Close to a Monopole Antenna

The effect of nearby human tissue is simulated by the Sonnet setup shown in Figure 30. Here, a 3 cm dielectric layer is introduced beneath the ILA antenna PCB to model the Human tissue. The distance between this “human tissue” layer and the antenna PCB is varied (by the “dist_bot” variable).

Different parts of the human body possess different dielectric and conductive properties [9]. Major fraction of the body (muscle, fat, brain, kidney, heart, blood, etc.) has relatively high dielectric constant (epsilon of 50 to 70) and a conductivity of ~1 to 2 S/m at the UHF frequency range. Only the hard tissues like bones has significantly lower epsilon and lower conductivity. Due to the dominance of the “soft” tissues, for further simulations an epsilon of 60 and a conductivity of 1 S/m is assumed for the human body.

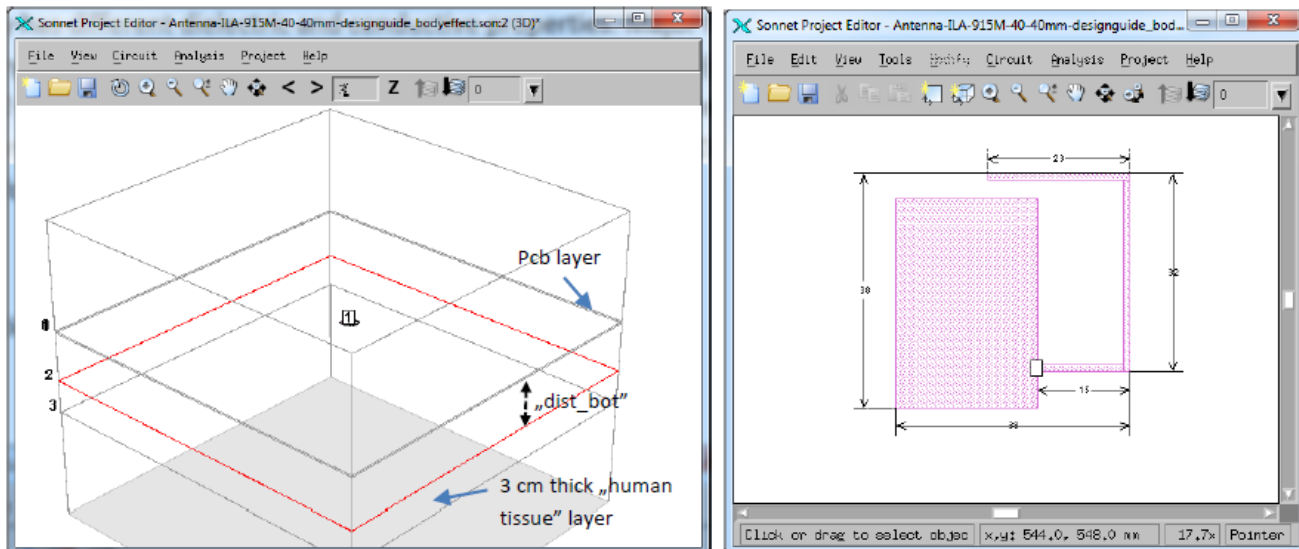


Figure 30. ILA Simulation Setup for the Human Body Effect Investigations

The Impedance simulation results are shown in Figure 31 and Figure 32. The antenna impedance changes significantly when the “Human Tissue” layer get very close to the antenna PCB, again, if it disturbs the reactive near field (i.e. if the gap ~5 mm). In these cases, besides the strong detuning, increase of the antenna real impedance can be observed due to the high losses introduced by the human body.

At higher distances (even if it is only higher by 15 to 20 mm) the antenna impedance and the resonance practically does not change anymore.

The antenna gain variations are simulated in Figure 31. As one can see, the gain collapses to the direction of the human body (bottom lobe at the figures) even at higher distances. The direction of radiation maximum is at Theta=0, away from the body as it was with large metal. However, with the body tissue the main lobe does not decrease so rapidly. Basically it changes very slightly or even can be considered as constant until the body is not closer than 20 mm. Significant gain drop can be observed only when the tissue is at 15 mm (~ 0.05 lambda) distance or closer.

But in typical handheld or wristband application, the antenna PCB is very close to the body, causing both detuning and gain drop (~6 to 8 dB) to occur. The detuning can be compensated for, but not the gain drop.

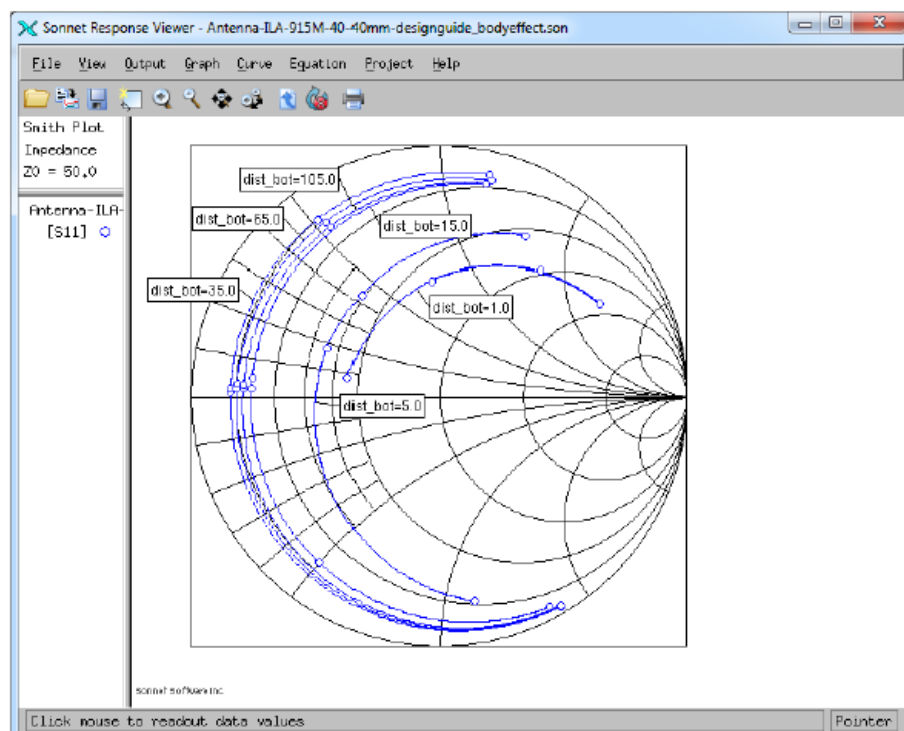


Figure 31. Input Impedance Dependence of the ILA on the “Human Body Tissue” Layer (3 cm thick, Er = 60, cond = 1 S/m) with Varying Distance Between (Denoted by “dist_bot”)

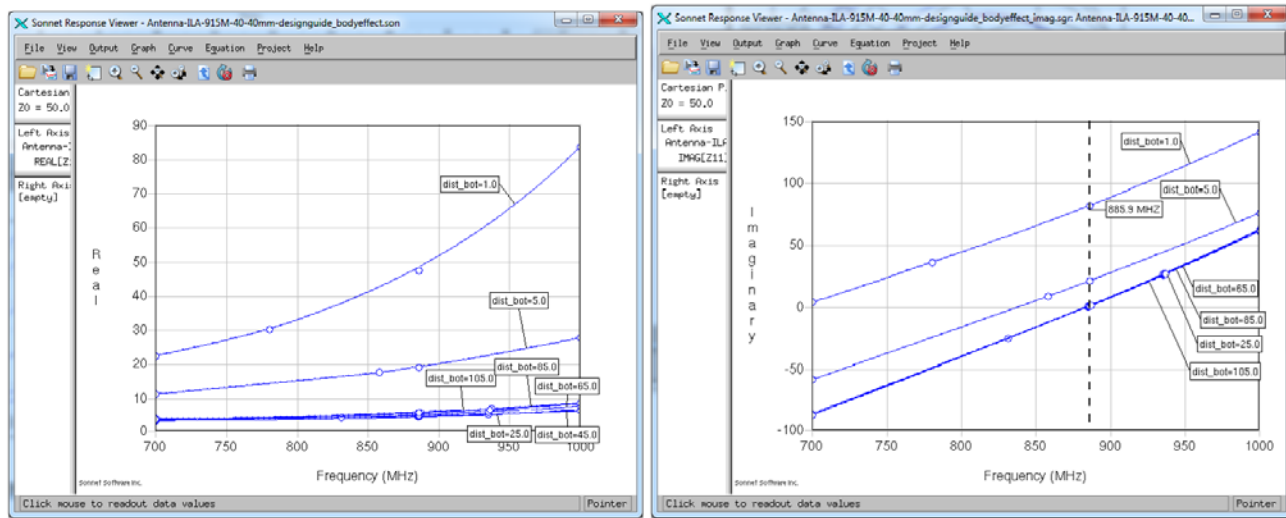
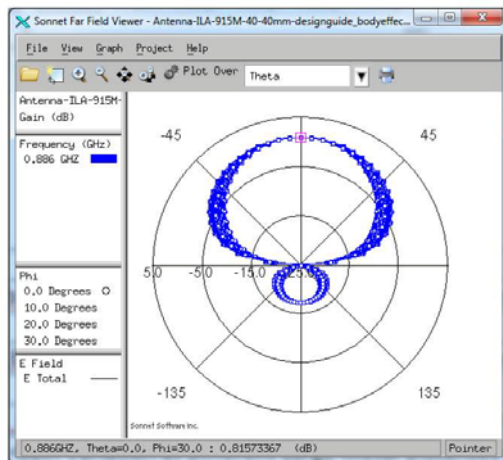
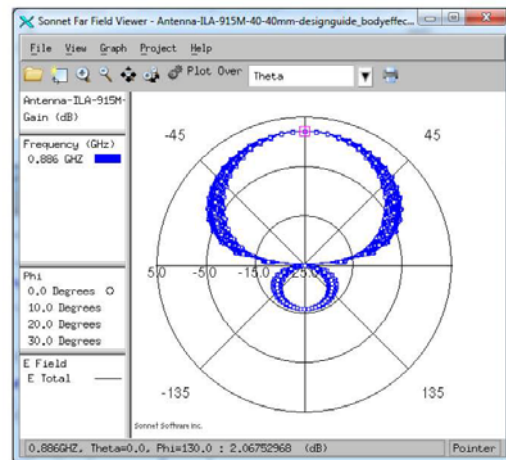


Figure 32. Simulated Real and Image Impedance with “Human Tissue” Layer

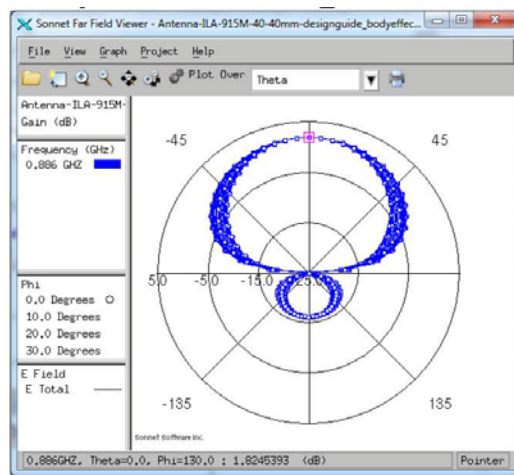
Note: In Figure 32, the substrate is a 1.55 mm thick FR4 with an epsilon of 4.5 and a tangent delta of 0.02. The parameter (“dist_bot”) of the curves is the distance between the antenna board and the Body Tissue in millimeters.



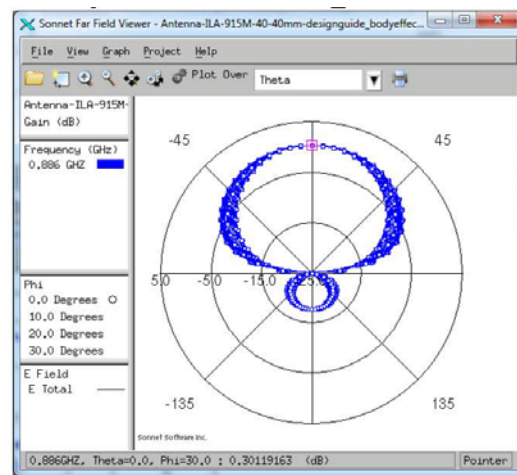
ILA gain with hand, “dist_bot”=105 mm



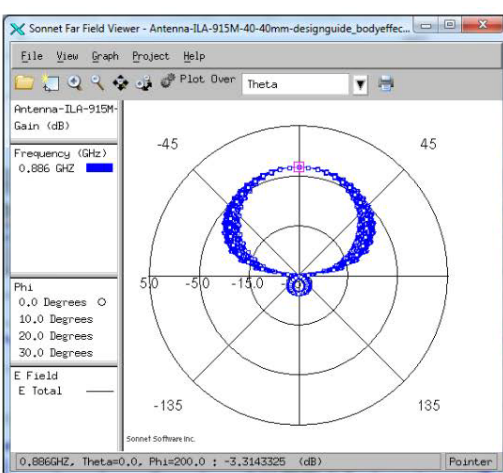
ILA gain with hand, “dist_bot”=45 mm



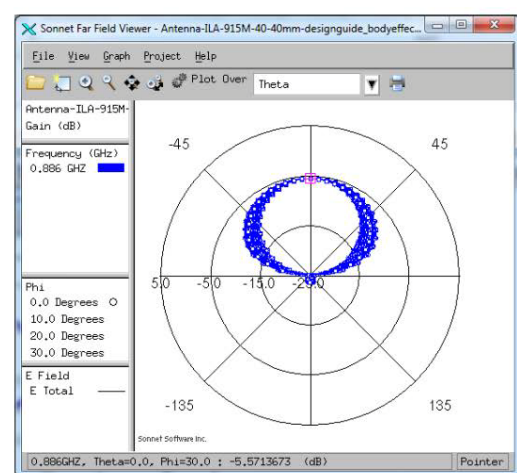
ILA gain with hand, “dist_bot”=25 mm



ILA gain with hand, “dist_bot”=15 mm



ILA gain with hand, “dist_bot”=5 mm



ILA gain with hand, “dist_bot”=1 mm

Figure 33. Simulated ILA Antenna Gain Variation at Different Human Body Distances (“dist_bot” Variable)

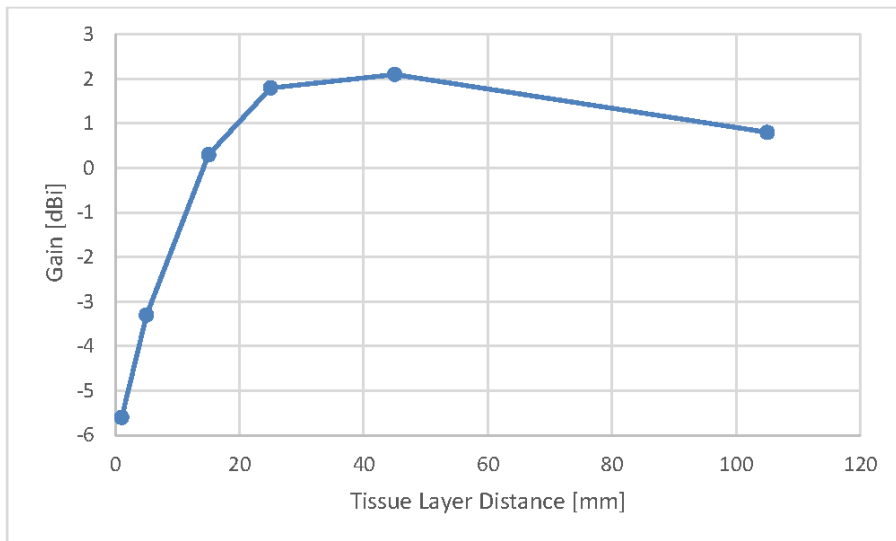


**Figure 34. Printed ILA with Parallel Large “Human Tissue” Layer.
Gain vs. “Tissue Layer” Distance**

4.5. Effect of Reduced Ground Size on Monopole Antennas

As shown in Section "2.7. Ground Plane as an Electrical Mirror" on page 6, a large ground metal behaves as an electrical mirror and creates the virtual ‘opposite pole’ of the monopole antenna. Without this virtual mirror antenna the monopole cannot work as intended. The performance of the monopole degrades rapidly if the ground size is not “very large”. As the small ground metal size is typical in keyfob/sensor/etc. applications in the UHF band, this problem is one of the most important to resolve during a monopole type antenna design.

The conclusion from the results of this chapter is that the antenna gain and range test result presented in the Single-ended Antenna Matrix Application Notes (AN768, AN782, AN847, AN848, AN849, and AN850) are valid only with the applied demo configuration, i.e. with the single-ended Antenna Board connected to the Pro2 PicoBoard through a male-to-male SMA transition and to the large WMB 930 Motherboard. Without these additional large boards (behaves as RF ground) the antenna gains and thus the ranges are significantly lower.

The harmful effects of a small ground plane are:

- Degradation of the real antenna impedance i.e. increase of the antenna Q.
- Detuning of the antenna first resonant frequency (usually it goes up from ~ 0.23 lambda to $\sim 0.28\ldots 29$ lambda monopole antenna length [1]).
- Degradation of the antenna gain, i.e., efficiency.
- Deterioration of the antenna radiation pattern.

The decrease of the antenna real impedance (increase of the Q) is critical as the match of a higher Q antenna is more difficult as it is more sensitive to technological spreading, has narrower bandwidth, and the matching loss is more critical. Unfortunately, decrease of the ground metal size causes significant decrease of the impedance. For example, if the infinite large perpendicular ground metal shrinks to a circle with a radius of a lambda, then the original $\sim 36 \Omega$ monopole impedance at resonance decreases to $\sim 28 \Omega$. The impedance degradation is even more significant in typical remote/sensor/etc. applications where the ground metal (which is usually the circuitry with the gaps filled with GND metal) is in the antenna plane and the GND dimensions are much smaller, usually in the range of 20 to 50 mm. In these typical customer applications the impedance at resonance is very low, around 3 to 10Ω only.

Next, the degradation of the printed ILA antenna impedance at lower PCB ground sizes is investigated with a series of ILA antenna simulations at 915 MHz where the PCB ground size is varied. The simulation setup is shown in Figure 35. The horizontal dimension of the ground metal (circuitry) is varied by the “W_GND” parameter. In Figure 35, the cases with two different “W_GND” parameter values (89 mm and 9 mm) are shown. The antenna trace length is also tuned (by the “L_trace” parameter) to maintain the series antenna resonance around 915 MHz at the different PCB ground sizes.

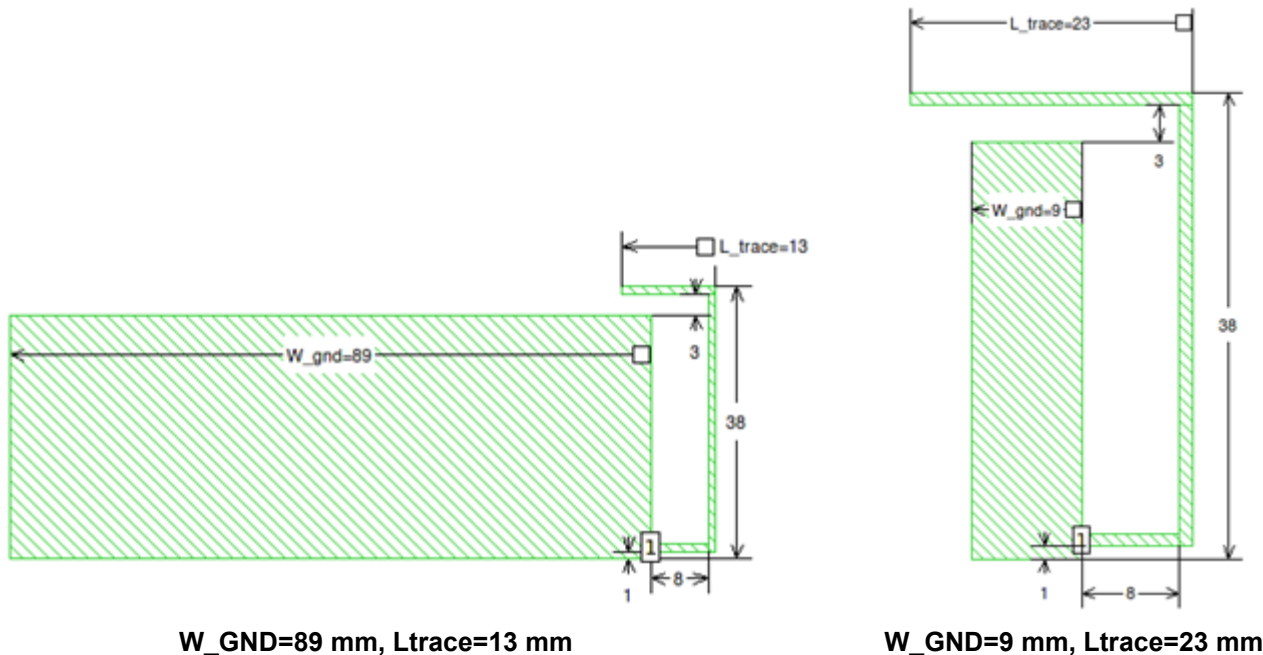
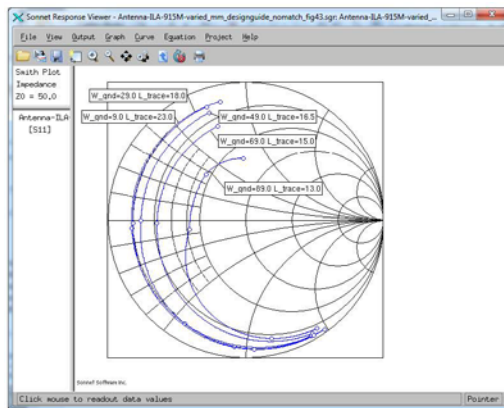


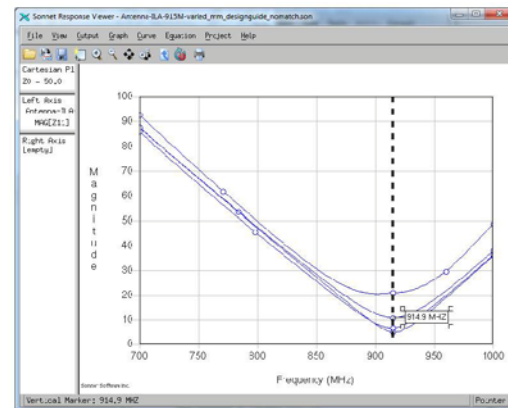
**Figure 35. ILA Simulation Setup in Sonnet with Variable PCB Ground Size
 (“W_GND” Parameter Runs in 20 mm Steps)**

Note: In Figure 35 above, the antenna trace is tuned (with the “L_trace” parameter) as well to maintain the resonance around 915 MHz.

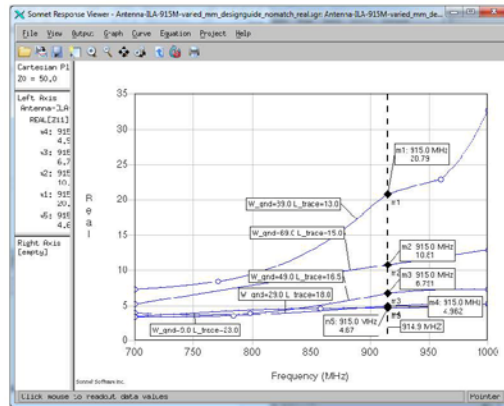
The simulated ILA antenna impedance of the setup of Figure 35 is shown in Figure 36 at different “W_GND” parameter values (and with properly adjusted “L trace” values to maintain the 915 MHz resonance). The real impedance at resonance monotonically increases with the increasing PCB ground size i.e. with the “W_GND” parameter. The increase is non-linear, and is the steepest from 69 to 89 mm (around quarter lambda long region as it is shown in the last figure).



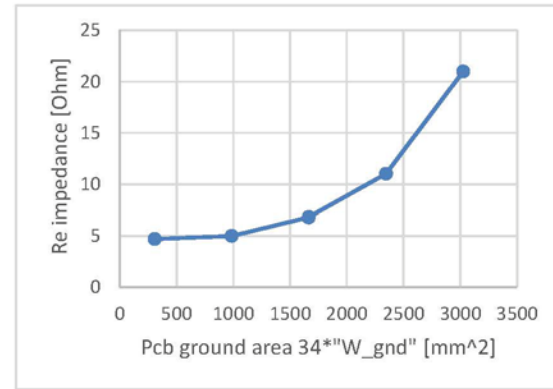
Smith Chart



Impedance Magnitude



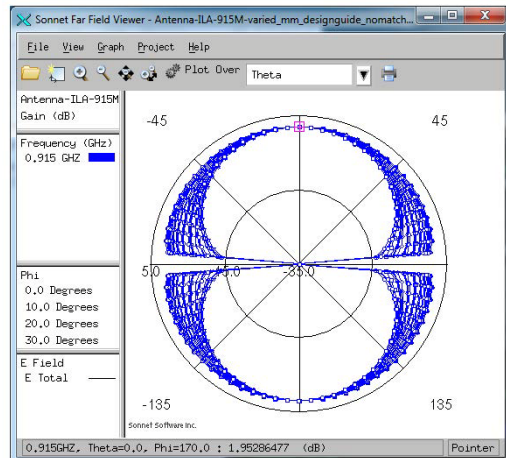
Impedance Real Part



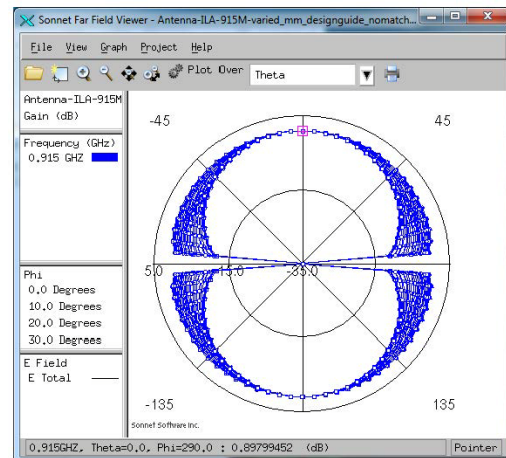
Real Impedance vs. PCB Ground Area

**Figure 36. Simulated Printed ILA Antenna Impedance at Different PCB Ground Sizes
(Antenna Trace Length is Varied as well to Maintain Resonance at ~915 M)**

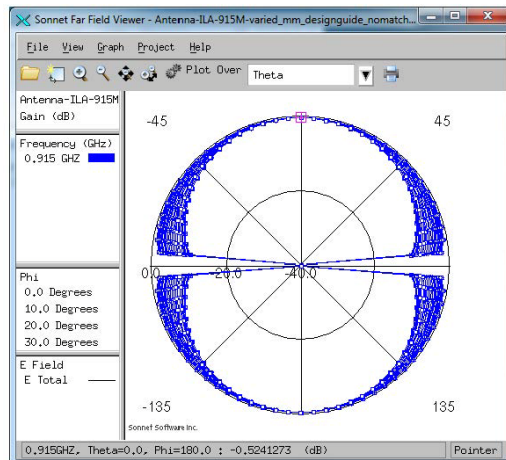
The gain variation with reduced GND sizes is investigated as well. Figure 37 shows the simulated gain patterns with the different PCB ground sizes. As can be seen from the last figure, the gain strongly depends on the PCB area.



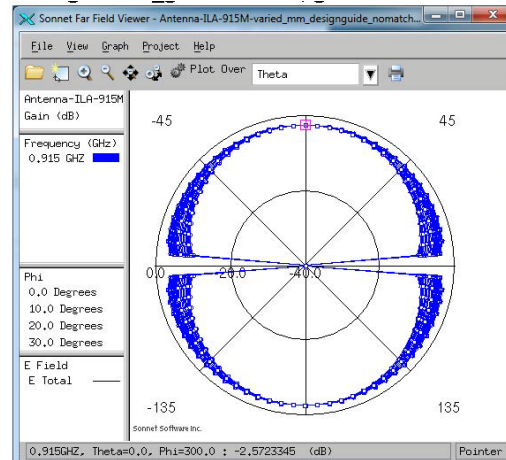
ILA gain "W_GND"=89 mm, gain=+2 dBi



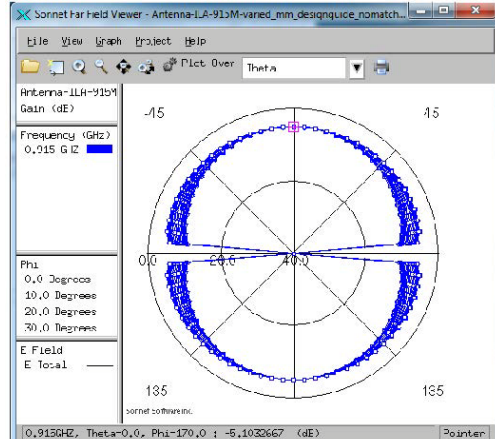
ILA gain "W_GND"=69 mm, gain=+0.9 dBi



ILA gain "W_GND"=49 mm, gain=-0.5 dBi



ILA gain "W_GND"=29 mm, gain=-2.6 dBi



ILA gain "W_GND"=9 mm, gain =-5.1 dBi

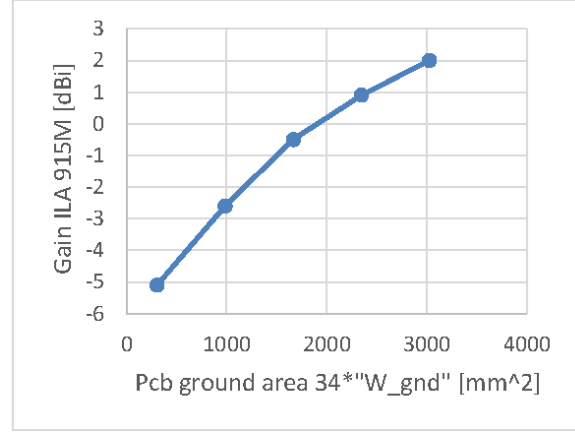


Figure 37. Simulated 915 MHz ILA Antenna Gain Variation at Different PCB Ground Sizes

A second series of investigations are done as well, where both the GND (circuitry) part and the total PCB size, including the ILA antenna area of 915 MHz radio remote boards are varied. The boards represent a typical final remote design in the given size. As shown in Figure 38, four total PCB sizes are investigated: a 40x40 mm, 30x30 mm, 20x20 mm, and a 10x10 mm board (the simulated boards are slightly smaller to have some (~2 mm) gap between the antenna trace and the PCB cutting edge).

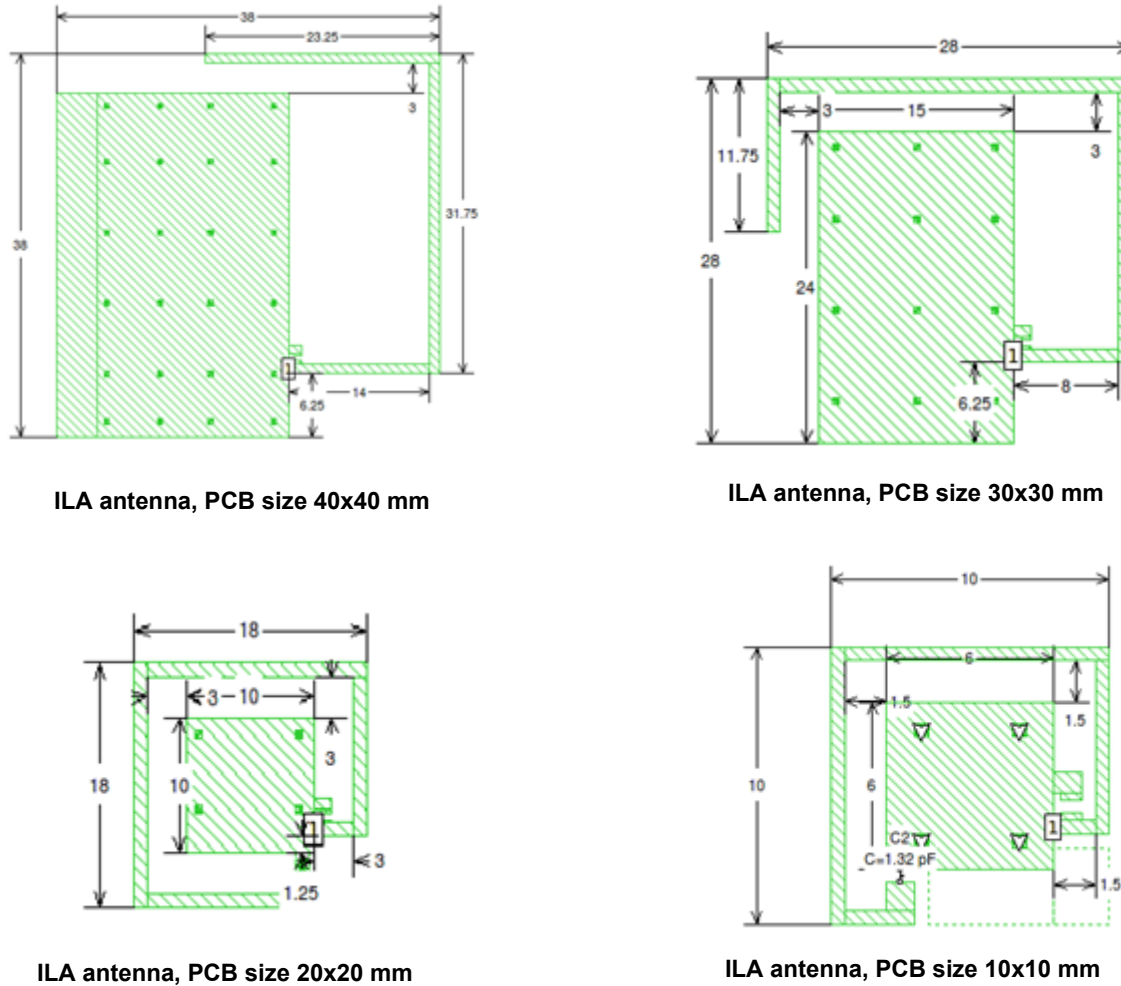


Figure 38. Simulated ILA Antenna Setups at Different PCB Sizes

In Figure 39, the gains of these four 915 MHz remote boards are shown (in the horizontal axis the total PCB size is shown). The gain is monotonically increasing with the increased PCB area, similar to the results of Figure 37. However, a significant difference is that at low PCB sizes (below the $\sim 1000 \text{ mm}^2$) the gain drops even more rapidly. The reason is that despite the first investigation (Figure 37), here the horizontal axis represents the total PCB area and the effective ground area is only a small fraction of this, especially at lower PCB sizes.

The 915 MHz outdoor and indoor ranges are estimated in these various total PCB sizes in Table 2. In these calculations, two identical units both applying Si4463 radios with +20 dBm TX power and with a typical RX sensitivity (with 40 kbps, 20 kHz dev GFSK and 0.1% BER link parameters) are used and the boards are facing with the direction of maximum radiation (peak gain values of Figure 39 are used). An additional 5 dB link budget margin is also applied, to mimic the degradation that usually occurs due to interferences. The assumed propagation constant is 3 for the outdoor and 4.5 for the indoor environment.

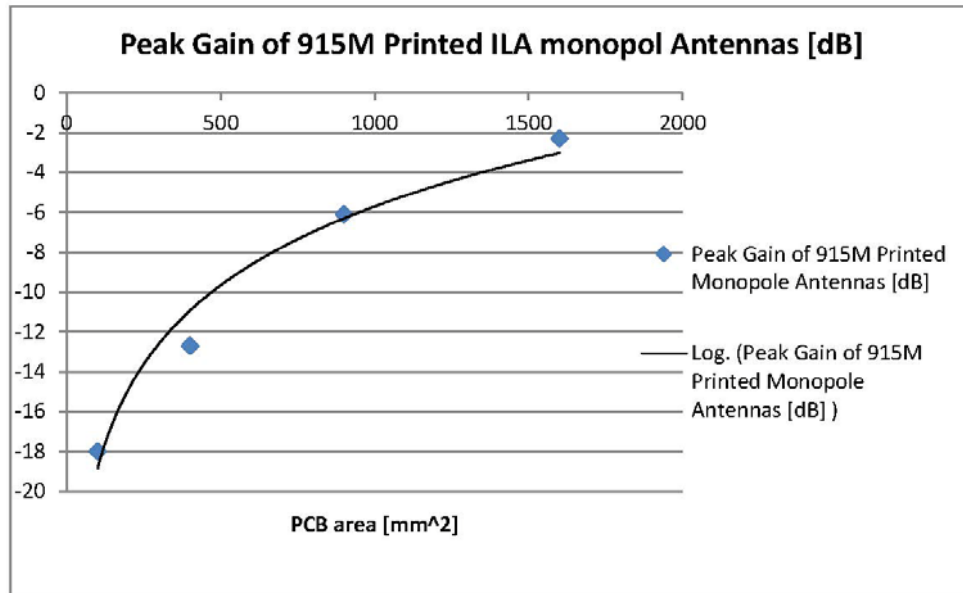


Figure 39. Peak Gain of 915 M Printed ILA Antennas Boards vs. Different Total PCB Size

Table 1. Range with 915 MHz Printed ILA Antenna Boards with Various Total PCB Sizes*

915 MHz Printed Monopole Antenna Summary	Total PCB Area (mm ²)	Antenna Maximum Gain (dBi)	Maximum Link Budget with Si4463 (dB)	Estimated Indoor Range (m)	Estimated Outdoor Range (m)
PCB size 10x10 mm	100	~ -18	~93	48	95
PCB size 20x20 mm	400	~ -12.7	~103.6	68	215
PCB size 30x30 mm	900	~ -6.1	~116.8	74	591
PCB size 40x40 mm	1600	~ -2.3	~124.4	88	1058

*Note: Range is estimated between two identical units with +20 dBm TX Power, 40 kbps, 20 kHz dev GFSK, and 0.1% BER Sensitivity. A 5 dB extra link budget margin is assumed to count interference effects.

Table 1 shows that at very small PCB sizes the antenna gain and the range drop significantly. The drop is even higher at lower frequencies where the PCB size is even smaller compared to the lambda.

The curves of Figure 37 and Figure 39 can be used as a way of estimating the gain for different PCB sizes at 915 MHz.

4.5.1. Frequency Dependency of the Gain with Constant PCB Size

Up until this point, the gain and impedance dependency on the ground metal dimensions have been investigated only at a single frequency (915 MHz). The reader may be interested in the method to rescale this knowledge to other frequencies as well.

In theory, at lower frequencies the PCB area (the horizontal axe in the figures) has to be rescaled with the square of the frequency ratio (e.g. a 915 MHz gain result with a PCB ground area of 1000 mm^2 ($\sim -3 \text{ dBi}$) is nearly valid to a PCB with a ground size of $(915/434)^2 \times 1000 \text{ mm}^2 = 4400 \text{ mm}^2$ at 434 MHz). However, this is only valid if the distance between the ground and the antenna trace changes inversely with the ratio of the frequencies (e.g. at 434 M, the antenna trace should be $915/434 = \sim 2.1$ times further from the ground than in 915 MHz).

If the antenna trace is at the same distance, than the gain drop is *much higher* at lower frequencies. To investigate this, a 434 MHz ILA structure is also simulated with various PCB ground sizes and the same antenna trace to PCB ground distance (8 mm) as it was at 915 MHz. Figure 40 shows the setup. At 434 MHz, the constant dimension of the PCB is increased as well (from 34 to 52 mm) to have gain values nearly at the same order as was with the 915 MHz case. Similarly to Figure 35 the “W_GND” variable is varied (between 49 and 89 mm in 20 mm steps) and the trace length (“L_trace”) is adjusted to have resonance at 434 MHz.

Figure 41 shows the simulated impedance and the “gain vs. PCB ground size” curves. As it is shown the impedance is nearly the same independently of the PCB ground size, moreover the real part is quite low even at these physically larger ground sizes. The gain is also quite low: e.g. the gain of the $69 \times 48 = \sim 3300 \text{ mm}^2$ PCB ground size case is $\sim -7.5 \text{ dBi}$ at 434 MHz. According to the theoretical rule, at 915 MHz, for the same gain a PCB ground size of $(434/915)^2 \times 3312 \text{ mm}^2 = 745 \text{ mm}^2$ would be required. But according to Figure 37, a board with a ground size of $\sim 200 \text{ mm}^2$ produces this gain at 915 MHz.

So the conclusion is that if the antenna trace is at the same distance from the ground, the gain drops more rapidly than expected (from the PCB size) at lower frequencies.

Or viewing from the reverse side: if the distance between the antenna trace and the ground is the same, the same PCB dimensions results in approximately 10 dB lower gain at 434 M than at 915 MHz in the regime of practically usable PCB dimensions (1000 to 3000 mm^2).

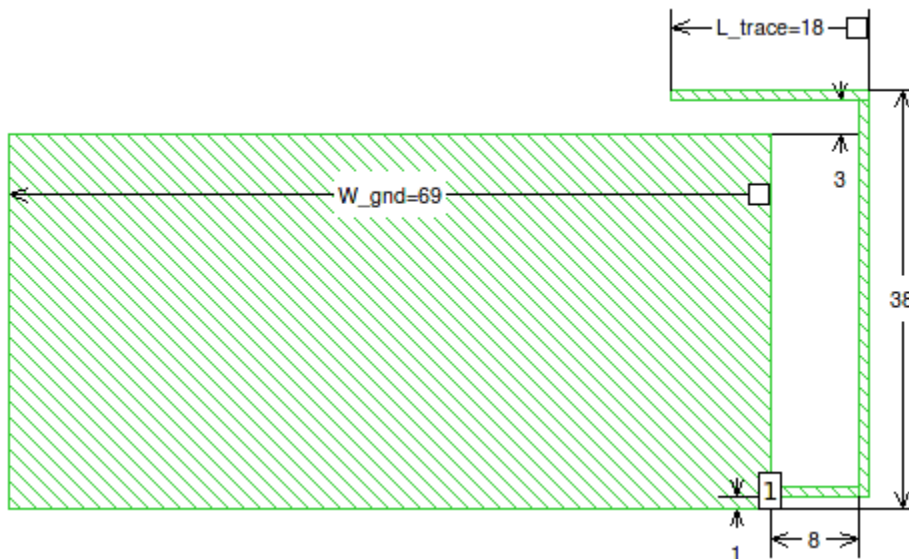


Figure 40. 434 M ILA Simulation Setup with Variable Ground Size (“W_GND” Runs in 20 mm Steps). The Variation of “L_trace” Maintains the Resonant Frequency at 434 MHz

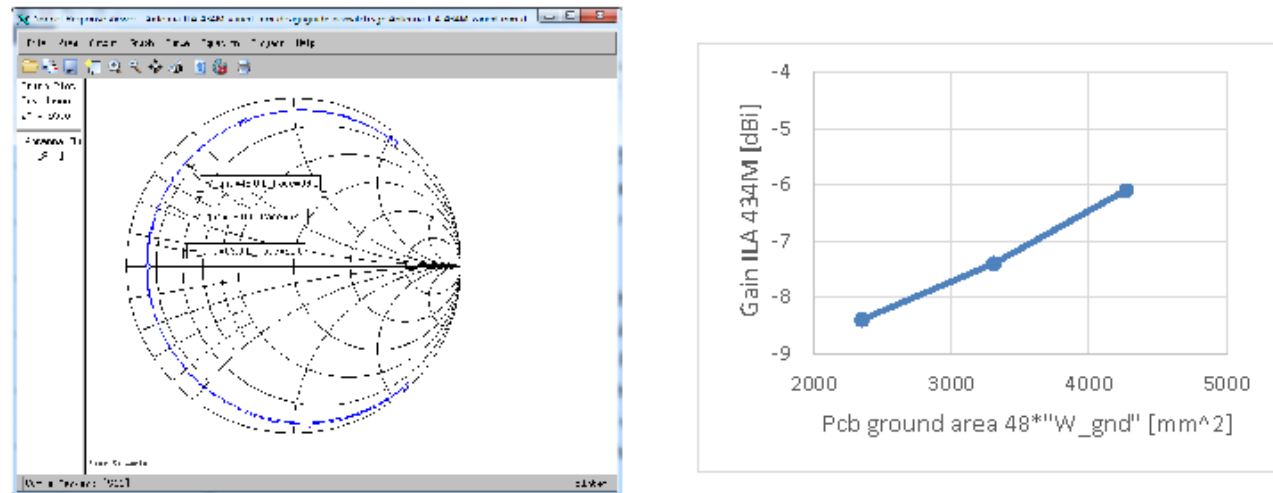


Figure 41. 434 M ILA Simulated Impedance and Gain with Different Ground Sizes (“W_GND” Runs in 20 mm Steps). Antenna Trace Length “L_trace” Variable Maintains the Resonance at 434 M

5. Design Steps of Printed ILA and IFA Antennas

Some description and behavior of ILA and IFA antennas can be found in [6]. Unfortunately, detailed design steps are not given. The aim of this chapter to present systematic way to design for both antenna types.

5.1. Design of Printed ILA Antennas

The printed ILA antenna is basically a bended monopole. So its behavior is close to the normal wire monopole (Section 2). The main difference is that in the case of a printed ILA the ground is in the plane of the antenna, and a significant (or main) part of the antenna trace is leaded in parallel with the ground boundary. Due to these properties, the ILA radiates with less efficiency (especially if it is close to the ground boundary) compared to a normal wire monopole with the same physical length.

Despite this, the basic behavior and the designs steps are very similar. As the ground size in the typical compact radio realizations is small, the residual real ILA impedance at resonance is much lower than $50\ \Omega$ and the antenna has high Q.

Due to the low impedance, the printed ILA antenna cannot be matched inherently to $50\ \Omega$, so external matching elements are required. Unfortunately, as the antenna Q is quite high in practical cases, the loss of the external matching is critical. The SMD capacitors in 0402 or 0201 sizes has a Q of approximately 200 to 300 at the UHF frequencies, while the SMD inductors has a Q of only 40 to 70 depending on type (multilayer or wirewound). Moreover, the price of an SMD inductor is 5 to 6 times higher than the price of a capacitor. Due to these facts, our primary aim is to use only one or two capacitors as external matching elements and avoid the usage of any external inductors.

During the design the effect of a nearby metal or hand has to be taken into account and if required, post tuning has to be done. Knowing the basic effects, the necessary tuning steps can be determined. First, the basic antenna design steps are presented without hand and metal effects. Later on, the impact of these effects are investigated and the antenna is tuned.

In the later design steps, the ILA configuration presented in Figure 18 is used as a starting point. The aim is to design a practically usable 915 MHz radio board with ILA fit into a $40 \times 40\text{ mm}$ form factor.

As it was mentioned earlier, the effect of a nearby PCB substrate cutting edge is not simulated in Sonnet, so the total PCB size is slightly (by 2 mm in each dimensions) lower than the available space to keep some gap between the antenna trace and the cutting edge. The effect of a PCB cutting edge close to the antenna trace is that the effective dielectric constant around the antenna trace decreases and thus the electrical length of the antenna will be shorter. From the theory, a rule is that the E field can be neglected at distances equal or higher than 3^*H , where H is the substrate thickness. Fortunately, Silicon Labs' experience is that at cutting edge distances higher than 2 mm (up to 1.6 mm thick FR4 substrate), the detuning can be easily compensated during the bench tuning phase. So in the upcoming example, a 2 mm gap is used at the two PCB sides with antenna traces close to them while the non-antenna PCB sides are situated right at the PCB cutting edges.

Due to the nearby PCB cutting edge and the thin substrate, the effective epsilon seen by the antenna trace is somewhere between the PCB FR4 substrate epsilon (~ 4.5) and the epsilon of the air. The effective epsilon depends slightly on the trace width and substrate thickness as well, but not as much as one would expect due to the very small PCB thickness compared to the lambda. Another important factor which determines the effective epsilon is the antenna structure. An antenna trace closer to the ground has higher value of distributed parasitic capacitance per unit length and, thus, higher phase rotation. Due to this, an antenna trace closer to the ground generates the same electrical length with shorter physical length, which is equivalent to having a higher effective epsilon.

As one can see from Figure 21 the resonance of the ILA of Figure 18 is at $\sim 890\text{ MHz}$. According to the literature [1], a monopole with a small ground has its first series resonance at higher than ~ 0.23 to 0.24 lambda electrical lengths, typically around ~ 0.29 lambda. Knowing this, the physical length of the antenna (68 mm) and the resonant frequency, effective dielectric constant of the investigated structure on the applied 1.55 mm thick FR4 can be estimated:

$$\lambda_{\text{eff_899MHz}} = \frac{68[\text{mm}]}{0.29} = 234.5[\text{mm}]$$

$$\epsilon_{\text{eff}} = \frac{c^2}{\lambda_{\text{eff}}^2 f^2} = \frac{(3 \times 10^8)^2}{(234.5 \times 10^{-3})^2 (889 \times 10^6)^2} \approx 2.07$$

The effective epsilon value around 2.1 is not surprising as the antenna is mostly surrounded by air and only a 1.55 mm thick FR4 is close to it. With a thinner FR4, the effective epsilon would be even lower. Also, the antenna trace is relatively far (~ 8 mm) from the ground. With this gap size, an effective epsilon somewhere between 2 and 2.1 can be used for antenna trace length estimations.

Here, the reader may notice that the antenna should work at 915 MHz, but its resonance is at a lower frequency (889 MHz). As shown in Figure 22, the impedance at resonance is very low, only $\sim 5 \Omega$. Matching a 5Ω resonant antenna impedance to 50Ω would be rather lossy with commonly available SMD elements, if a two-element matching with at least one inductor was required.

To avoid this, the antenna is designed to have longer electrical length, for example, at the operating frequency it is already over resonance and, thus, has a proper inductive input impedance. Then this inductive input impedance can be matched by one parallel input capacitance to 50Ω . Due to the higher Q of the SMD capacitors, the matching loss is lower in this way.

Perform the following detailed steps:

1. The antenna length is adjusted to have an inductive antenna admittance with $1/50 = 0.02$ Siemens real part at the operating frequency. This step is shown in Figure 42 where the simulated antenna impedance is plotted on the admittance Smith chart. The admittance real and imaginary parts are displayed here with normalized values:

$$Y_{\text{NORM}} = \frac{Y}{Y_0} = \frac{Y}{0.02}$$

So, a displayed normalized admittance real part of 1 corresponds to 0.02 Siemens real part in real life.

Unfortunately, the length of the antenna in Figure 18 is short as it does not have enough phase shift to be at the 1 normalized real admittance circle at 915 MHz, as shown on Figure 42A.

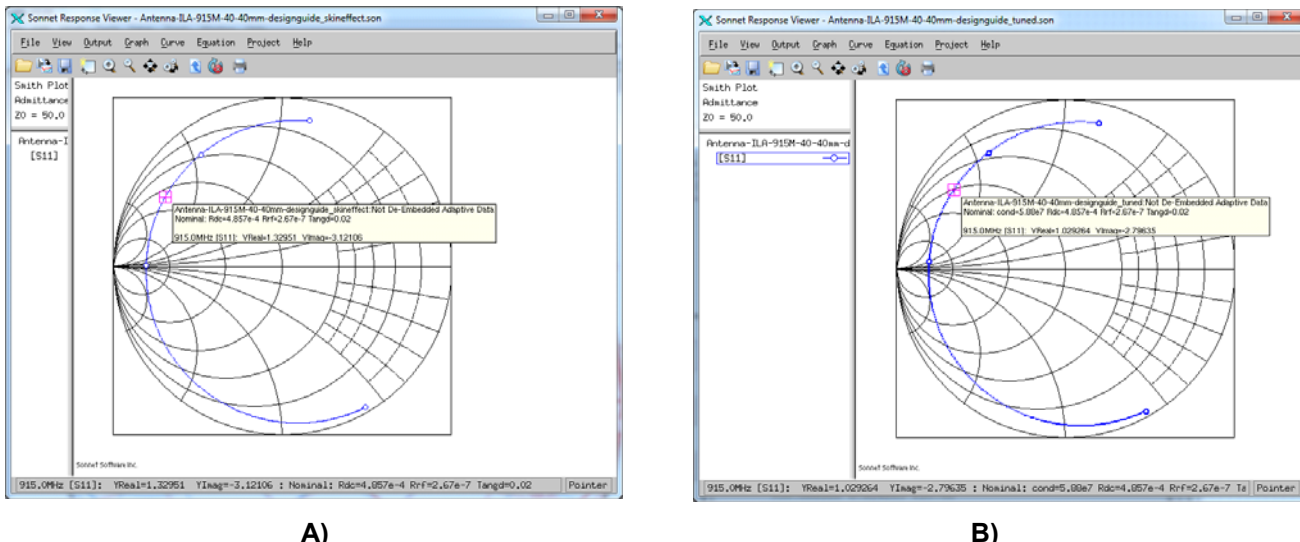
With slight increase of the physical length (from 68 to 68.25 mm) the admittance can be tuned to be at the 1 normalized real admittance circle (Figure 42B).

It is interesting to determine the modified electrical length of the antenna trace at 915 MHz:

$$\lambda_{\text{eff_915MHz}} = \frac{V_{\text{eff}}}{f} = \frac{C}{f \times \sqrt{\epsilon_{\text{eff}}}} = \frac{3 \times 10^8}{(915 \times 10^6) \times \sqrt{2.07}} = 228[\text{mm}]$$

$$l_{\text{elect_915MHz}} = \frac{l_{\text{phy}}}{\lambda_{\text{eff_915MHz}}} = \frac{68.25}{228} = 0.299 \lambda_{\text{eff_915MHz}}$$

So in order to have an antenna input admittance real part of ~ 0.02 Siemens, the antenna trace electrical length should be around 0.3 lambda at the operating frequency. Using this rule and assuming an effective dielectric constant between 2...2.1 (depending on PCB thickness), one can estimate the necessary physical antenna trace length at any UHF frequency.



A)

B)

Figure 42. 915 MHz ILA Antenna Admittance
A) Before Tuning (L = 68 mm); B) After Tuning (L = 68.25 mm)

2. Connecting a proper parallel SMD capacitor to transform the impedance to 50 Ω (i.e. to the center of the Smith chart).

In this second step, the residual imaginary admittance part after Step 1 is eliminated by adding a parallel capacitor at the ILA antenna input. This step is illustrated on the Smith chart in Figure 43 together with the matching, which is a parallel 9.7 pF, or it can be calculated quite easily knowing the residual admittance imaginary part. As shown in Figure 43, after the first step, the impedance is $\sim 5.8 + j - 15.8 \Omega$. From this, the admittance at this point is $\sim 0.02 - j0.056$, meaning the real part is 0.02 Siemens as expected. The parallel capacitance should eliminate the imaginary part of the admittance. So, the required parallel cap is:

$$C_{\text{par}} = \frac{-\text{Im}Y}{\omega} = \frac{0.056}{2\pi(915 \times 10^6)} = 9.74 \times 10^{12} [\text{F}] = 9.74 [\text{pF}]$$

which is identical to the result of Figure 43.

It should be noted that these are the results with an ideal capacitor. A real SMD capacitor has parasitics and losses. The equivalent circuit of a 0402 SMD cap with C0G dielectric is a series-resonant RLC with a typical inductor value of $\sim 0.7 \text{ nH}$ and R value of 0.5 Ω.

The impedance locus with this RLC is quite different from the ideal cap case as shown in Figure 44. Here, the main reason for the deviation is the series parasitic inductance. Figure 45 shows the parasitic inductance compensated case in which the capacitance value is decreased to 8 pF to have the impedance close to the center of the Smith chart. The loss has no significant effect on the locus.

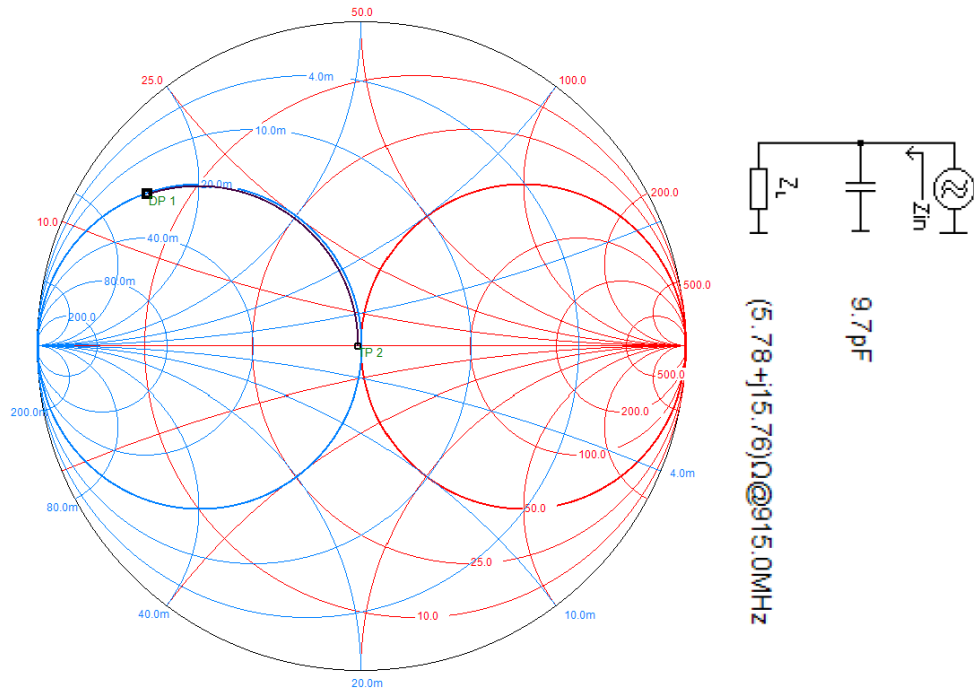


Figure 43. Tuning of the 915 MHz ILA Antenna by an Ideal Parallel Capacitor at the Input

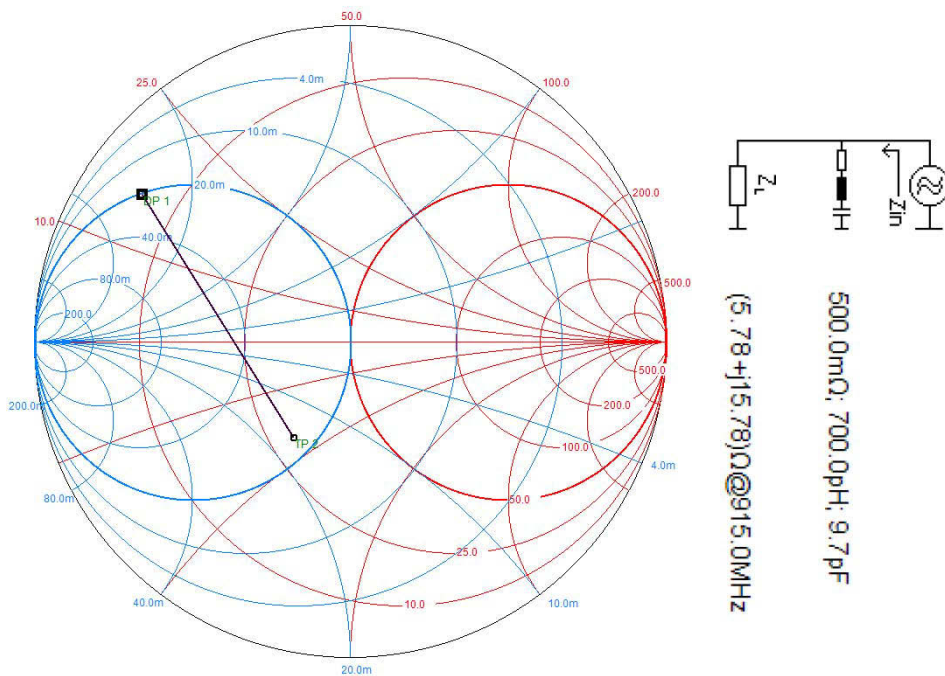


Figure 44. Deteriorated Tuning Result with the Parasitics (Series Inductance and Loss) of the Parallel Tuning Cap Introduced

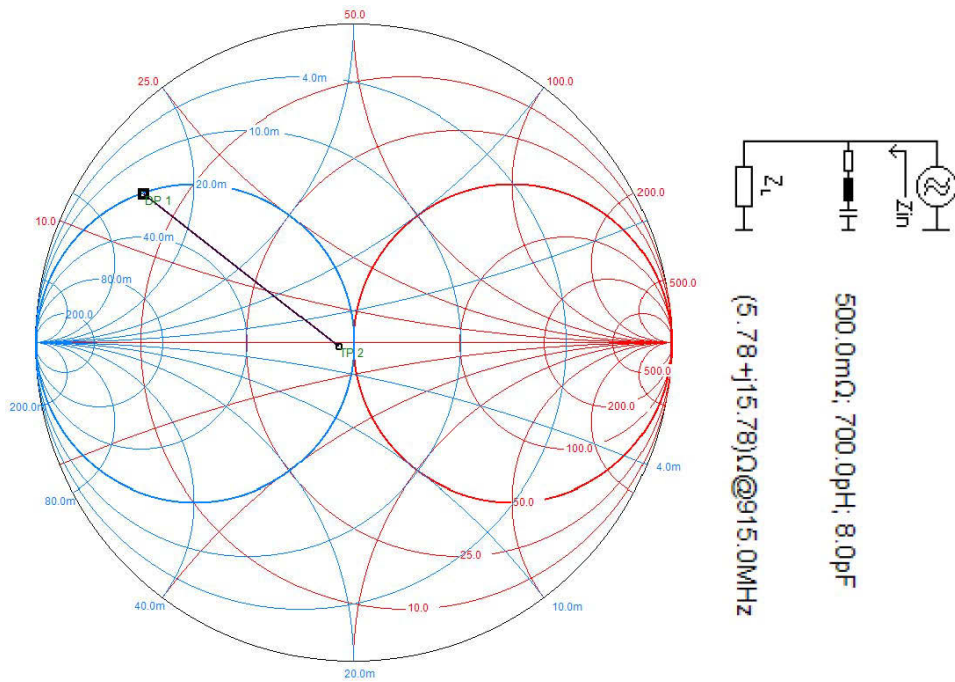


Figure 45. Compensation of the Parallel Cap Parasitics by Properly Decreasing the Value

The compensated capacitance value can be calculated analytically as well. By neglecting the loss, the imaginary part of the admittance of a series LC is:

$$\text{Im}Y_{LC} = \frac{\omega C}{1 - \omega^2 LC}$$

The imaginary part of the antenna admittance should be compensated by this:

$$\text{Im}Y_{LC} = -\text{Im}Y$$

From the above, the compensated C value can be derived:

$$C = \frac{|\text{Im}Y|}{\omega + |\text{Im}Y| \omega^2 L}$$

After substituting:

$$C = \frac{0.056}{2\pi \times 915 \times 10^6 + 0.056 \times (2\pi \times 915 \times 10^6)^2 \cdot 0.7 \times 10^{-9}} = 7.95[\text{pF}]$$

It must be noted that the final trace length and capacitance value can be determined during bench tuning on the final PCB with the final nearby objects (e.g. plastic, battery etc.), but the steps required during bench tuning are the same as those detailed above.

5.2. Design of IFA Antennas

The Inverted F Antenna (IFA) applies a small loop parallel with the monopole close to the antenna input. A typical example of this antenna type is the Panic Button IFA antennas in the 434, 868, and 915 MHz Antenna Matrix. Figure 46 shows the 868 M Panic Button IFA (WES0035).



Figure 46. 868 M Panic Button IFA

An IFA antenna can be considered as a normal ILA antenna with a parallel connected small loop close to the antenna input. As the small loop can be modeled quite well with a discrete shunt inductor, the IFA can be modeled by an ILA with a shunt inductor at the input. The parallel inductor generates a parallel resonance with the ILA at the frequency regions where the ILA shows capacitive impedance, below the ILA series resonance point. Thus, the IFA can be resonated at lower frequencies than the inherent series resonant frequency of the ILA structure. Since the IFA resonance is parallel, the residual impedance at resonance can be adjusted as needed, and can be increased to even higher values (50 to 200 Ω). This fact does not change the resulting Q of the antenna. As the Q of the parallel small loop is very high (~100 or more), it has practically no influence on the overall IFA Q, which is then approximately identical to the Q of the ILA structure. The ILA Q is usually also quite high (~10 or more) with small grounds, and thus, the operation is rather narrowband.

The resonant frequency and impedance depend on the electrical length of the ILA and the inductor value. The whole procedure can be best followed on the Smith chart. Figure 47 shows the original 868 MHz ILA simulation setup, where an additional ideal parallel tuning inductor (denoted by "Lpar") is introduced. Figure 48 shows the simulated antenna impedance curves on the Smith chart (the admittance diagram is shown here with the constant conductance (admittance real part) and susceptance (admittance imaginary part) curves) in the 400 to 1200 MHz frequency range. The parameter of the curves is the parallel inductor value.

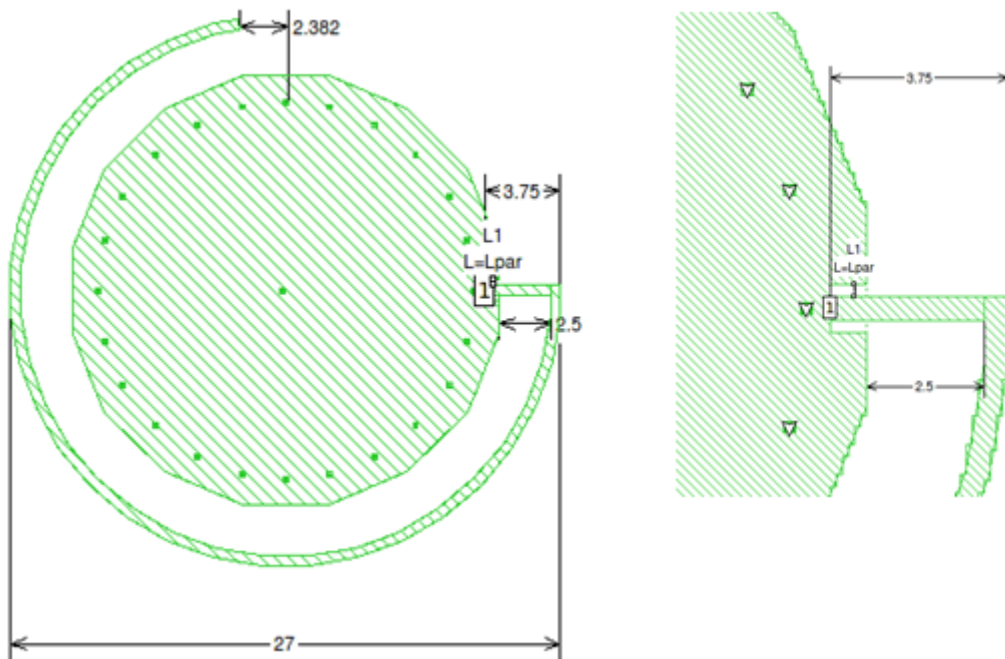


Figure 47. Simulated 868 M ILA Structure before Tuning with Parallel Tuning Inductor at the Input

The reference curve with high value ($L_{par} = 60 \text{ nH}$) of parallel inductor is highlighted. The impedance of the 60 nH parallel inductor in this UHF frequency range is so high that it has practically no effect on the antenna impedance, and, thus, this curve roughly coincides with the original ILA impedance curve.

As can be seen, the series resonance is around 840 MHz and is nearly independent of the L_{par} value. Also, the ILA antenna was originally designed to have $\sim 20 \text{ mSie}$ conductance with inductive susceptance at $\sim 868 \text{ MHz}$ in order to tune it with a proper parallel cap. This design approach was already detailed for the 915 MHz ILA in Section “5.1. Design of Printed ILA Antennas”.

The other, capacitive 20 mSie conductance point of the $L_{par} = 60 \text{ nH}$ curve is at $\sim 808 \text{ MHz}$ (marked). By adjusting (decreasing) the L_{par} value, this point moves upwards along the constant 20 mSie conductance curve (along the red arrow) to the center of the diagram. The impedance curves are also “gliding” when the L_{par} is decreasing, as indicated by the green arrow. Significant change starts only below 9 nH and accelerates below 6 nH . The proper L_{par} value is $\sim 2 \text{ nH}$, with which the impedance at resonance is $\sim 50 \Omega$ at $\sim 811 \text{ MHz}$. So, the frequency of the capacitive 20 mSie conductance point with $L_{par} >= 60 \text{ nH}$ and the frequency of the 50Ω resonant point with $L_{par} = 2 \text{ nH}$ is practically identical, as expected.

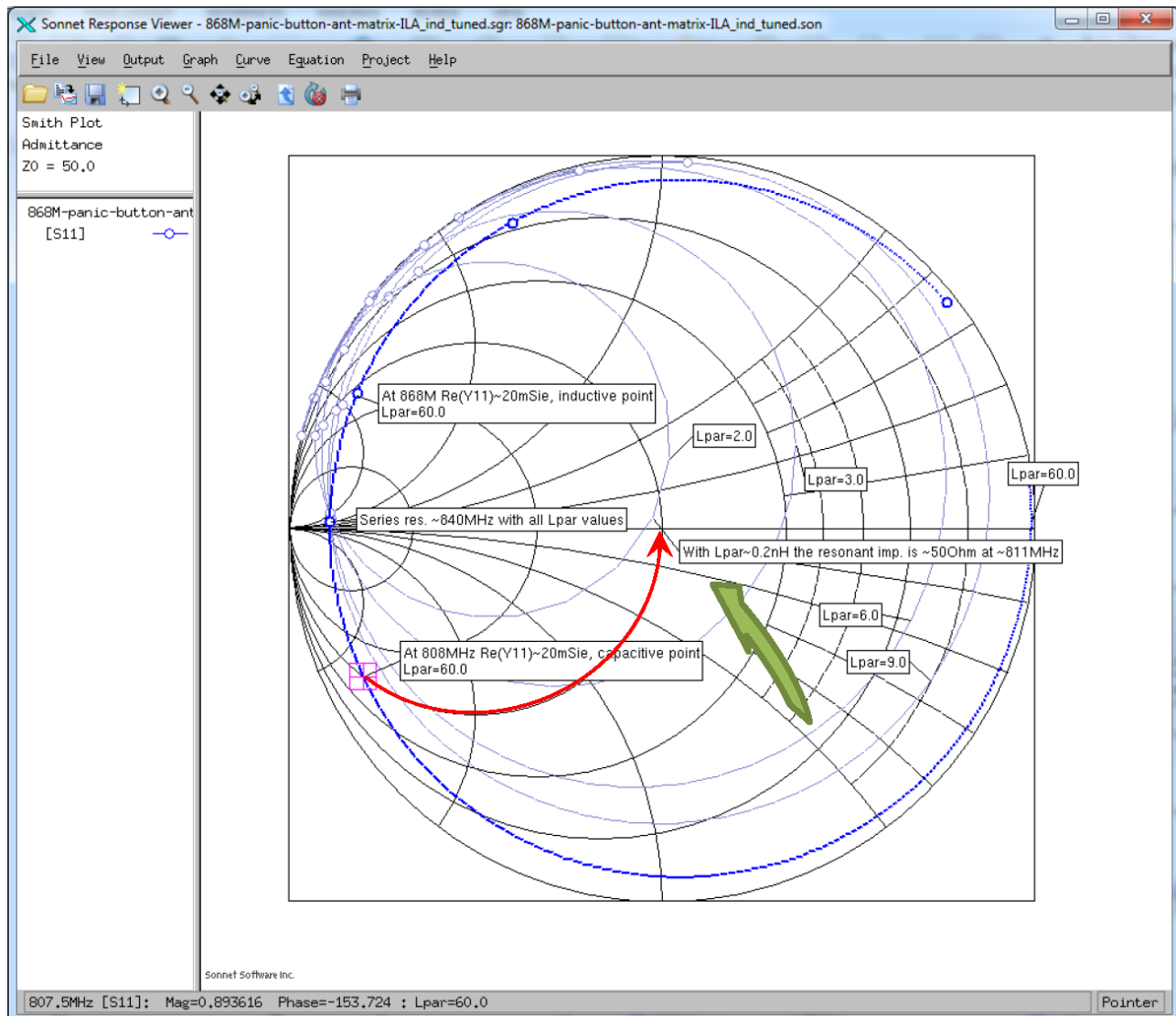


Figure 48. Impedance Gliding of the Starting ILA + Parallel Inductor Combo if the Parallel Tuning Inductor Value at the Input is Varied

Based on these observations, the design steps of the IFA antenna can be determined:

1. The antenna length needs to be adjusted to have a capacitive antenna admittance with $1/50 = 0.02$ Siemens real part at the operating frequency.
2. Proper parallel inductor value has to be determined for parallel resonance at the operating frequency with 50Ω residual impedance (i.e., at the center of the Smith chart).
3. Design of a loop that realizes the calculated parallel inductor value.

For the first step, the effective epsilon has to be calculated as was done for the 915 MHz ILA in Section “5.1. Design of Printed ILA Antennas”. Knowing the series resonant frequency (~838 MHz), the physical length of the antenna trace (~63.5 mm), and assuming again [1] that the electrical length at resonance is 0.29 lambda due to the small ground size, the effective epsilon can be calculated:

$$\lambda_{\text{eff_838MHz}} = \frac{63.5[\text{mm}]}{0.29} = 219[\text{mm}]$$

$$\epsilon_{\text{eff}} = \frac{c^2}{\lambda_{\text{eff}}^2 f^2} = \frac{(3 \times 10^8)^2}{(219 \times 10^{-3})^2 (838 \times 10^6)^2} \approx 2.67$$

The effective epsilon calculated here is much higher than what was derived for the 915 MHz ILA structure in Section 5.1, despite the same FR4 thickness (1.5 mm). This is because in the 868 MHz panic button structure, the gap size between the antenna trace and the ground is only 2.5 mm. The much smaller gap size results in higher parallel trace distributed capacitance per unit length, and thus, higher phase shift per unit length. So a typical rule for the effective epsilon with 2 to 3 mm gap and 1.5 mm FR4 thickness is 2.5 to 2.7.

The antenna trace electrical length at the capacitive 20 mSie conductance frequency point (808 MHz) can be calculated from the series resonant frequency (838 MHz), and from the fact that at series resonance, the electrical length is ~ 0.29 lambda for monopoles with small ground plane:

$$l_{\text{elect_808MHz}} = l_{\text{elect_838MHz}} \frac{808\text{MHz}}{838\text{MHz}} = 0.29 \frac{808}{838} \approx 0.28 \lambda_{\text{eff_838MHz}}$$

So a rule is that the trace electrical length should be ~ 0.28 lambda at the targeted operating frequency (868 MHz). The lambda at 868 MHz can be calculated with the aid of the effective epsilon:

$$\lambda_{\text{eff_868MHz}} = \frac{c}{f \sqrt{\epsilon_{\text{eff}}}} = \frac{3 \times 10^8}{868 \times 10^6 \sqrt{2.67}} \approx 211.5[\text{mm}]$$

By knowing the lambda at 868 MHz, the required physical trace length for 868 MHz operation can be calculated:

$$l_{\text{phy_868MHz}} \approx 0.28 \lambda_{\text{eff_868MHz}} = 0.28 \times 211.5[\text{mm}] = 59.2[\text{mm}]$$

That is, the trace length of the antenna has to be decreased to 59.2 mm to tune up the frequency of the capacitive 20 mSie conductance point to 868 MHz. Figure 49 shows the modified antenna structure (the trace is a 0.5 mm wide donut, with 13.25 mm radius and a 241° angle). Figure 50 shows the simulated impedance curves with various Lpar values. In Figure 50, the admittance values shown are normalized values (to 0.02 Siemens):

$$Y_{\text{NORM}} = \frac{Y}{Y_0} = \frac{Y}{0.02}$$

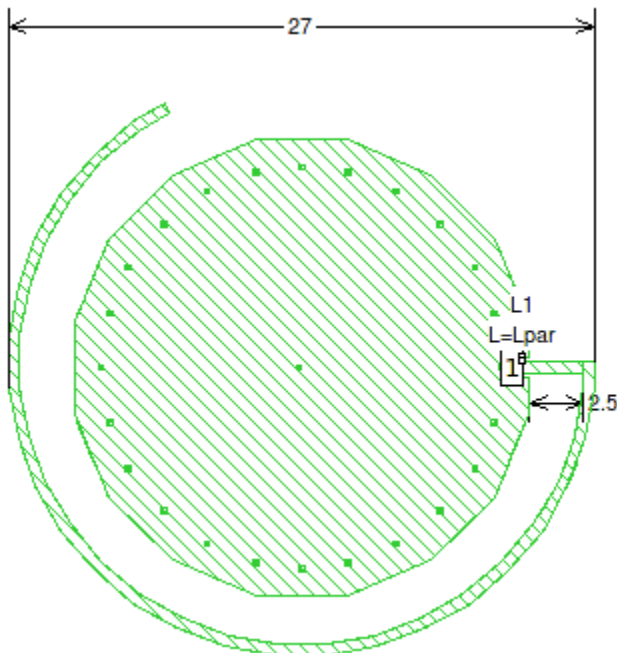


Figure 49. Tuned 868 M ILA Structure with Parallel Tuning Inductor at Input

With the calculated 59.2 mm trace length, the normalized conductance is 0.995 at 868 M (Lpar is high (≥ 60 nH)). This is very close to the target normalized value of one (i.e., close to the real target value of 20 mSie). By decreasing the Lpar value to 2 nH, this point shifts near to the center of the Smith chart as is shown by the dashed red arrow. However, on the Lpar = 2 nH curve, the 868 M point is not exactly at the center of the chart, and the normalized conductance is slightly lower than one. Also, the real resonance is at a slightly higher frequency: 870 MHz.

These facts clearly show that the calculated 59.2 mm total length is slightly shorter than the optimum. However, the calculated value is a good estimation, which can be used as a starting point for further optimization or bench tuning.

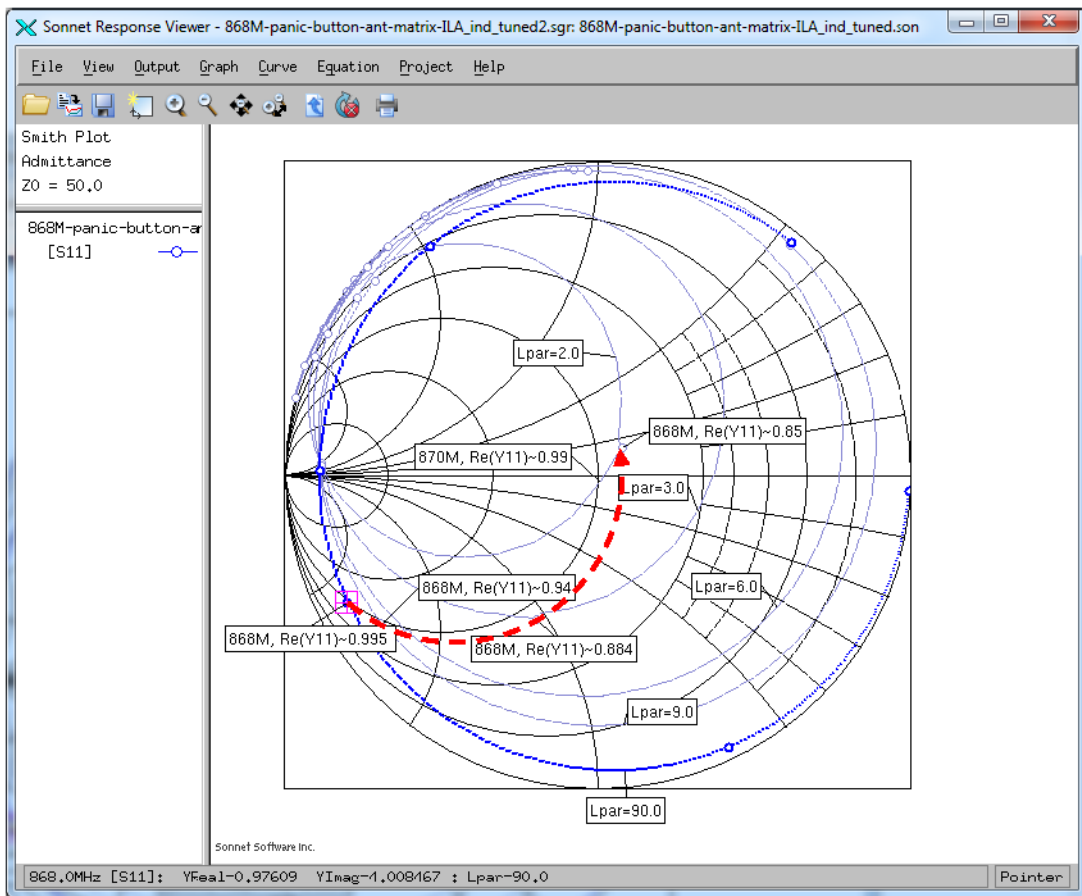


Figure 50. ILA Impedance Curves with Various Parallel L (Lpar) Values

Note: In Figure 50, the red arrow shows the $\text{Re}(Y_{11}) = 20 \text{ mSie}$ point shifting at 868 MHz caused by a 2 nH parallel inductor. *For the second step, the antenna trace susceptance at the capacitive 20 mSie conductance point needs to be determined with a high Lpar value (60 nH or a higher). This is shown in Figure 51.* According to this, the normalized susceptance (denoted by B_{868}) is ~ 4 , which corresponds to a real value of $4 \times 20 \text{ mSie} = 80 \text{ mSie}$.

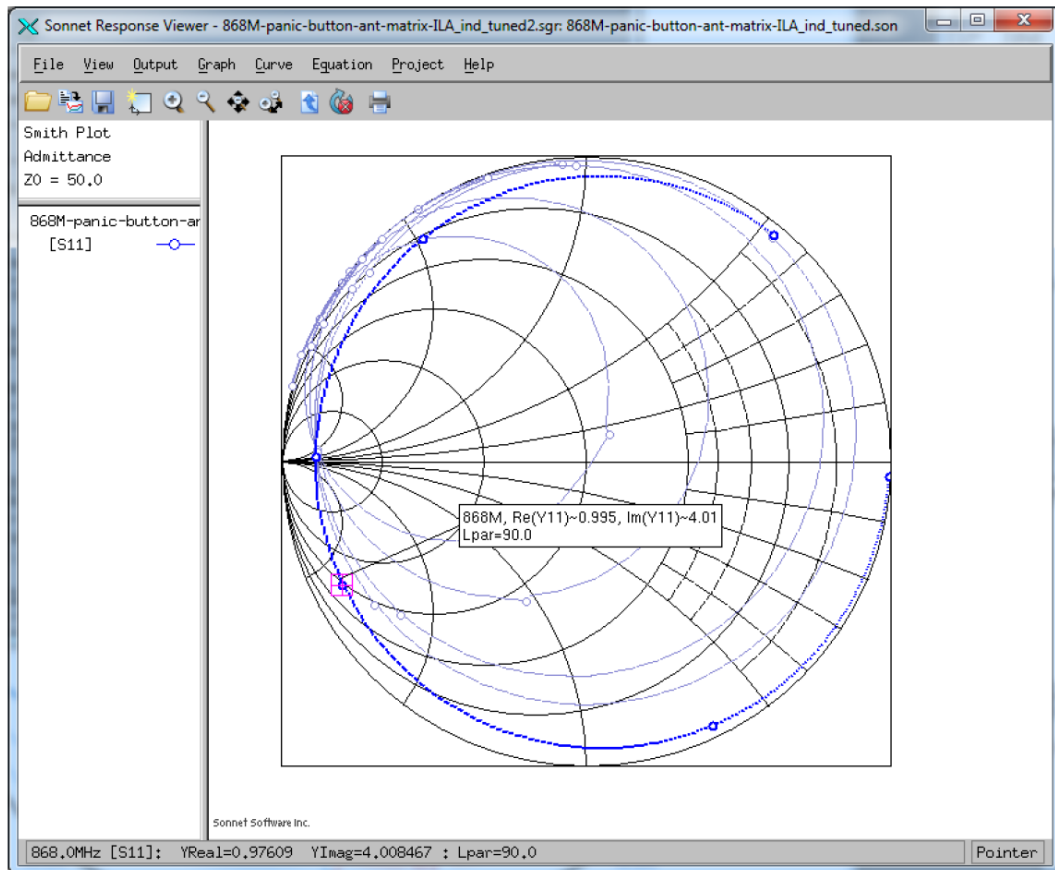


Figure 51. 868 M ILA Admittance After Trace Length Tuning without the Parallel Tuning Inductor

This capacitive 80 mSie susceptance must be compensated by the Lpar:

$$L_{\text{par}} = \frac{1}{2\pi f B_{868}} = \frac{1}{2\pi \times 868 \times 10^6 \times 8 \times 10^{-2}} = 2.29\text{nH}$$

The calculated 2.29 nH value is very close to the 2 nH result from the simulations.

In the third step, the area of the small loop should be estimated. Here, the logical step could be to determine the loop area, which yields nearly the above calculated value of inductance (~2 nH). Unfortunately, the small loop is not connected right at the ILA input (as is the case with the ideal Lpar), but it has a common route with the monopole. Due to this, the optimum loop inductance value may differ slightly from the ideal Lpar at the feeding point.

The loop inductance can be estimated by the formula given in [2]. For that, the dimensions are defined in Figure 52.

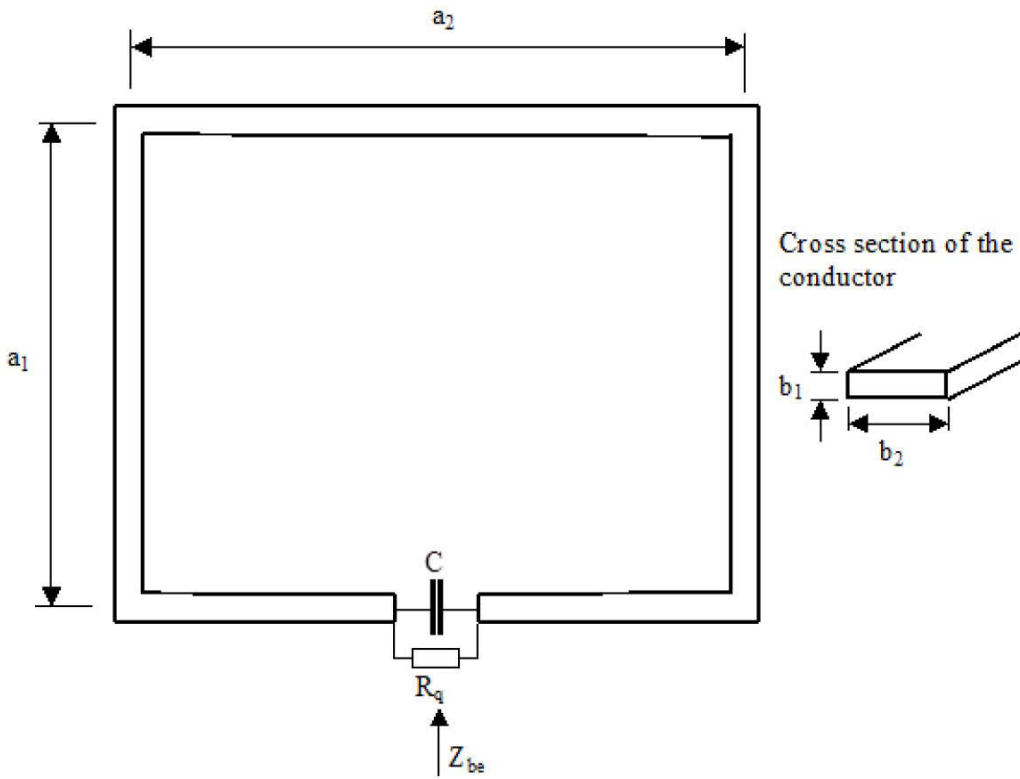


Figure 52. Loop Dimensions for Inductance Calculation

The loop inductance can be calculated:

$$L = \frac{2\mu_0\sqrt{a_1 a_2}}{\pi} \left[\ln \frac{\sqrt{a_1 a_2}}{b} - 0.774 \right]$$

where:

$$b = 0.35b_1 + 0.24b_2$$

According to this equation, a 1.5 mm x 1.5 mm size loop (2.25 mm² area) with 0.5 mm trace width generates approximately 2 nH loop inductance.

In Figure 53, a small loop is connected to the ILA of Figure 49. In the resulting IFA setup, the loop width can be varied. Figure 54 shows the simulated impedance with various loop widths (1, 1.5, and 2 mm). As one can see, the loop with 1 mm width is too small and the impedance is too high. The impedance curve goes close to the center if the width is 1.5 mm. In this case, the inner gap area of the loop is $\sim 1 \times 2.5 \text{ mm} = 2.5 \text{ mm}^2$, which is close to the predicted value (if the area is calculated by using the middle of the traces, then the calculated area is higher). The optimum loop area to hit the center point is slightly smaller, so it is even closer to the calculation.

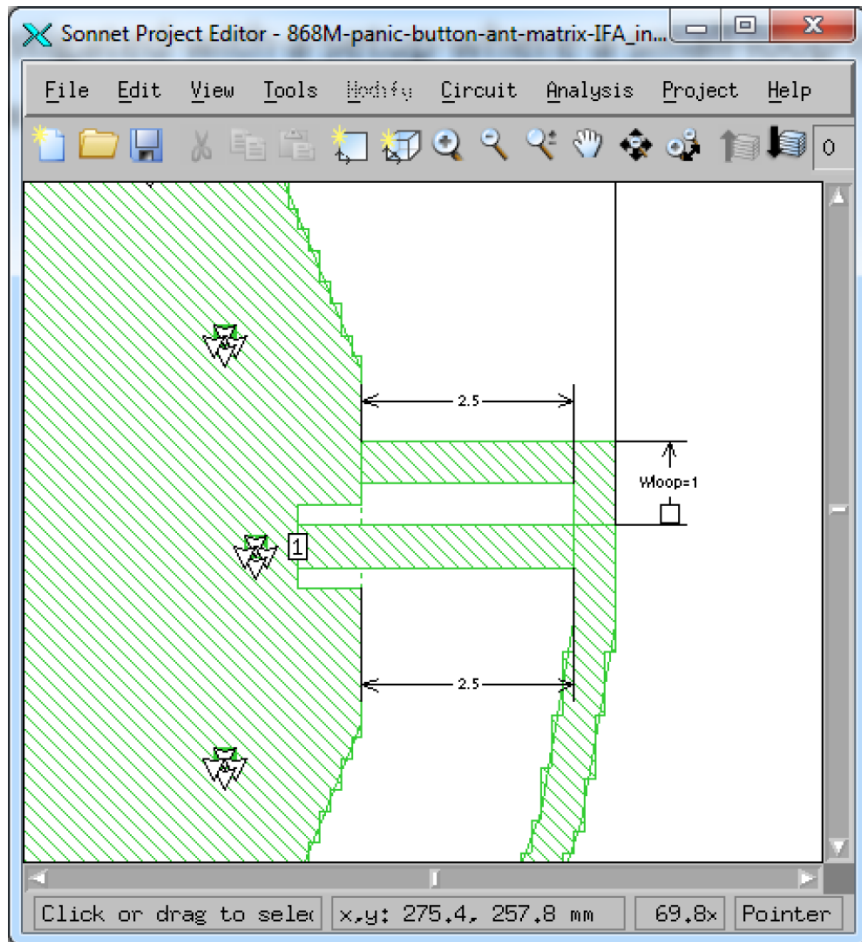


Figure 53. Simulated 868 M IFA Originated from the Tuned ILA + Parallel Inductor Combo by Replacing the Inductor with a Proper Small Loop

However, the introduction of the small loop increased the resonant frequency up to ~888 MHz. A possible explanation for this is that the common route of the ILA and the loop does affect the ILA's electrical length, and thus, a further increase of the ILA length is required. By increasing the ILA trace length by ~1.4 mm (total angle of the donut is 247°, and the total trace length $59.2 + 1.4 = 60.6$ mm) the resonance can be tuned down to 868 M as shown in Figure 55.

This design example shows that using these methods to determine trace length and small loop area yields a good starting point for final tuning. The tuning is also quite logical: the resonant frequency can be tuned by the trace length, while the impedance at resonance can be tuned by the small loop area. This is detailed in the next section.

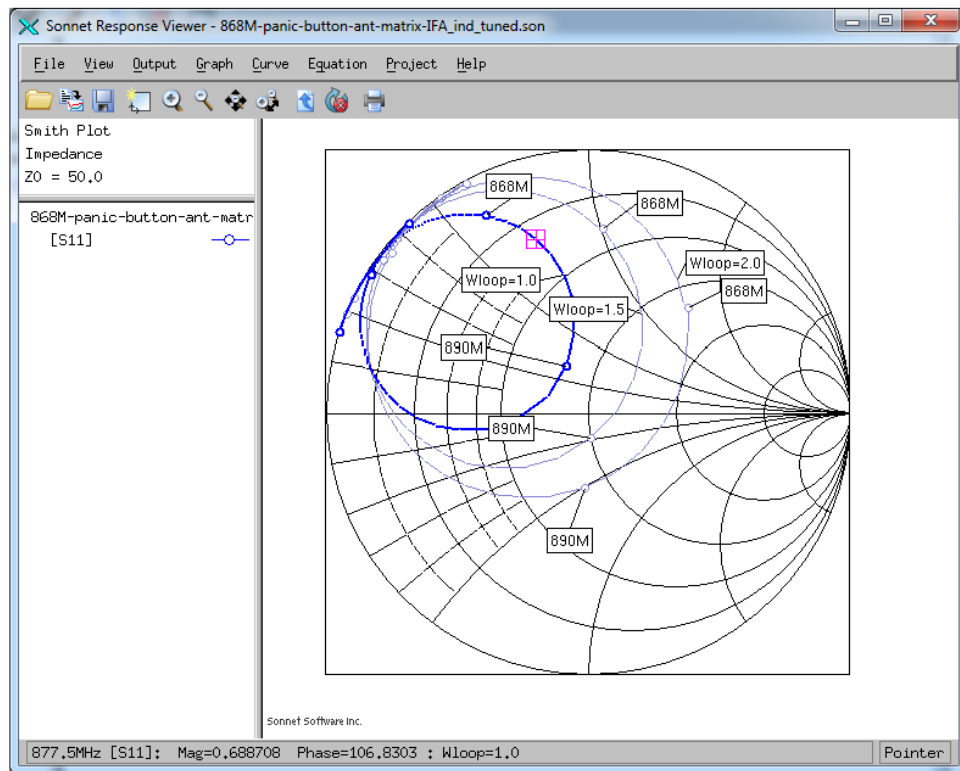


Figure 54. Simulated 868 M IFA Impedance with Various Loop Widths

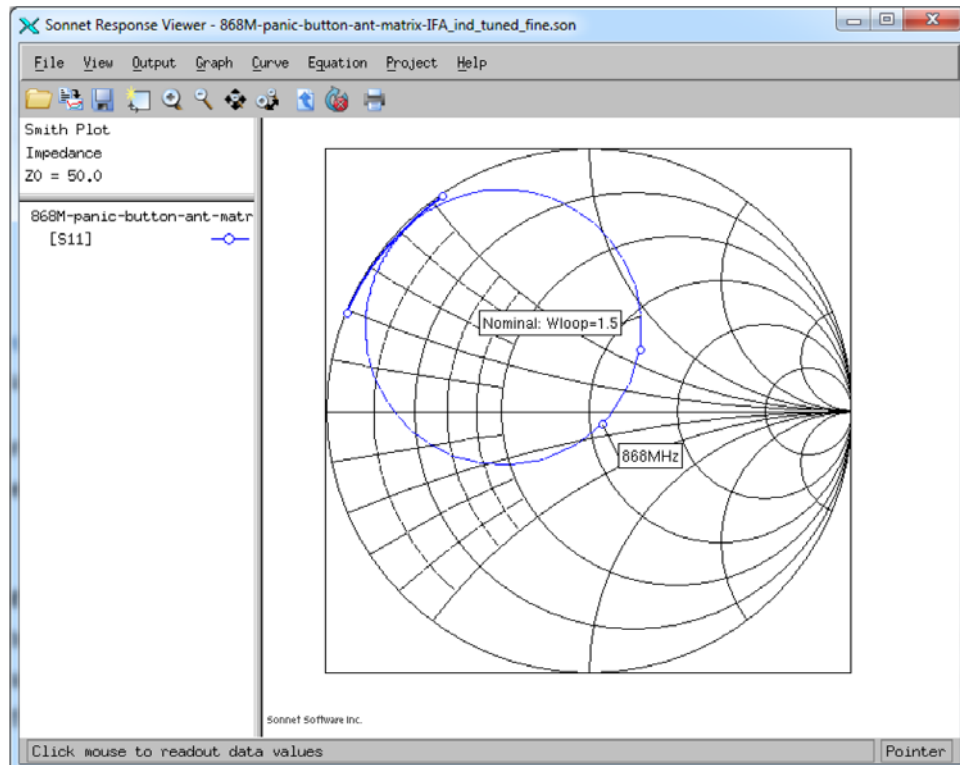


Figure 55. Impedance Curve of the Final Tuned 868 M IFA

5.2.1. Tuning of the IFA Antenna

As mentioned earlier, there are two distinct ways to tune an IFA antenna:

- By varying the antenna trace length to tune the resonant frequency.
- By modifying the small loop area to change the impedance at resonance.

This is demonstrated here in separate simulations.

The effect of varying the antenna trace length is shown in Figure 56 and Figure 57. The length of the antenna trace determines only the resonant frequency and has a negligible effect on the impedance at resonance. So with the trace length variation, the resonant frequency can be tuned independently of the impedance.

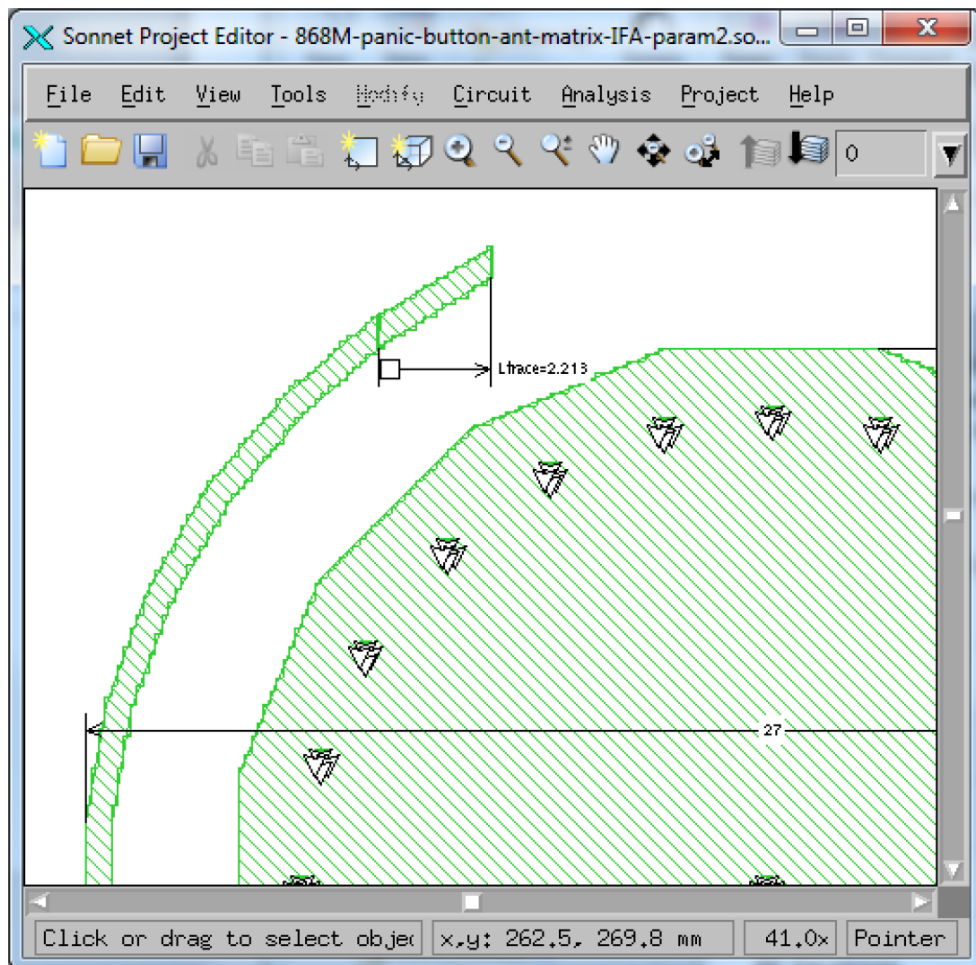


Figure 56. Investigation of the Effect of Antenna Trace Length by Sweeping “Ltrace” (Trace Length) Dimension Parameter

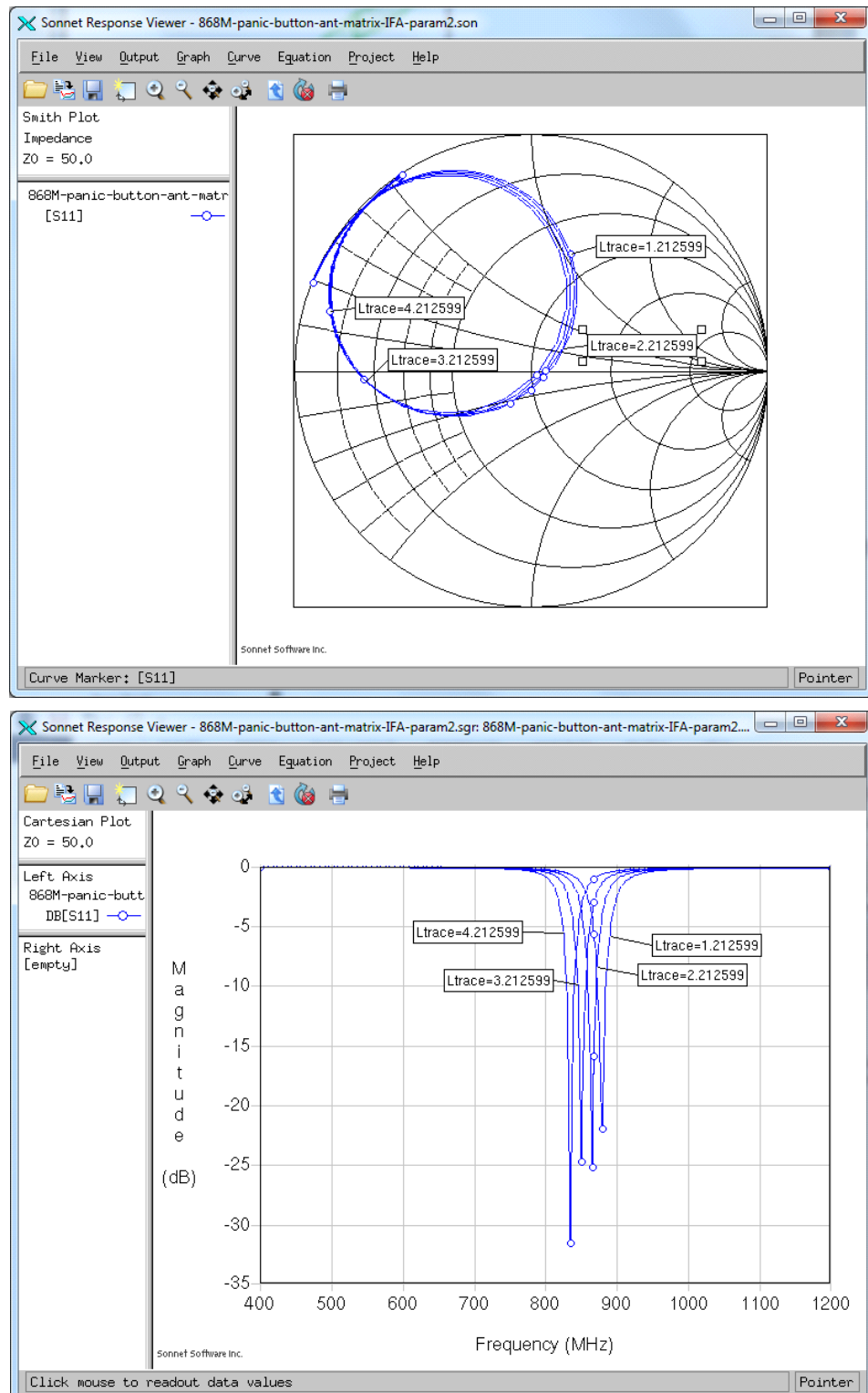


Figure 57. Effect of the Antenna Trace Length by Sweeping “Ltrace” (Trace Length) Dimension Parameter

Note: In Figure 57 above, the variation of the trace length changes only the resonant frequency (the higher the length, the lower the frequency), while the impedance practically does not change.

The effect of the variation of the loop width is shown in Figure 58 and Figure 59. At higher loop areas, the impedance at resonance increases, and the resonant frequency shifts down slightly.

So by varying the loop area, the impedance at resonance can be adjusted with minor changes in the resonant frequency.

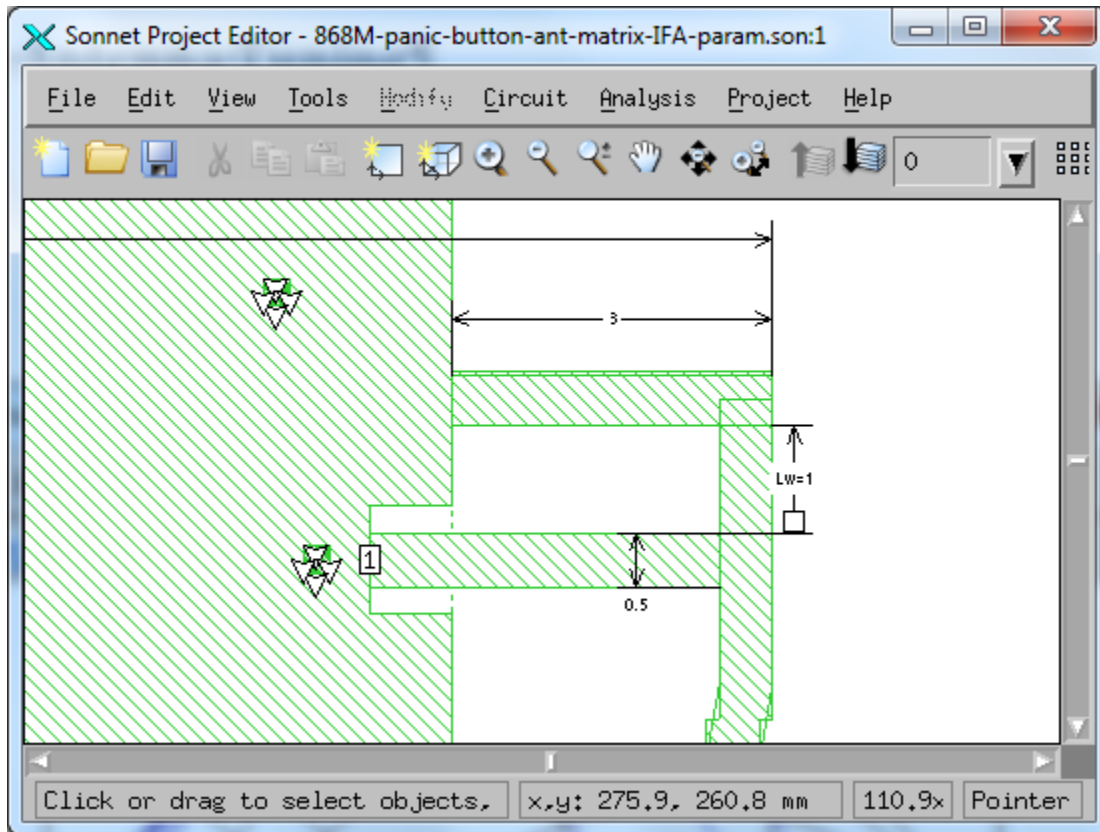


Figure 58. Investigation of the Effect of the Loop Area: by Sweeping “Lw” (Loop Width) Dimension Parameter the Loop Area Changes

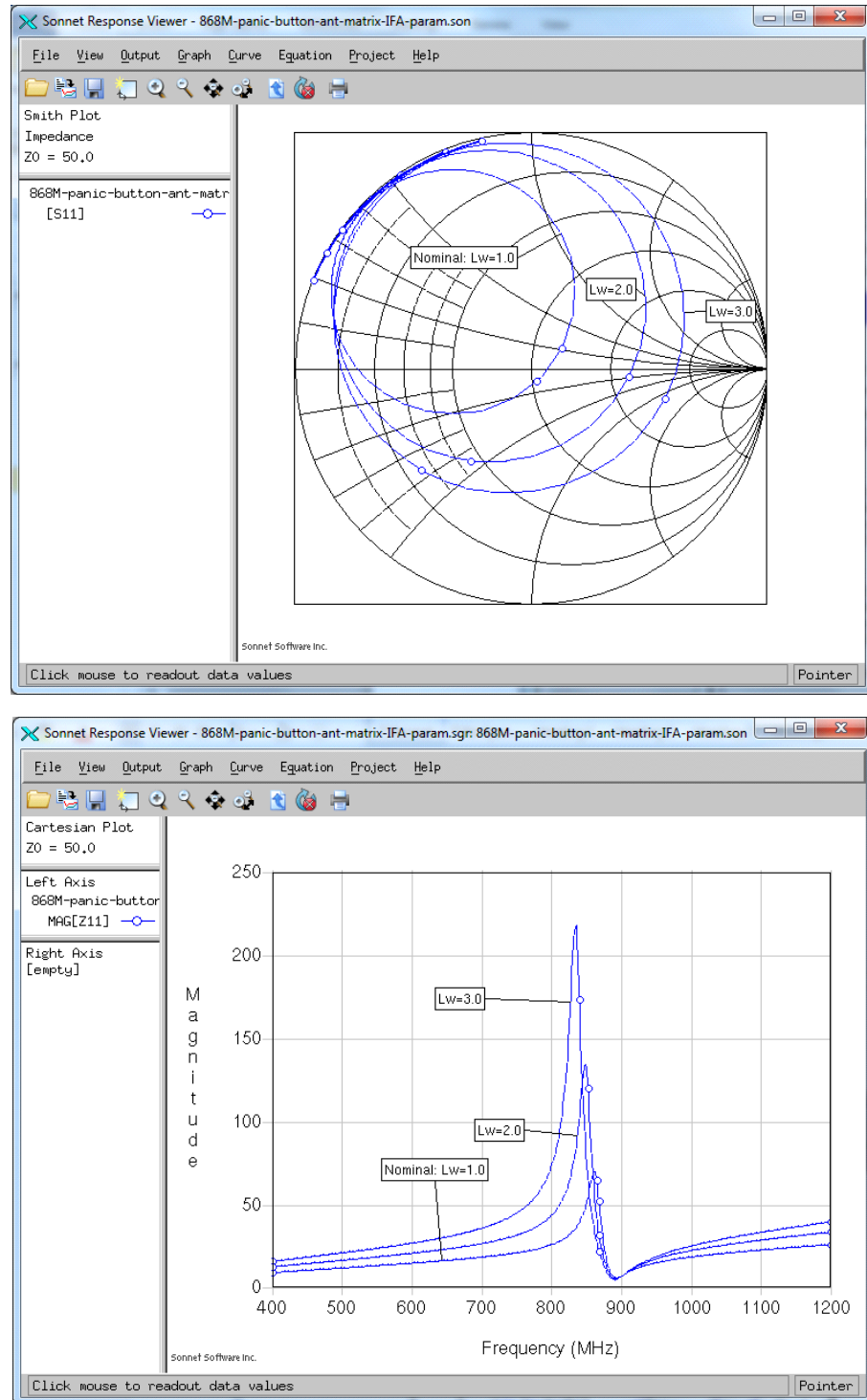


Figure 59. Effect of the Loop Area

Note: In Figure 59 above, at higher loop areas (the “Lw” (loop width) parameter changes between 1 and 3 mm in 1 mm steps) the impedance at resonance is higher. The resonant frequency also shifts down slightly at higher loop areas.

Based on the above investigations, the IFA antenna design steps are the following:

1. Set the antenna trace to have resonance at the desired frequency.
2. Tune the small loop area to have the targeted impedance at resonance.
3. Fine-tune the antenna trace to set the resonant frequency again.
4. Repeat the above three steps in case of nearby human body, plastic, or metal effect.

Unfortunately, the IFA antenna design cannot be fully finished with purely analytical methods. Final optimization with EM software and/or bench tuning is required.

6. Secondary Effects of Impedance Measurement and Tuning

The impedance of a printed monopole antenna usually requires bench tuning since some secondary effects are not taken into account during simulations:

- Effect of PCB cutting edge at ~2 mm distance from the antenna trace cannot be simulated in Sonnet
- Spreading of the epsilon in real substrates
- Spreading of PCB thickness
- Effect of connecting SMA (behaves as a perpendicular ground), PicoBoard, and LCD (or MCU) baseboard
- Hand effect

The following are required modifications during bench tuning of ILA or IFA antennas:

1. Varying of the antenna trace.
2. Modifying (increasing) small loop area.
3. Input matching network (usually a parallel cap) tuning, if required.

Next, the bench tuning process is demonstrated on the 868 M Panic Button IFA (WES0035) antenna.

This antenna is first tuned with the SMA and with the PicoBoard and Motherboard, but without battery, plastic, and strong hand effect. The setup is shown in Figure 60. With this setup, the antenna trace has to be shortened by 5 mm compared to the simulated case, and the small loop area is increased slightly. Parallel cap still not required at the antenna input after the modifications. Figure 61 shows the modified structure.

The impedance is measured at the modified/tuned antenna structure input (with reference plane shift) with the final picoboard configuration and with a hand holding the main board (i.e., with weak hand effect far from the antenna board) as shown in Figure 60. The measured impedance and S11 is given in Figures 62 and 63. Without the weak hand effect on the mainboard, the impedance is only slightly mistuned: the resonant frequency shifts down by ~5 MHz, but the S11 is still much better than -10 dB.

It should be emphasized that in typical panic button applications, the grounding environment and the strength of the hand effect is different. In real panic button applications, instead of the SMA connector, SMA male-male transition, picoboard, and baseboard, only a lithium coin battery can increases the ground size. So further impedance tuning is required, and the radiation is usually weaker. This situation is discussed in detail in Section 7.

Also, in wrist applications the very close parallel hand has a strong detuning effect. In these applications, further impedance tuning is required, and the radiation efficiency degrades strongly (see Section "7.5. Hand Effect" on page 79 for more information).



Figure 60. DUT in the Final Measurement Setup with Weak Hand Effect (Holding the Base Board)

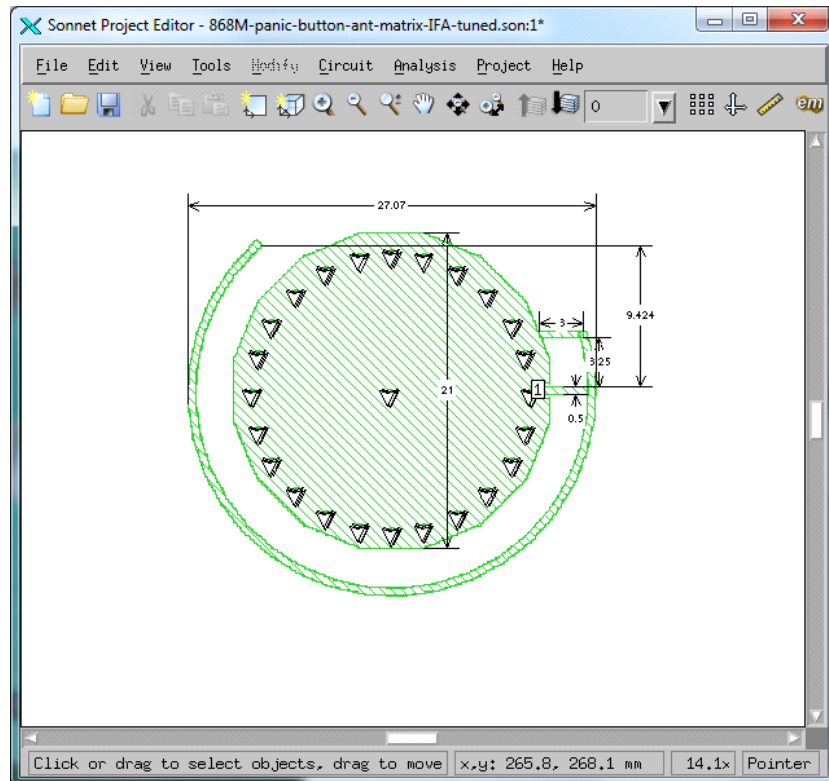
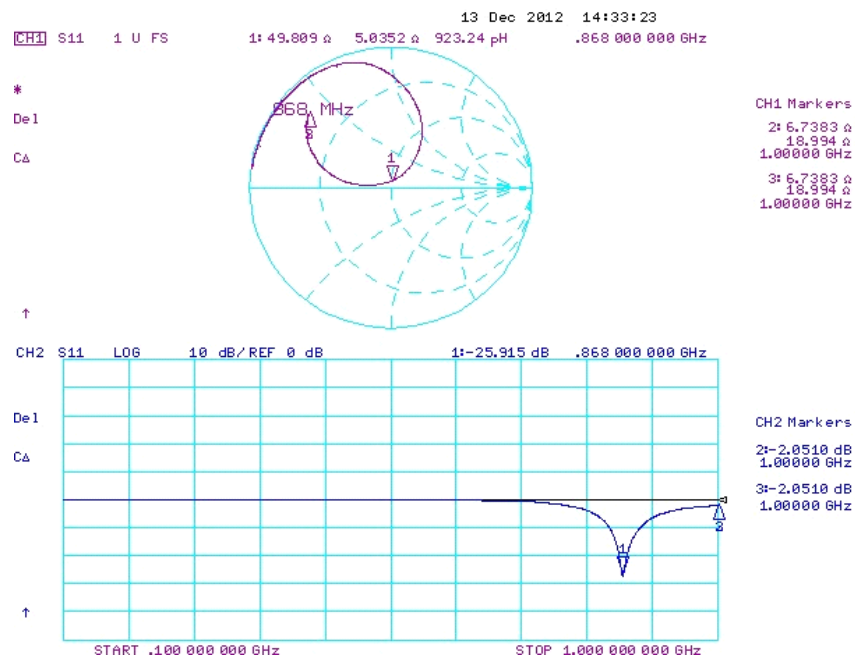
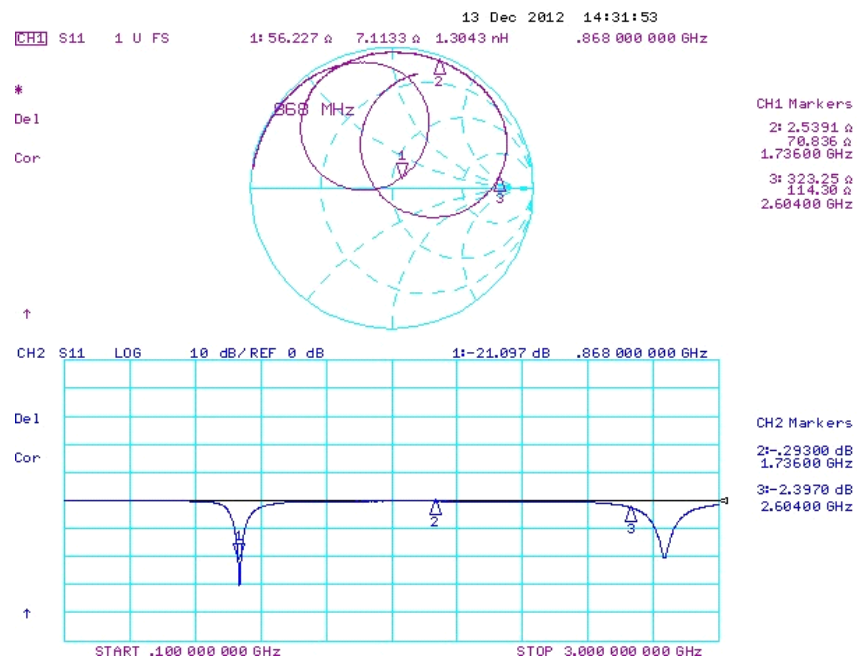


Figure 61. Fine-tuned Layout with New Parameters (5 mm Shorter Arm, Bigger Area Small Loop)



**Figure 62. Measured Impedance up to 1 GHz.
Tuned 868 M Panic IFA with Weak Hand Effect on the Main Board**



**Figure 63. Measured Impedance up to 3 GHz.
Tuned 868 M Panic IFA with Weak Hand Effect on the Main Board**

7. Radiation Measurement and Range Estimations of Pure Matrix Antenna Boards without External PicoBoard and WMB-930 Motherboard

7.1. Introduction

In the Single-ended Antenna Matrix application notes (AN782: “868 MHz Antenna Matrix (WES0030-01-AMS868-01) Measurement Reports”; AN848: “915 MHz Single-ended Antenna Matrix Measurement Reports”; and AN850: “434 MHz Single-ended Antenna Matrix Measurement Reports”) the small antenna boards are measured with a radio PicoBoard connected through a male-to-male SMA transition and with the large MWB-930 wireless Motherboard as shown in Figure 64. Due to the connected large additional boards, the measured antenna gains and range test results are much better than the typical application applying the antenna boards alone.

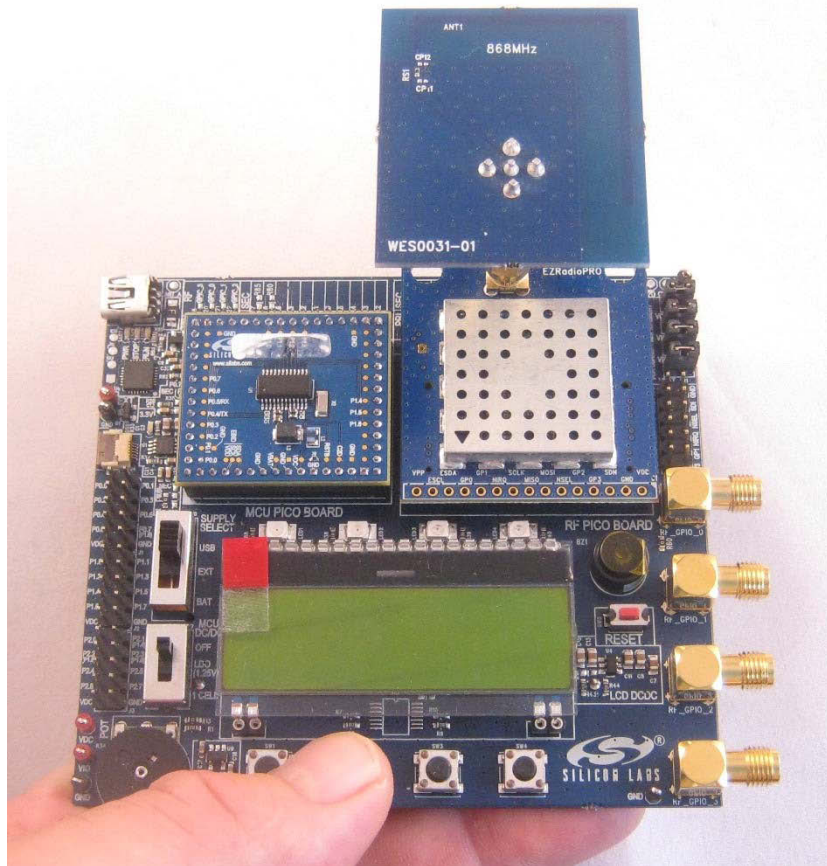


Figure 64. Antenna Boards Connected to the PicoBoard and the Motherboard

Note: In Figure 64, the antenna boards connected to the PicoBoard and the Motherboard are as measured in application notes: AN782, AN848, and AN850.

Radiation measurements of single-ended small antenna boards alone are challenging in the UHF frequency range. The main reason is that in the case of typical (practically small) application boards (like the matrix antenna boards), there is not enough large ground metal in the vicinity of the antenna to supply the good electrical mirror necessary for efficient operation of single-ended antennas. Because of this, the RF signal leaks from the antenna board ground to the connected large Motherboard or PicoBoard ground. These large metals may radiate much more strongly than the antenna board itself, hiding the antenna radiation and making the actual antenna measurements impossible.

The situation does not improve if only the pure small antenna boards are tested through a coax feed line. Here, the RF signal leaks to the outer surface of the feeding coax, which again radiates very well and usually exceeds the original antenna board radiation. So the radiation gain of the pure antenna board also cannot be measured in these configurations.

To determine the pure antenna board gains and estimate the ranges in a typical real application, a new gain test method is applied in which the leaking surface RF currents on the coax feed line are blocked by a properly-tuned 'bazooka' (sometimes called a 'sleeve') balun, as shown in Figure 65 (with the 434 M panic button antenna).

In theory, ferrites can also be used to block radiation from the coax feed line. However, the losses introduced by the ferrites also reduce the ground currents on the original antenna board and thus, reduce its radiation. The advantage of a properly-tuned bazooka balun is that it shows high impedance at the board ground connection point, thereby blocking the leakage without disturbing the antenna board ground RF currents, and thus, not excessively reducing the gain.

However, during the tests of very small, weakly-radiating antennas, even the blocking of the balun may not be enough to fully eliminate the coax feed line radiation. In these cases, the best results can be achieved if ferrites are used after the balun to kill all residual leakage RF currents on the coax [7]. With this configuration, the ferrites are isolated from the antenna board by the balun and, thus, the antenna radiation is not significantly disturbed. This test structure (called C&B&F) is used later to estimate the pure antenna board gain (see Figure 66). The antenna is separated from the coax feed line by the balun and the ferrites are periodically located along the coax. The distance between them is approximately 15 cm, less than half lambda at all measured frequencies.

The built 'bazooka' balun structures and their tuning is detailed in "Appendix B—Bazooka Balun Design and Tuning" on page 93.



Figure 65. Antenna Measurement with “Bazooka” Balun

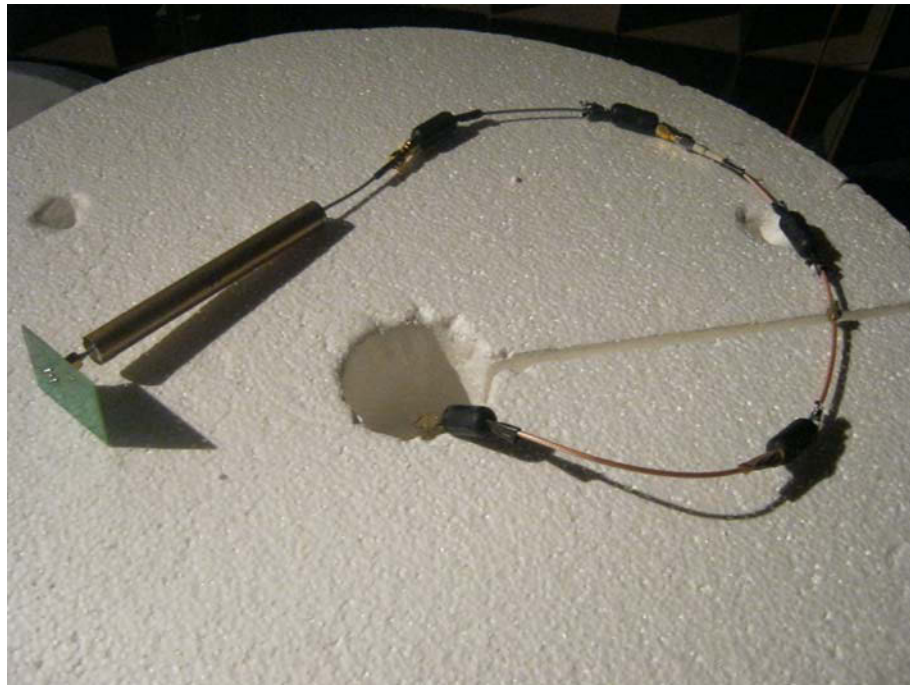


Figure 66. Antenna Feeding Coax with Ferrites and Bazooka Balun

7.2. Gain Measurements on Pure Antenna Matrix Boards and Comparison of Test Methods

When testing for gain, the antenna matrix boards are fed from a generator through a coax cable. Since the goal is to measure the pure antenna gain, the effect of the coax feed line needs to be eliminated. Here, the radiation patterns of different measurement configurations are compared with: a sleeve balun, balun and ferrites, or ferrites only. The maximum radiation in the XY plane is compared to the naked coax case in Table 2 for vertical polarization and in Table 3 for horizontal polarization.

In the tables, the maximum XY cut gain measurement results of the "Antenna Board + PicoBoard + Motherboard" configuration (denoted as P&M) are also given as published in AN782, AN848, and AN850.

It has to be noted that all matrix antennas are tuned and matched (S_{11} is better than ~ -10 dB) in the applied measurement configuration by using the classical lumped element matching methods [8]. The matching networks for the naked coax, for the coax and balun, and for coax, balun, and ferrite configurations are given in "Appendix C—Matching Circuits and Measured S_{11} of the Antenna Boards with Naked Coax, with Coax and Balun (C&B), and with Coax, Balun, and Ferrite (C&B&F) Configurations" on page 98. As was described earlier, the C&B&F configuration measures the pure antenna board properties with the best accuracy (the balun isolates the board from the coax quite well, and the residual RF leakage is neutralized by the ferrites). Due to this, the matching network of the C&B&F can be used as a tuning starting point in real application developments where the pure antenna board is usually applied without any large extra boards (e.g., PicoBoard and MotherBoard). Unfortunately, some bench tuning is usually required in real units in the presence of typical secondary effects of the battery, plastic, or hand.

According to Table 2, with vertical polarization the insertion of the balun (C&B configuration) reduces the radiation significantly for most of the antennas (the 7th column shows the gain change compared to the naked coax case). This is expected since the vertical polarized radiation in the XY cut is mainly coming from the fed coax and not from the antenna boards (except for the meander monopoles where the main polarization of antenna board radiation is the vertical one). The planar antennas dominant radiation polarization coincides with the PCB plane, so in the XY cut, it is the horizontal one (except the meander monopole).

By introducing the ferrites after the balun (C&B&F configuration), the radiation decreases even more since the ferrites suppress the residual coax radiation generated by the RF leakage through the balun. This experience proves that the radiation of the pure antenna boards with vertical polarization is so weak that coax radiation even after the balun is still higher. Adding the ferrites, the antenna board radiation measurement becomes more accurate with vertical polarization.

The 5th column shows the radiation change if only the ferrites are used on the coax (called C&F) without the balun. The boards, which radiate very weakly in the C&B&F configuration (WES0031), do not suffer as great a radiation drop with ferrite only. So the ferrite alone cannot suppress the coax radiation as efficiently and yields less accurate results. Based on this conclusion, the gain results of the C&B&F configuration are used for any further process.

It is also in agreement with the expectations that the antenna boards alone (~in C&B&F configuration) radiate much less than with the large PicoBoard and Motherboard (P&M configuration). The last column shows the difference. The weaker radiation of the pure antenna boards results in significantly smaller ranges in real applications compared to the range test results published in AN782, AN848, and AN850.

However, there are some exceptions such as the 868/915 MHz meander monopoles (WES0037 and WES0117 in the C&B&F configuration). These meander monopoles radiate with nearly the same efficiency as they did with the additional large boards (as in P&M configuration). It seems that the SMA and the small ground metal on the meander board is enough for efficient meander antenna operation. Unfortunately, this is not the case with the 434 M meander, where the large boards are required for good efficiency.

The horizontally polarized results (see Table 4) have the highest importance since theoretically, this is the main radiation polarization of the pure planar matrix antenna boards (the exception again being the meander monopoles). The first observation is that the horizontally polarized radiation also decreases strongly with the C&B&F configuration (8th column) compared to the naked coax case. The reason is that the coax feed makes curls around the turntable during rotation and in the case of high leakage RF currents (i.e. without the balun and ferrites), the coax radiation in the horizontal polarization can be significantly stronger than the original small antenna board radiation. With the balun and ferrite (C&B&F), the coax radiation is reduced, and the residual antenna board radiation can be acquired. These horizontally polarized gain results are the closest to real pure antenna board radiation values. Thus, they are used to predict the achievable range (except again the meander monopoles where the vertical polarized gain results are used).

The horizontal radiation degradation is also significant if one compares the C&B&F horizontal gain results with those of the PicoBoard and Motherboard (P&M) configuration (as in AN782, AN848, and AN850). The delta is shown in the last column of Table 3. The highest radiation degradation mostly occurs with the small antennas (WES0033/35/36/38, WES0113/115/116/118, WES0075/76/78), with the meander monopoles (WES0037, WES0117, WES0078) and with the 434 M helical (WES0074). Degradation with the small antennas is expected since they cannot radiate efficiently without an extra ground. The degradation with pure meander monopoles is also expected since these types of antennas radiate mainly with vertical polarization, and any significant horizontal radiation in the P&M configuration is mainly generated by the additional boards only. However, the radiation degradation of the 434 M helical board is surprising. It shows that the applied ground metal size on the antenna board is not large enough for the helical antenna at 434 M.

Table 2. Maximum Vertical XY Gain [dBi] of Different Radiation Measurement Configurations

	Antenna Board Only				Fed by PicoBoard and Motherboard* (P&M)	Delta Gain (C&B)-(C)	Delta Gain (C&B&F)-(C)	Delta Gain C&F)-(C)	Delta Gain (C&B&F) - (P&M)
	Coax (C)	Coax + Balun (C&B)	Coax + Balun + Ferrite (C&B&F)	Coax + Ferrite (C&F)					
868 MHz									
WES0031_01	-1.9	-10.4	-24.7	-11.2	-1.9	-8.5	-22.8	-9.3	-22.8
WES0032_01	-5.6	-26.9	-23.7	-14.5	-4.9	-21.3	-18.1	-8.9	-18.8
WES0033_01	-6.8	-19.9	-22.0	-15.2	-4.2	-13.1	-15.2	-8.4	-17.8
WES0034_01	-2.8	-13.9	-17.2	-11.7	-3.8	-11.1	-14.4	-8.9	-13.4
WES0035_01	-4.6	-8.4	-12.4	-11.8	-3.3	-3.8	-7.8	-7.2	-9.1
WES0036_01	-4.6	-9.3	-14.8	-11.8	-3.2	-4.7	-10.2	-7.2	-11.6
WES0037_01	-2.1	-3.0	-1.3	-4.8	-0.5	-0.9	0.8	-2.7	-0.8
WES0038_01	-5.7	-9.8	-15.0	-13.6	-8.1	-4.1	-9.3	-7.9	-6.9
WES0039_01	-17.4	-17.6	-22.5	-25.3	-7.3	-0.2	-5.1	-7.9	-15.2
Ref monopl					-2.5				
915 MHz									
WES0111_01	-4.2	-8.9	-13.6	-12.6	-5.3	-4.7	-9.4	-8.4	-8.3
WES0112_01	-9.4	-19.7	-23.0	-16.3	-7.7	-10.3	-13.6	-6.9	-15.3
WES0113_01	-14.6	-21.4	-22.8	-18.1	-8.1	-6.8	-8.2	-3.5	-14.7
WES0114_01	-5.7	-11.5	-15.0	-11.1	-2.8	-5.8	-9.3	-5.4	-12.2
WES0115_01	-6.9	-9.5	-12.1	-14.1	-5.2	-2.6	-5.2	-7.2	-6.9
WES0116_01	-5.7	-10.2	-12.6	-14.3	-4.2	-4.5	-6.9	-8.6	-8.4
WES0117_01	-3.2	-0.3	-2.2	-5.4	-2.1	2.9	1.0	-2.2	-0.1
WES0118_01	-7.4	-10.2	-11.7	-15.9	-6.6	-2.8	-4.3	-8.5	-5.1
WES0119_01	-19.5	-18.4	-29.1	-24.2	-12.5	1.1	-9.6	-4.7	-16.6
Ref monopl					-1.9				
Note: As in application notes AN848, AN850, and AN782.									

Table 2. Maximum Vertical XY Gain [dBi] of Different Radiation Measurement Configurations (Continued)

	Antenna Board Only				Fed by PicoBoard and Motherboard* (P&M)	Delta Gain (C&B)-(C)	Delta Gain (C&B&F)-(C)	Delta Gain C&F)-(C)	Delta Gain (C&B&F) - (P&M)
	Coax (C)	Coax + Balun (C&B)	Coax + Balun + Ferrite (C&B&F)	Coax + Ferrite (C&F)					
434 MHz									
WES0071_01	-7.7	-11.0	-16.4	-11.6	-5.3	-3.3	-8.7	-3.9	-11.1
WES0072_01	-5.9	-13.8	-18.3	-12.0	-7.7	-7.9	-12.4	-6.1	-10.6
WES0073_01	-9.3	-16.7	-20.6	-13.6	-12.5	-7.4	-11.3	-4.3	-8.1
WES0074_01	-5.5	-13.0	-15.9	-10.3	-2.2	-7.5	-10.4	-4.8	-13.7
WES0075_01	-6.1	-10.3	-13.5	-11.5	-5.2	-4.2	-7.4	-5.4	-8.3
WES0076_01	-7.1	-10.7	-12.8	-11.6	-4.2	-3.6	-5.7	-4.5	-8.6
WES0077_01	-8.0	-13.9	-15.2	-10.9	0	-5.9	-7.2	-2.9	-15.2
WES0078_01	-11.3	-11.5	-15.3	-13.7	-14.8	-0.2	-4.0	-2.4	-0.5
Ref monopl					0.3				

Note: As in application notes AN848, AN850, and AN782.

Table 3. Maximum Horizontal XY Gain [dBi] of Different Radiation Measurement Configurations

	Antenna Board Only				Fed by PicoBoard and Motherboard* (P&M)	Delta Gain of (C&B)-(C)	Delta Gain of (C&B&F)-(C)	Delta Gain of (C&F)-(C)	Delta Gain of (C&B&F)-(P&M)
	Coax (C)	Coax & Balun (C&B)	Coax + Balun + Ferrite (C&B&F)	Coax + Ferrite (C&F)					
868 MHz									
WES0031_01	-5.5	-5.9	-8.9	-9.7	-4	-0.4	-3.4	-4.2	-4.9
WES0032_01	-10.6	-16.7	-15.7	-11.0	-5.7	-6.1	-5.1	-0.4	-10.0
WES0033_01	-12.0	-11.9	-13.7	-13.2	-3.6	0.1	-1.7	-1.2	-10.1
WES0034_01	-8.8	-5.4	-8.6	-9.3	-3.9	3.4	0.2	-0.5	-4.7
WES0035_01	-8.3	-11.6	-17.9	-16.7	-2.6	-3.3	-9.6	-8.4	-15.3
WES0036_01	-7.4	-11.0	-18.4	-16.6	-3.9	-3.6	-11.0	-9.2	-14.5
WES0037_01	-6.2	-11.3	-23.2	-19.3	-4.4	-5.1	-17.0	-13.1	-18.8
WES0038_01	-9.3	-13.0	-18.3	-17.7	-6.7	-3.7	-9.0	-8.4	-11.6
WES0039_01	-6.5	-6.9	-6.0	-7.5	-5.8	-0.4	0.5	-1.0	-0.2
Ref monopl					-22.0				
915 MHz									
WES0111_01	-7.6	-5.3	-7.2	-10.2	-5.2	2.3	0.4	-2.6	-2.0
WES0112_01	-13.8	-13.1	-17.6	-15.2	-12.2	0.7	-3.8	-1.4	-5.4
WES0113_01	-14.6	-16.1	-16.0	-20.4	-10.6	-1.5	-1.4	-5.8	-5.4
WES0114_01	-5.5	-5.6	-8.8	-11.7	-6.1	-0.1	-3.3	-6.2	-2.7
WES0115_01	-10.2	-11.4	-18.1	-19.1	-9.1	-1.2	-7.9	-8.9	-9.0
WES0116_01	-9.8	-11.4	-17.4	-17.8	-7.4	-1.6	-7.6	-8.0	-10.0
WES0117_01	-9.7	-10.4	-21.7	-21.7	-8.5	-0.7	-12.0	-12.0	-13.2
WES0118_01	-15.0	-13.7	-19.8	-23.5	-10.3	1.3	-4.8	-8.5	-9.5
WES0119_01	-5.9	-6.3	-8.4	-7.1	-5.4	-0.4	-2.5	-1.2	-3.0
Ref monopl					-22.2				
Note: As in application notes AN848, AN850, and AN782.									

Table 3. Maximum Horizontal XY Gain [dBi] of Different Radiation Measurement Configurations (Continued)

	Antenna Board Only				Fed by PicoBoard and Motherboard* (P&M)	Delta Gain of (C&B)-(C)	Delta Gain of (C&B&F)-(C)	Delta Gain of (C&F)-(C)	Delta Gain of (C&B&F)- (P&M)
	Coax (C)	Coax & Balun (C&B)	Coax + Balun + Ferrite (C&B&F)	Coax + Ferrite (C&F)					
434 MHz									
WES0071_01	-6.1	-9.2	-10.3	-13.5	-5.2	-3.1	-4.2	-7.4	-5.1
WES0072_01	-6.7	-7.1	-8.7	-11.4	-12.2	-0.4	-2.0	-4.7	3.5
WES0073_01	-8.2	-11.8	-11.9	-10.8	-5.4	-3.6	-3.7	-2.6	-6.5
WES0074_01	-7.4	-7.5	-11.1	-12.2	2.1	-0.1	-3.7	-4.8	-13.2
WES0075_01	-9.5	-10.6	-16.3	-14.9	-9.1	-1.1	-6.8	-5.4	-7.2
WES0076_01	-9.7	-10.9	-17.0	-16.2	-7.4	-1.2	-7.3	-6.5	-9.6
WES0077_01	-5.4	-10.5	-19.6	-17.4	-1.9	-5.1	-14.2	-12.0	-17.7
WES0078_01	-10.4	-10.7	-19.7	-17.8	-9.6	-0.3	-9.3	-7.4	-10.1
Ref monopl					-10.1				
Note: As in application notes AN848, AN850, and AN782.									

7.3. Range Estimations Based on Pure Antenna Board Gain Measurement Results

In the previous chapter, the variation of the gain was measured if the PicoBoard and the Motherboard were eliminated from the vicinity of the antenna board. Here, the outdoor range is estimated using the new gain data.

The range calculation can be followed in Table 4. The 2nd and 3rd columns summarize the measured maximum gain and range test results of the Antenna Board, PicoBoard, and Motherboard (P&M) configuration in the normal front direction (see Figure 67), as given in the measurement application notes: AN782, AN848, and AN850. This data is also given in the table for the reference monopoles, both vertical and horizontal polarization.

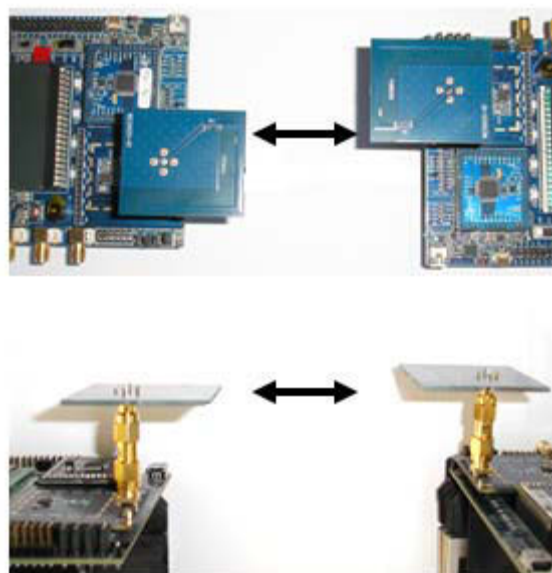


Figure 67. Horizontal and Vertical Polarized Normal Front Direction in Range Measurements

The reason for using the normal front direction (X axes are facing, i.e. XY cut 0° or XZ 270° direction) results is that in this direction, the range test data are available for both vertical and horizontal polarization of the antenna boards (with 50 kbps at 868/915 M and 40 kbps at 434 M). Also, it is important to highlight the open site outdoor propagation is different for the vertical and horizontal polarized waves due to the different magnitude and phase of the ground reflection coefficient. The maximum of the range data reflects a kind of propagation optimum where the stronger radiation polarization of the P&M configuration coincides with the polarization of lower propagation loss. If the measured configuration radiates mostly to one polarization (as is the case with the reference monopoles), then the propagation properties of this dominant polarization have to be taken into account. However, with the P&M configuration, the radiated power (i.e. gain) in the two polarizations are usually close together (the difference is typically 1 to 3 dB, see Tables 2 and 3). Due to this, the propagation properties in both polarizations influences the range. So depending on the radiated energy distribution between the two polarizations, the overall propagation factor is slightly changing with the different antenna types.

So the first step is the calculation of the P&M configuration propagation factors from the measured maximum range data and from the measured maximum gain data (extracted from the pattern measurements in AN782, AN848, and AN850) in the normal, forward direction. These propagation factors are given in the 4th column in Table 4.

As a second step, the range with the P&M configuration is predicted to the direction of maximum radiation in the XY plane using the calculated propagation factor for each antenna board. These maximum XY ranges are presented in the 8th column of Table 4. For the range calculations, the polarization with higher maximum XY gain data is used from Tables 2 and 3. The higher maximum XY gain data can be found in Table 4, 5th column.

In the third step, the available range is predicted with the pure antenna boards to the direction of maximum radiation in the XY plane. For the calculation, the measured gain data with the bazooka balun and ferrites (C&B&F configuration) are used in the theoretical dominant polarization of the antenna boards (the vertical (Table 2) for the meanders and horizontal (Table 3) for all other types). It has to be noted that in the case of some very small antennas (WES0035/0036/0038/0115/0116/0118/0075/0076/0078), the measured XY gain is still higher in the theoretically weaker vertical polarization, even if the balun and the ferrites are applied (C&B&F configuration). The reason is that with these very small and thus poorly radiating antennas, the main horizontally-polarized antenna radiation is still lower than the balun and ferrite suppressed vertically-polarized coax feed line radiation. To predict the range with these pure antenna boards, the vertical coax radiation must be disclosed and the horizontally polarized gains must only be applied according to theory. This is shown in the 6th column of Table 4. The only exceptions are the meander monopoles where the theoretically-dominant, vertically-polarized gain results are used. The polarization applied is also indicated in the 6th column.

Since the pure antenna boards radiate mainly to the theoretically dominant polarizations, the propagation factor of these (vertical for the meander monopoles; horizontal for all other antennas) are used for the range predictions. The propagation factor for the horizontal and vertical polarization is extracted from the reference monopoles' vertically- and horizontally-polarized measured range and gain data ("reference monopole" rows in Table 4) with the P&M configuration. Here, the PicoBoard and Motherboard helps the reference monopoles to be the dominant radiators, and they radiate mostly to the polarization of their axes.

The predicted maximum XY range data for the same pure antenna boards used in both sides of the link are shown in the 9th column of Table 4. As expected, the pure antenna range is very low (on the order of 100 to 150 M) with the very small, very poor gain antennas (like the WES0035/0036/0038/0115/0116/0118/0075/0076/0078).

The last column shows the range reduction (by percentage) compared to the P&M configuration. As expected, without the large PicoBoard and Motherboard, the small antenna radiation collapses and the range drops drastically (by 90 to 95%). Unfortunately, the reduction is still significant with the larger antenna boards as well. The lowest reduction can be seen with the 868 and 915 M BIFA (WES0039/0119), and meander monopoles (WES0037/0117). However, at 434 M, even these antennas suffer a large range reduction, which shows that the help of the large additional boards (PicoBoard and Motherboard) are more important on lower-frequency bands.

It should be noted that the range does not collapse so drastically if the pure antenna board is used only on one side of the link and the reference monopole (with the PicoBoard and Motherboard) on the other side.

Table 4. Gain and Range Test Results Comparison (Antenna Board + PicoBoard + Motherboard (P&M) Configurations Compared to the Coax Fed Pure Antenna Boards Measured with Balun and Ferrite (C&B&F))

	Maximum of XY 0° or XZ 270° Gain and Range Test Results, with PicoBoard & Motherboard ¹ (P&M)			Measured Maximum XY Gain [dBi]			Predicted Outdoor Range in XY Cut, Maximum Direction [m], Using Est. Prop.Factor		
	Gain [dBi] (P&M)	Outdoor Range [m] (P&M)	Estimated Propagation Factor	(P&M)	Antenna Board with only Coax & Balun & Ferrite (C&B&F)	Gain Delta [dB] (C&B&F)-(P&M)	(P&M)	Antenna Board with only Coax & Balun & Ferrite (C&B&F)	Range Reduction without large boards %
868 MHz²									
WES0031_01	-3.4	1596	2.53	-1.9	-8.9 H	-7.0	2097	626	70.1
WES0032_01	-5.5	1660	2.37	-4.9	-15.7 H	-10.8	1865	179	90.4
WES0033_01	-3.2	1296	2.63	-3.6	-13.7 H	-10.1	1208	259	78.6
WES0034_01	-4.3	1815	2.42	-3.8	-8.6 H	-4.8	1996	662	66.8
WES0035_01	-4.3	1657	2.46	-2.6	-17.9 H	-15.3	2279	119	94.8
WES0036_01	-4.6	1667	2.43	-3.2	-18.4 H	-15.2	2173	109	95.0
WES0037_01	-2.6	2104	2.48	-0.5	-1.3 V	-0.8	3105	2467	20.5
WES0038_01	-6.5	1186	2.43	-6.7	-18.3 H	-11.6	1142	111	90.3
WES0039_01	-2.7	1743	2.55	-5.8	-6.0 H	-0.2	995	1068	-7.3
Ref monopol H	-2.5	2054	2.50						
Ref monopol V	-2.5	2000	2.51						

Notes:

1. As in application notes AN848, AN850, and AN782.
2. Range is tested with +13dBm cond. power, Rx sens: -104.5 dBm (50 kbps, 25KHz dev, 0.1% PER,10 byte packets, 99 KHz RXBW).
3. Range is tested with +13dBm cond. power, Rx sens: -106.3 dBm (50 kbps, 25KHz dev, 0.1% PER,10 byte packets, 103.06 KHz RXBW).
4. Range is tested with +8.8 dBm cond. power, Rx sens: -105.5 dBm (40 kbps, 20KHz dev, 0.1% PER,10 byte packets, 82.64 KHz RXBW).

Table 4. Gain and Range Test Results Comparison (Antenna Board + PicoBoard + Motherboard (P&M) Configurations Compared to the Coax Fed Pure Antenna Boards Measured with Balun and Ferrite (C&B&F)) (Continued)

	Maximum of XY 0° or XZ 270° Gain and Range Test Results, with PicoBoard & Motherboard ¹ (P&M)			Measured Maximum XY Gain [dBi]			Predicted Outdoor Range in XY Cut, Maximum Direction [m], Using Est. Prop.Factor		
	Gain [dBi] (P&M)	Outdoor Range [m] (P&M)	Estimated Propagation Factor	(P&M)	Antenna Board with only Coax & Balun & Ferrite (C&B&F)	Gain Delta [dB] (C&B&F)-(P&M)	(P&M)	Antenna Board with only Coax & Balun & Ferrite (C&B&F)	Range Reduction without large boards %
915 MHz³									
WES0111_01	-5.7	1834	2.37	-5.2	-7.2 H	-2.0	1697	859	49.4
WES0112_01	-8.7	1272	2.29	-7.7	-17.6 H	-9.9	1298	125	90.4
WES0113_01	-7.5	1245	2.38	-8.1	-16.0 H	-7.9	932	168	81.9
WES0114_01	-2.9	1857	2.55	-2.8	-8.8 H	-6.0	1608	639	60.3
WES0115_01	-4.5	1724	2.47	-5.2	-18.1 H	-12.9	1280	114	91.1
WES0116_01	-3.2	1572	2.60	-4.2	-17.4 H	-13.2	1122	130	88.4
WES0117_01	-2.6	2080	2.53	-2.1	-2.2 V	-0.1	1934	1984	-2.6
WES0118_01	-5.6	1142	2.55	-6.6	-19.8 H	-13.2	811	83	89.7
WES0119_01	-5	1806	2.42	-5.4	-8.4 H	-3.0	1411	688	51.2
Ref monopol H	-1.9	2696	2.49						
Ref monopol V	-1.9	2460	2.52						
Notes:									
1. As in application notes AN848, AN850, and AN782.									
2. Range is tested with +13dBm cond. power, Rx sens: -104.5 dBm (50 kbps, 25KHz dev, 0.1% PER,10 byte packets, 99 KHz RXBW).									
3. Range is tested with +13dBm cond. power, Rx sens: -106.3 dBm (50 kbps, 25KHz dev, 0.1% PER,10 byte packets, 103.06 KHz RXBW).									
4. Range is tested with +8.8 dBm cond. power, Rx sens: -105.5 dBm (40 kbps, 20KHz dev, 0.1% PER,10 byte packets, 82.64 KHz RXBW).									

Table 4. Gain and Range Test Results Comparison (Antenna Board + PicoBoard + Motherboard (P&M) Configurations Compared to the Coax Fed Pure Antenna Boards Measured with Balun and Ferrite (C&B&F)) (Continued)

	Maximum of XY 0° or XZ 270° Gain and Range Test Results, with PicoBoard & Motherboard ¹ (P&M)			Measured Maximum XY Gain [dBi]			Predicted Outdoor Range in XY Cut, Maximum Direction [m], Using Est. Prop.Factor		
	Gain [dBi] (P&M)	Outdoor Range [m] (P&M)	Estimated Propagation Factor	(P&M)	Antenna Board with only Coax & Balun & Ferrite (C&B&F)	Gain Delta [dB] (C&B&F)-(P&M)	(P&M)	Antenna Board with only Coax & Balun & Ferrite (C&B&F)	Range Reduction without large boards %
434 MHz⁴									
WES0071_01	-1.4	1151	3.09	-10.27	-5.2 H	5.1	268	514	-91.6
WES0072_01	-5.2	838	2.96	-7.7	-12.2 H	-4.5	494	185	62.6
WES0073_01	-5	886	2.95	-11.87	-5.4 V	6.5	264	646	-145.1
WES0074_01	-0.2	1194	3.16	-11.07	2.1 H	13.2	215	1496	-596.6
WES0075_01	-4.5	992	2.93	-5.2	-9.1 H	-3.9	772	291	62.3
WES0076_01	-3.2	842	3.11	-4.2	-7.4 H	-3.2	636	373	41.4
WES0077_01	3	1349	3.33	0	-15.2 H	-15.2	786	145	81.6
WES0078_01	-5.6	386	3.36	-19.67	-9.6 H	10.1	50	270	-443.3
Ref monopol H	0.3	1315	3.15						
Ref monopol V	0.3	1779	3.01						

Notes:

- As in application notes AN848, AN850, and AN782.
- Range is tested with +13dBm cond. power, Rx sens: -104.5 dBm (50 kbps, 25KHz dev, 0.1% PER,10 byte packets, 99 KHz RXBW).
- Range is tested with +13dBm cond. power, Rx sens: -106.3 dBm (50 kbps, 25KHz dev, 0.1% PER,10 byte packets, 103.06 KHz RXBW).
- Range is tested with +8.8 dBm cond. power, Rx sens: -105.5 dBm (40 kbps, 20KHz dev, 0.1% PER,10 byte packets, 82.64 KHz RXBW).

7.4. Effect of a 2032 Coin Battery in Typical Application Conditions

In typical applications, the pure antenna boards are used with batteries. A popular type is the lithium coin cell (e.g., 2032). The battery is a large metal one and from the RF point of view, usually connected to ground so it can enlarge the GND size and/or shield the antenna. Depending on the battery's relative position to the antenna, it can help or severely hinder the useful radiation.

If the battery does not overlap with the antenna trace and falls outside of the "antenna area", it will usually increase the ground size significantly, helping the useful radiation. However, it works best if the battery is perpendicular to the antenna axis. If the battery is above a larger ground (circuit) area and away from the antenna, then it is mostly neutral from a radiation point of view. Lastly, if the battery directly overlaps the antenna trace or covers the antenna area, then it usually significantly decreases the antenna radiation.

It is important to note that in the first and third cases above, the antenna impedance detunes, so tuning of the antenna match is required.

The measured radiation (gain) results with a 2032 coin cell are given in Table 5. For some antenna boards (typically with the small size antennas—not for all) the matching network must be properly modified so it is matched with the battery (by using the classical lumped element matching methods [8]). The matching networks and the S11s with the coin cell are detailed in "Appendix D—Matching Circuits and Measured S11 of the Antenna Boards with Coax, Balun, Ferrite, and Battery (C&B&F&Bat) Configurations" on page 102. Radiation is significantly better than -10 dB in all cases. In Appendix D, the photos of the antenna boards with the coin cell are also shown.

In Table 5, gains with the battery are given in the 4th column. The 5th column next to it shows the gain without battery (from Table 4). The 3rd column shows the applied polarization. The gain difference with and without the battery is shown in the 6th column. As can be seen, the difference is practically negligible for all antenna types, so the 2032 coin cell has practically no influence on the gain. These results are expected for antenna boards having large ground with the battery situated above (e.g., WES0031/0113/0071/0072/0112/0072/0039/0119/0079). It is surprising that the small boards (panic buttons, small ILA, etc.) with the battery have larger ground. In theory, it could improve their radiation (here, the coin cells do not overlap the antenna traces).

The ranges are compared in the last three columns if the same pure antenna board unit is used at both (TX and RX) sides of the link. Since the gains are not changing significantly with the coin cell, the predicted ranges (7th column) are nearly the same as without the battery (8th column). So the range is still very low with the small antenna boards (WES0035/0036/0038/0075/0076/0078/0115/0116/0118).

The meander monopoles also have the following interesting results with the battery:

- At 434 M, the slightly larger, coin-cell-sized ground is not enough to have better range.
- At 868 and 915 M, the battery has no influence on the gain and range. They have nearly the same good gain and range as with the extra Motherboard and PicoBoard.

Table 5. Gain and Range Test Results Comparison of Coax Fed Pure Antenna Board + Balun + Ferrite Configurations with (C&B&F&Bat) and without (C&B&F) Coin Cell Battery

	Estimated Propagation Factor	Measured Maximum XY Gain [dBi]			Predicted Outdoor Range in XY Cut, Max. Direction [m], Using Estimated Propagation Factor			
		Antenna Board with Coax & Balun & Ferrite & Bat (C&B&F&Bat)	Antenna Board with Coax & Balun & Ferrite (C&B&F)	Gain Delta [dB] (C&B&F&Bat)-(C&B&F)	Antenna Board with Coax & Balun & Ferrite & Bat (C&B&F&Bat)	Antenna Board with Coax & Balun & Ferrite (C&B&F)	Range Reduction without large boards (%)	
868 MHz¹								
WES0031_01	2.53	H	-6.7	-8.9	2.2	939	626	33.3
WES0032_01	2.37	H	-17.1	-15.7	-1.4	138	179	-29.4
WES0033_01	2.63	H	-14.7	-13.7	-1.0	215	259	-20.2
WES0034_01	2.42	H	-8.7	-8.6	-0.1	650	662	-1.9
WES0035_01	2.46	H	-18.2	-17.9	-0.3	113	119	-5.7
WES0036_01	2.43	H	-17.0	-18.4	1.4	141	109	22.7
WES0037_01	2.48	V	-0.8	-1.3	0.5	2704	2467	8.8
WES0038_01	2.43	H	-17.6	-18.3	0.7	126	111	12.1
WES0039_01	2.55	H	-6.8	-6.0	-0.8	922	1068	-15.9
Ref monopol H	2.50							
Ref monopol V	2.51							

Notes:

1. Range is tested with +13dBm cond. power, Rx sens: -104.5 dBm (50 kbps, 25KHz dev, 0.1% PER,10 byte packets, 99 KHz RXBW).
2. Range is tested with +13dBm cond. power, Rx sens: -106.3 dBm (50 kbps, 25KHz dev, 0.1% PER,10 byte packets, 103.06 KHz RXBW).
3. Range is tested with +8.8dBm cond. power, Rx sens: -105.5 dBm (40 kbps, 20KHz dev, 0.1% PER,10 byte packets, 82.64 KHz RXBW).

Table 5. Gain and Range Test Results Comparison of Coax Fed Pure Antenna Board + Balun + Ferrite Configurations with (C&B&F&Bat) and without (C&B&F) Coin Cell Battery (Continued)

	Estimated Propagation Factor	Measured Maximum XY Gain [dBi]				Predicted Outdoor Range in XY Cut, Max. Direction [m], Using Estimated Propagation Factor		
		Antenna Board with Coax & Balun & Ferrite & Bat (C&B&F&Bat)	Antenna Board with Coax & Balun & Ferrite (C&B&F)	Gain Delta [dB] (C&B&F&Bat)-(C&B&F)	Antenna Board with Coax & Balun & Ferrite & Bat (C&B&F&Bat)	Antenna Board with Coax & Balun & Ferrite (C&B&F)	Range Reduction without large boards (%)	
915 MHz²								
WES0111_01	2.37	H	-9.0	-7.2	-1.8	616	859	-39.6
WES0112_01	2.29	H	-17.5	-17.6	0.1	128	125	1.8
WES0113_01	2.38	H	-15.6	-16.0	0.4	181	168	7.1
WES0114_01	2.55	H	-10.5	-8.8	-1.7	466	639	-37.0
WES0115_01	2.47	H	-17.8	-18.1	0.3	121	114	5.4
WES0116_01	2.60	H	-17.3	-17.4	0.1	132	130	1.8
WES0117_01	2.53	V	-1.1	-2.2	1.1	2426	1984	18.2
WES0118_01	2.55	H	-21.1	-19.8	-1.3	65	83	-27.2
WES0119_01	2.42	H	-8.5	-8.4	-0.1	675	688	-1.9
Ref monopol H	2.49							
Ref monopol V	2.52							

Notes:

1. Range is tested with +13dBm cond. power, Rx sens: -104.5 dBm (50 kbps, 25KHz dev, 0.1% PER,10 byte packets, 99 KHz RXBW).
2. Range is tested with +13dBm cond. power, Rx sens: -106.3 dBm (50 kbps, 25KHz dev, 0.1% PER,10 byte packets, 103.06 KHz RXBW).
3. Range is tested with +8.8dBm cond. power, Rx sens: -105.5 dBm (40 kbps, 20KHz dev, 0.1% PER,10 byte packets, 82.64 KHz RXBW).

Table 5. Gain and Range Test Results Comparison of Coax Fed Pure Antenna Board + Balun + Ferrite Configurations with (C&B&F&Bat) and without (C&B&F) Coin Cell Battery (Continued)

	Estimated Propagation Factor	Measured Maximum XY Gain [dBi]			Predicted Outdoor Range in XY Cut, Max. Direction [m], Using Estimated Propagation Factor			
		Antenna Board with Coax & Balun & Ferrite & Bat (C&B&F&Bat)	Antenna Board with Coax & Balun & Ferrite (C&B&F)	Gain Delta [dB] (C&B&F&Bat)- (C&B&F)	Antenna Board with Coax & Balun & Ferrite & Bat (C&B&F&Bat)	Antenna Board with Coax & Balun & Ferrite (C&B&F)	Range Reduction without large boards (%)	
434 MHz³								
WES0071_01	3.09	H	-10.5	-10.3	-0.2	238	245	-3.0
WES0072_01	2.96	H	-8.3	-8.7	0.4	328	310	5.7
WES0073_01	2.95	H	-11.9	-11.9	0.0	194	194	0.0
WES0074_01	3.16	H	-11.1	-11.1	0.0	218	218	0.0
WES0075_01	2.93	H	-17.9	-16.3	-1.6	81	102	-26.4
WES0076_01	3.11	H	-17.7	-17.0	-0.7	83	92	-10.8
WES0077_01	3.33	V	-15.1	-15.2	0.1	147	145	1.5
WES0078_01	3.36	H	-22.4	-19.7	-2.7	42	62	-48.4
Ref monopole H	3.15							
Ref monopole V	3.01							
Notes:								
1. Range is tested with +13dBm cond. power, Rx sens: -104.5 dBm (50 kbps, 25KHz dev, 0.1% PER,10 byte packets, 99 KHz RXBW).								
2. Range is tested with +13dBm cond. power, Rx sens: -106.3 dBm (50 kbps, 25KHz dev, 0.1% PER,10 byte packets, 103.06 KHz RXBW).								
3. Range is tested with +8.8dBm cond. power, Rx sens: -105.5 dBm (40 kbps, 20KHz dev, 0.1% PER,10 byte packets, 82.64 KHz RXBW).								

7.5. Hand Effect

As all matrix antenna boards basically comprise a monopole derivative type antenna, they are sensitive to the vicinity of the human hand. The human hand detunes the antennas and thus, tuning of the matching networks is required. The hand also has strong effect on the radiation, as detailed in Section 4.4.

However, not all matrix antenna types are practical to use in remotes or close to the hand. The wire helical, chip, meander, and BIFA antennas are less proper due to their larger size and/or higher price.

The antennas that best fit the remote and hand applications are panic-button antennas and the small/medium ILAs (or IFAs). Therefore, these antennas are retuned here with strong hand effect (using the matching with the coin cell battery and bazooka balun as a starting point), meaning if the PCB is directly touched.

Here, a big problem is that detuning and thus the new matching strongly depends on the position and distance of the hand. The hand behaves as a lossy dielectric. So if a hand is close to the antenna trace, it increases effective electrical length and thus detunes the antenna. Also, it usually degrades the radiation if it is parallel with the human body, as detailed in Sections 2.7 and 4.4. However, antenna traces perpendicular to the human body will radiate better, so the hand position is critical. The users' hand material and structure (fat and water content, size, etc.) has influence as well.

In the upcoming measurements, the antennas are held by hand positions which are typical during applications. However, in these tests the hand directly touches the antenna PCB, which results in the strongest possible detuning and gain degradation. Under actual conditions, the PCB is usually wrapped with a plastic that maintains 1 to 2 mm distance between the antenna and the body, making the hand effect weaker. So the present tests deal with a kind of worst-case hand effect scenario. Later on a panic button, antenna behavior is investigated with several distances between the antenna and hand.

Figure 68 shows the four antennas with the hand touch in the tests. The medium ILAs are held in a typical remote position with a virtual thumb push-button in the middle. The panic buttons and the small ILA are fully surrounded by the hand right beneath the PCB, as these antennas usually lay on the body (such as a wrist). All antennas here are measured with the bazooka balun and with the 2032 coin cell.

The left column of Figure 69 shows the detuning effect of the 868 M antennas with the original battery, balun, ferrite, and battery match if the hand introduced. As one can see, the detuning is significant, shown by the antennas resonances shifting down in frequency

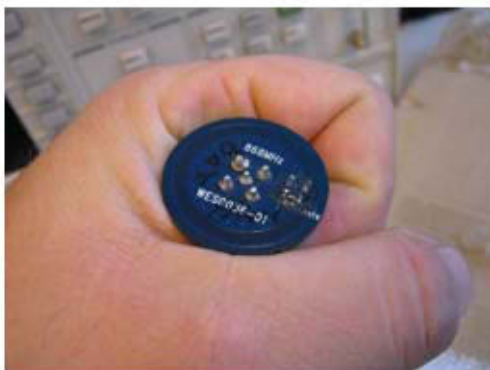
The right column shows the S11 after hand tuning. All S11 is better than -10 dB. The new matching networks and the measured S11 after tuning are detailed in “Appendix E—Matching Circuits and Measured S11 of the Antenna Boards with Coax + Balun + Ferrite + Battery + Hand (C&B&F&Bat&H) Configurations” for all three bands (868, 915, and 434 M).



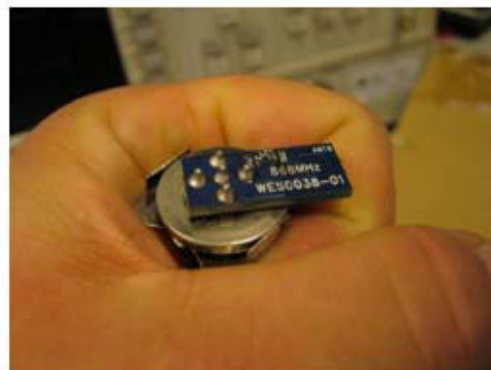
WES0031/0111/0071: Medium ILA



WES0035/0115/075: Panic IFA



WES0036/0116/076: Panic ILA



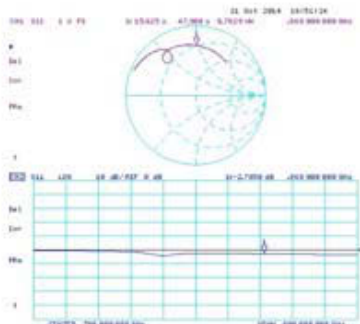
WES0038/0118/078: Small ILA

Figure 68. Small Matrix Antennas with Strong (Direct Touch) Hand Effect

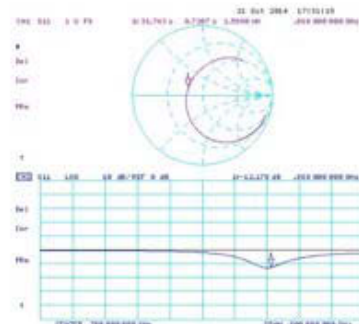
The gains of the tuned antennas with hands in proximity are detailed in Table 6. Here again, the 3rd column shows the polarization applied, which is the horizontal one in these antenna types. The 4th column shows the gain with hands present. The 5th column shows the original gain without the hand effect (from Table 6). The 6th column shows the difference. The difference is typically around 5 to 6 dB at 868 and 915 MHz, and lower at 434 MHz.

From the gain data, the outdoor range degradation can also be predicted with the help of the propagation factor values estimated from the reference monopole range tests. The ranges are compared in the 7th, 8th, and 9th columns if the same unit is used at the TX and RX side. With hand present (7th column), the range reduction is 60 to 80% (9th column) at 868/915 M bands, even if the antenna is matched. At 434 M, the reduction is smaller.

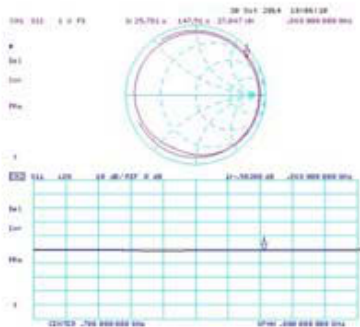
The reduction is much less if the remote antenna held by the hand is used only at one side of the link. The last column shows the range in this typical real life case when the reference monopole (with the PicoBoard and Motherboard) is used at the other side of the link. The ranges are significantly higher in this case.



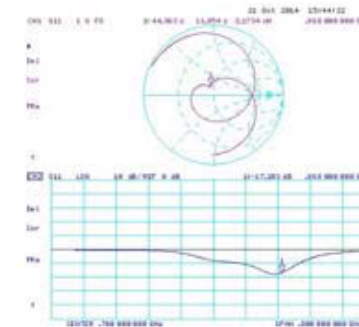
WES0031 with hand (original C&B&F&Bat match)



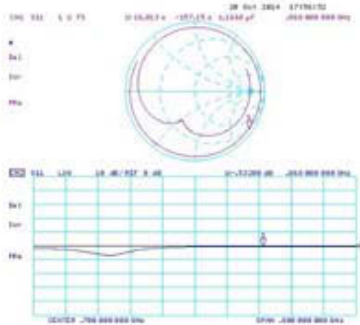
WES0031 with hand (new C&B&F&Bat&Hand match)



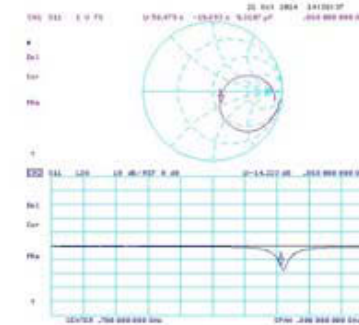
WES0035 with hand (original C&B&F&Bat match)



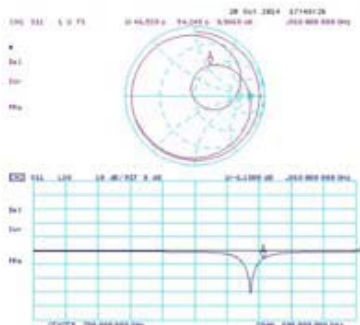
WES0035 with hand (new C&B&F&Bat&Hand match)



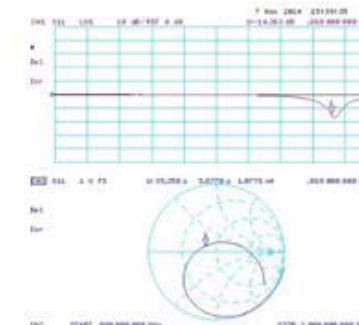
WES0036 with hand (original C&B&F&Bat match)



WES0036 with hand (new C&B&F&Bat&Hand match)



WES0038 with hand (original C&B&F&Bat match)



WES0038 with hand (new C&B&F&Bat&Hand match)

Figure 69. S11 of the Tested Pure Antenna Boards with Hand

Note: In Figure 69, the left column is the case with the original match, and the right column is the tuned case.

Table 6. Gain and Range Test Results Comparison of Coax Fed Pure Antenna Board + Balun + Ferrite + Battery Configurations with (C&B&F&Bat&Hand) and without (C&B&F&Bat) Hand Effect

Estimated Propagation Factor		Measured Maximum XY Gain [dBi]			Predicted Outdoor Range in XY Cut, Maximum Direction [m], Using Estimated Propagation Factor				Reference Monopole and (C&B&F&Bat&H) Board on Link Sides
		Antenna Board with Coax & Balun & Ferrite & Bat & Hand (C&B&F&Bat&H)	Antenna Board with Coax & Balun & Ferrite & Bat (C&B&F&Bat)	Gain Delta [dB] (C&B&F&Bat&H) - (C&B&F&Bat)	Same TX and RX units on Link Sides				
					Antenna Board with Coax & Balun & Ferrite & Bat & Hand (C&B&F&Bat&H)	Antenna Board with Coax & Balun & Ferrite & Bat (C&B&F&Bat)	Range Change (%) with Hand		
868 MHz¹									
WES0031_01	2.53	H	-11.6	-6.7	-4.9	381	939	-59.4	1389
WES0035_01	2.46	H	-24.3	-18.2	-6.1	37	113	-67.5	482
WES0036_01	2.43	H	-21.5	-17.0	-4.5	62	141	-56.3	538
WES0038_01	2.43	H	-26.4	-17.6	-8.8	25	126	-80.2	509
Ref monopol H	2.50		-2.5						
Ref monopol V	2.51		-2.5						
915 MHz²									
WES0111_01	2.37	H	-14.6	-9.0	-5.6	218	616	-64.5	1237
WES0115_01	2.47	H	-22.8	-17.8	-5.0	48	121	-60.4	547
WES0116_01	2.60	H	-22.9	-17.3	-5.6	47	132	-64.5	573
WES0118_01	2.55	H	-25.3	-20.1	-5.2	30	79	-61.8	442
Ref monopol H	2.49		-1.9						
Notes:									
1. Range is tested with +13dBm cond. power, Rx sens: -104.5 dBm (50 kbps, 25KHz dev, 0.1% PER,10 byte packets, 99 KHz RXBW).									
2. Range is tested with +13dBm cond. power, Rx sens: -106.3 dBm (50 kbps, 25KHz dev, 0.1% PER,10 byte packets, 103.06 KHz RXBW).									
3. Range is tested with +8.8dBm cond. power, Rx sens: -105.5 dBm (40 kbps, 20KHz dev, 0.1% PER,10 byte packets, 82.64 KHz RXBW).									

Table 6. Gain and Range Test Results Comparison of Coax Fed Pure Antenna Board + Balun + Ferrite + Battery Configurations with (C&B&F&Bat&Hand) and without (C&B&F&Bat) Hand Effect (Continued)

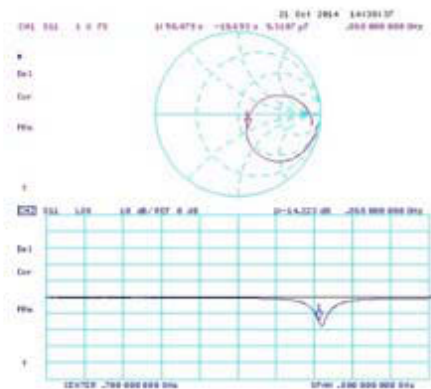
	Estimated Propagation Factor	Measured Maximum XY Gain [dBi]			Predicted Outdoor Range in XY Cut, Maximum Direction [m], Using Estimated Propagation Factor				Reference Monopole and (C&B&F&Bat&H) Board on Link Sides
		Antenna Board with Coax & Balun & Ferrite & Bat & Hand (C&B&F&Bat&H)	Antenna Board with Coax & Balun & Ferrite & Bat (C&B&F&Bat)	Gain Delta [dB] (C&B&F&Bat&H) - (C&B&F&Bat)	Same TX and RX units on Link Sides				
Ref monopol V	2.52	−1.9							
434 MHz³									
WES0071_01	3.09	H	−14.6	−10.5	−4.1	131	238	−45.1	337
WES0075_01	2.93	H	−21.3	−17.9	−3.4	49	81	−39.2	196
WES0076_01	3.11	H	−19.1	−17.7	−1.4	68	83	−18.5	199
WES0078_01	3.36	H	−23.1	−22.4	−0.7	38	42	−9.7	141
Ref monopol H	3.15		0.3						
Ref monopol V	3.01		0.3						
Notes:									
1. Range is tested with +13dBm cond. power, Rx sens: -104.5 dBm (50 kbps, 25KHz dev, 0.1% PER,10 byte packets, 99 KHz RXBW).									
2. Range is tested with +13dBm cond. power, Rx sens: -106.3 dBm (50 kbps, 25KHz dev, 0.1% PER,10 byte packets, 103.06 KHz RXBW).									
3. Range is tested with +8.8dBm cond. power, Rx sens: -105.5 dBm (40 kbps, 20KHz dev, 0.1% PER,10 byte packets, 82.64 KHz RXBW).									

Finally, antenna behaviors are shown for the case where the hand does not directly touch the PCB but is held approximately 2 to 4 mm away. These are the typical distances if the PCB is in a plastic case and/or a coin cell is present between the PCB and the hand.

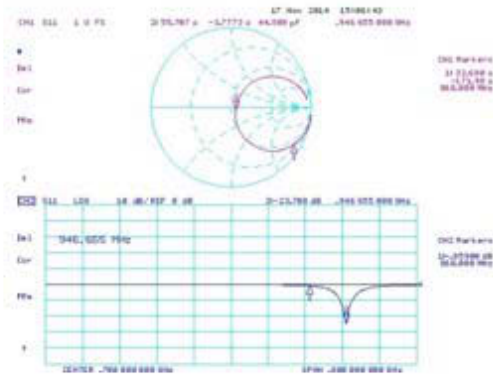
Figure 70 shows the original direct PCB touch, 2 mm gap and 4 mm gap cases and the measured impedances (S_{11}) with the WES0036 antenna. Here, the matching is the new battery, balun, ferrite, and hand (C&B&F&Bat&Hand) match optimized for direct PCB touch as given in Figures 91, 92 and 93.

As can be seen, the resonant frequency shifts significantly upwards as the gap between the hand and the PCB increases: with a 2 mm gap the frequency is ~946 MHz, while with a 4 mm gap the frequency is ~966 MHz. This is a typical effect with all the four investigated antenna types (medium/small ILA, and panic buttons).

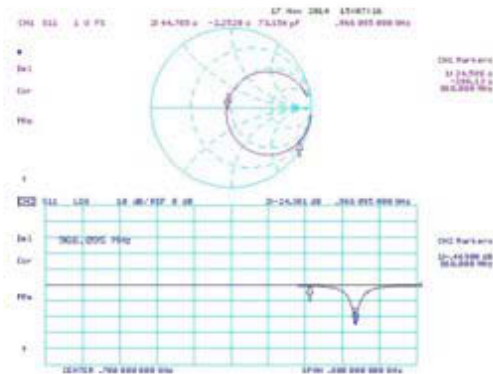
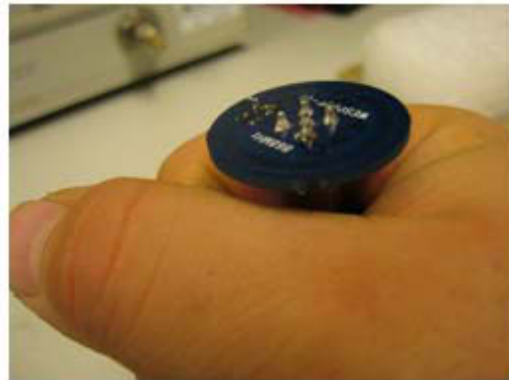
To tune the antenna back to 868 MHz, the introduction of a proper series inductance is required. For example, with ~4 mm gap the impedance at 868 MHz is $\sim 25-j206 \Omega$. If one compensates the capacitive $-j206 \Omega$ reactance, the antenna impedance will be close enough to the 50Ω point to have nearly -10 dB S_{11} ($S_{11} = (25-50)/(25+50) = -0.33$, $|S_{11}|^{dB} = 20\log(0.33) \sim -10$ dB). For the compensation, a series connected inductor is required with proper value.



WES0036 with direct PCB touch (new C&B&F&Bat&Hand match)



WES0036 with ~2 mm PCB hand gap (new C&B&F&Bat&Hand match)



WES0036 with ~4 mm PCB hand gap (new C&B&F&Bat&Hand match)

Figure 70. 868 M Panic Button ILA Antenna with Different Distances between the Hand and the Antenna Board.

Note: In Figure 70, the right column shows the detuning of the S11 for various cases. The match is optimized for the direct touch.

However, the WES0036 C&B&F&Bat&Hand match has a series 1.8 pF (Figure 92) capacitor. This cap has to be removed first. The reactance of the 1.8 pF cap at 868 MHz is:

$$X_{\text{ser_cap}} = \frac{-1}{2\pi f C} = \frac{-1}{2\pi \times 868 \times 10^6 \times 1.8 \times 10^{-12}} = -101.9\Omega$$

By substituting it from the antenna impedance, the residual impedance is: $Z_{\text{ant_new}} = Z_{\text{ant}} - jX_{\text{ser_cap}} = \sim 25 - j206 + j102 = \sim 25 - j104 \Omega$. So after removing the series 1.8 pF, the capacitive reactance needing to be compensated is $\sim -104 \Omega$. This can be done with a 19 nH series inductor.

The starting point (denoted by DP1) in Figure 71 shows the $Z_{\text{ant_new}}$ impedance. With a 18 nH series inductor, which is a real E12 series value, the impedance is close enough for the center to have an S11 close to -10 dB.

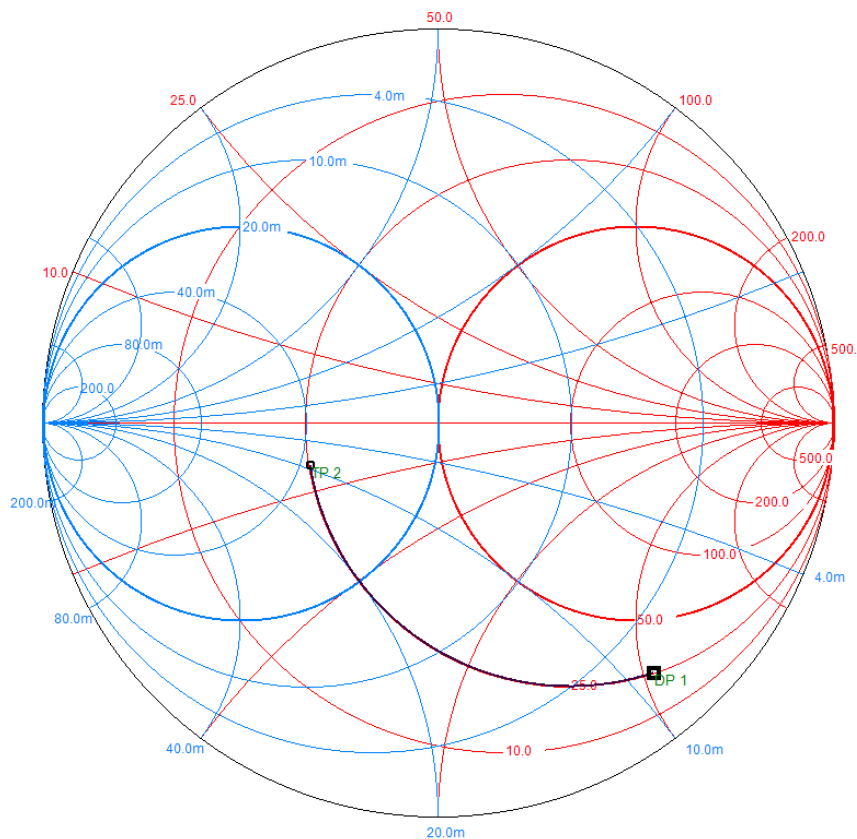


Figure 71. Tuning of the 868 M Panic Button ILA to 4 mm Gap Case with a Series 18 nH Inductor

Better matching can be achieved if the first parallel 1.8 pF capacitor value in the match (Figure 92) is only decreased and not fully removed. By decreasing it to 1.2 pF the $Z_{\text{ant_new}}$ impedance is transformed to $\sim 53 - j147 \Omega$ as it is shown in Figure 72 by the TP2 point. From here, a series 27 nH shifts the impedance very close to the center of the diagram (TP3). So with ideal tuning elements, the new antenna matching circuit fits for the 4 mm gap case (between the PCB and the hand) is a parallel 1.2 pF capacitor at the antenna input followed by a series 27 nH inductor. Unfortunately, due to the parasitics, some post bench tuning is required to finalize the values with real SMD elements.

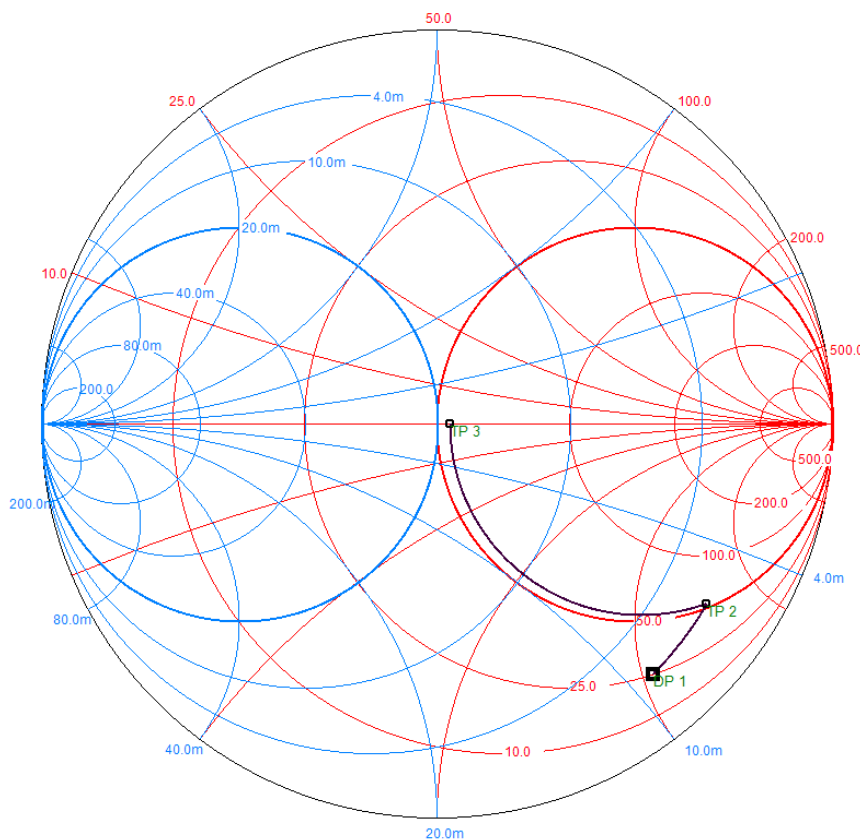


Figure 72. Tuning of the 868 M Panic Button ILA to 4 mm Gap Case with a Series 1.2 pF Capacitor and a 27 nH Parallel Inductor

APPENDIX A—DIPOLE ANTENNA RADIATION CALCULATIONS

Total Radiated Power of the Hertz Dipole

The total radiated power of a Hertz dipole can be calculated by integrating the power density (given in Section “3.1.2. Total Radiated Power and Radiation Resistance of the Herz Dipole”) to the whole space spherical surface around the antenna. Figure 73 shows the calculation method:

1. The power radiated to small circular areas is calculated at a given θ .
2. The radiation to these small areas are integrated over the entire θ range.

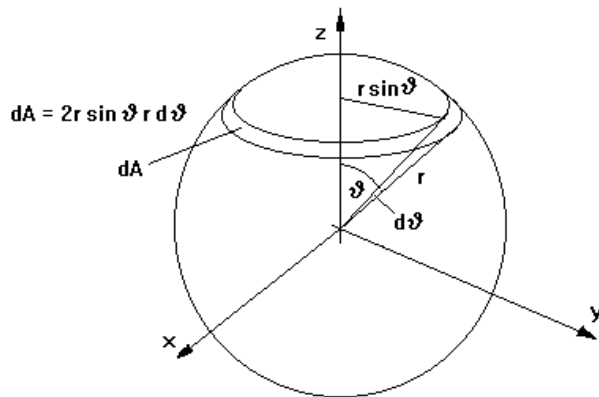


Figure 73. Calculation of the Total Radiated Power of the Herz Dipole

$$P_S = \iint_A S dA = \int_0^\pi \int_0^{2\pi} 2\pi r^2 \sin \theta \, d\theta \, d\phi = \frac{30\pi^2 I^2}{\lambda^2} \int_0^\pi \sin^3 \theta \, d\theta$$

As:

$$\int_0^\pi \sin^3 \theta \, d\theta = \frac{4}{3}$$

The total radiated power:

$$P_S = 40\pi^2 I_0^2 \left(\frac{dz}{\lambda} \right)^2$$

Gain of the Hertz Dipole Antenna

As shown in Section 3.1.2, the generated fields and power density depend only on the elevation. They are at maximum if $\theta=90^\circ$:

$$S_{\max} = \frac{15\pi I_0^2 dz^2}{\lambda^2 r^2}$$

By definition, the antenna directivity is:

$$D_A = \frac{\text{Radiation in the direction of maximum}}{\text{Ideal isotropic radiation with same total radiated Rf power}} = \frac{S_{\max}}{S_0}$$

The ideal isotropic antenna radiation with the same total radiated power can be calculated as:

$$S_0 = \frac{P_S}{4\pi r^2}$$

So, the directivity (at maximum i.e. at $\theta=90^\circ$) is:

$$D = \frac{S_{\max}}{S_0} = \frac{\frac{15\pi I_0^2 dz^2}{\lambda^2 r^2}}{\frac{P_S}{4\pi r^2}} = \frac{60\pi^2 I_0^2 dz^2}{P_S \lambda^2} = \frac{60\pi^2 I_0^2 \left(\frac{dz}{\lambda}\right)^2}{40\pi^2 I_0^2 \left(\frac{dz}{\lambda}\right)^2} = 1.5, \text{ or } +1.76 \text{ dB}$$

Calculation of the Generated Field of a Normal Dipole

A large dipole/monopole antenna can be divided into smaller dipoles in which the current distribution can be considered as constant. Thus, their field can be described by the Herz dipole results. The weighted sum (with the current distribution) of the radiations of these small dipoles yields the radiated field of the larger dipole.

The calculation of one small partial dipole field is shown in Figure 74.

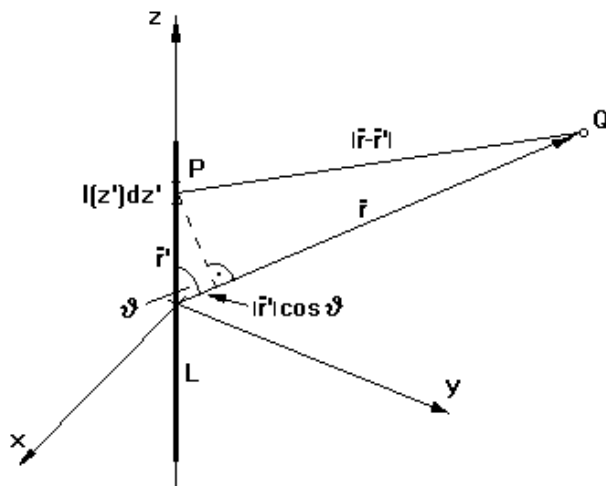


Figure 74. Calculation of the Far Field of a Small Partial Dipole Part of a Large Dipole

The far field of one Herz dipole section (given in Section 3.1.1) at the position of z' can be described by the following equation:

$$dE_\theta = j60\pi \frac{I(z') dz'}{\lambda |r - r'|} e^{-j\theta |r - r'|} \sin \theta$$

The total field generated by the antenna can be calculated by integrating the fields of the small dipoles over the entire antenna length. For that, the current distribution (denoted by $I(z')$ in the following equation) has to be known.

$$E_\theta = j \frac{60\pi}{\lambda} \sin \theta \int_L I(z') \frac{e^{-j\theta |r - r'|}}{|r - r'|} dz'$$

For the calculation, the vector differences in the exponent and in the denominator need to be calculated. From Figure 74, the exponent can be approximated in the following way:

$$|r - r'| \approx |r| - |r'| \cos \theta = r - r' \cos \theta$$

If the Q point is far, the denominator can be approximated in a trivial way:

$$|r - r'| \approx |r| = r$$

With these approximations, the total radiated field formula is much simpler:

$$E_\theta = j \frac{60\pi e^{-j\theta r}}{\lambda r} \sin \theta \int_L I(z') e^{j\theta z' \cos \theta} dz'$$

As mentioned earlier, in a real antenna the current distribution is sinusoidal along the antenna axis (Z axis):

$$I(z') = I_m \sin [\beta (1 - |z'|)] = \begin{cases} I_m \sin [\beta (1 - z')] & z' > 0 \\ I_m \sin [\beta (1 + z')] & z' < 0 \end{cases}$$

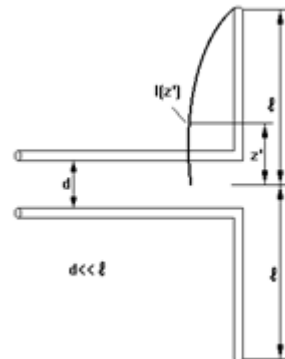


Figure 75. Sinusoidal Current Distribution Along a Large Dipole

Substituting this current distribution into the integral the final field formula yields:

$$E_\theta = j \frac{60\pi I_m e^{-j\theta r}}{\lambda r} \sin \theta \left[\int_{-1}^0 \sin [\beta (1 + z')] e^{j\beta z' \cos \theta} dz' + \int_0^1 \sin [\beta (1 - z')] e^{j\beta z' \cos \theta} dz' \right]$$

$$E_\theta = j60I_m \frac{e^{-j\theta r}}{r} \frac{\cos(\beta 1 \cos \theta) - \cos(\beta 1)}{\sin \theta}$$

where I_m is the maximum of the sinusoidal current distribution.

Electric Field of Short ($L=2l \leq \lambda/2$) Dipole Antennas

In the case of long dipole antennas ($L = 2l > \lambda/2$), the current maximum is somewhere on the antenna and depends on the length. For short antennas ($L = 2l \leq \lambda/2$), the current has a maximum at the feed point. Unfortunately, in the case of short antennas, because one dipole arm (or the monopole antenna) is shorter than a quarter wavelength, the current at the input ($I(0)$) is lower than the possible sinusoidal maximum (I_m). In this case, the I_m has to be calculated from the input current value and from the antenna length.

$$I(0) = I_m \sin \beta l$$

$$I_m = \frac{I(0)}{\sin \beta l}$$

So the integrated electric field for short antennas ($L=2l \leq \lambda/2$) is:

$$E_\theta = j60 \frac{I(0)}{\sin(\beta l)} \frac{e^{-j\theta r}}{r} \frac{\cos(\beta l \cos \theta) - \cos(\beta l)}{\sin \theta}$$

Total Radiated Power and Radiation Resistance of a Normal Dipole (Monopole)

As the E and H fields are known the generated power density, at r distance they can be calculated as well:

$$S = \text{Re}(E \times H^*) = \frac{|E(\theta)|^2}{240\pi}$$

The total radiated power can be calculated by integrating the power density over the whole spherical surface surrounding the antenna:

$$P_S = \int_A S dA = 30I_m^2 \int_0^\pi \frac{[\cos(\beta l \cos \theta) - \cos(\beta l)]^2}{\sin^2 \theta} d\theta$$

From the total radiated power the radiation resistance can be calculated:

$$R_{Rm} = \frac{2P_S}{I_m^2} = 60 \int_0^\pi \frac{[\cos(\beta l \cos \theta) - \cos(\beta l)]^2}{\sin^2 \theta} d\theta \quad (\text{if } L = 2l > \lambda/2)$$

If the total dipole antenna length is shorter than half lambda (or in the case of a monopole, shorter than quarter lambda) the current maximum is at the feeding point and the radiation resistance is modified:

$$R_{in} = \frac{R_m}{\sin^2 \beta l} = \frac{60}{\sin^2 \beta l} \int_0^\pi \frac{[\cos(\beta l \cos \theta) - \cos(\beta l)]^2}{\sin^2 \theta} d\theta \quad (\text{if } L = 2l = \lambda/2)$$

Unfortunately, this integral cannot be derived in closed form. Numerical solution yields the radiation resistance versus the dipole length curve, which is shown in Section 3.2.1 on page 14.

Dipole (Monopole) Radiation Pattern and Directivity

For dipoles shorter than 1.25 wavelengths ($l/\lambda \leq 0.625$), the direction of max radiation is at $\theta_{max}=90^\circ$ and the E field radiation pattern can be separated to a maximum and a normalized pattern part:

$$E(\theta) = E_{\max} F(\theta)$$

where:

$$E_{\max} = j60I_m \frac{e^{-j\beta r}}{r} (1 - \cos \beta l)$$

$$F(\theta) = \frac{\cos(\beta l \cos \theta) - \cos \beta l}{(1 - \cos \beta l) \sin \theta}$$

In the case of a half-wave dipole (quarter lambda monopole) where $\beta l = 2\pi/\lambda * \lambda/4 = \pi/2$, the normalized pattern become simpler:

$$F(\theta) = \frac{\cos\left(\frac{\pi}{2} \cos \theta\right)}{\sin \theta}$$

The directivity can be calculated from the total radiated power and thus from the radiation resistance:

$$D = \frac{S_{\max}}{S_0} = \frac{S_{\max}}{\frac{P_S}{4\pi r^2}} = \frac{2(1 - \cos \beta l)^2}{\int_0^\pi \frac{[\cos(\beta l \cos \theta) - \cos \beta l]^2}{\sin^2 \theta} d\theta} = \frac{120}{R_{Rm}} (1 - \cos \beta l)^2$$

R_{Rm} is the radiation resistance corresponding to the maximum of the current. If the dipole antenna length ($2l$) is shorter than 0.5λ , then the radiation resistance corresponding to the input current has to be used in the above gain formula:

$$R_{Rin} = \frac{R_{Rm}}{\sin^2 \beta l}$$

APPENDIX B—BAZOOKA BALUN DESIGN AND TUNING

A picture of a bazooka balun is shown in Figure 76. It consists of a cylinder around the feeding cable with a short at one end (Figure 77). The other cylinder end, which is facing to the antenna board, is an open (Figure 78). The cylinder and the feeding cable outer conductor form a transmission line for the leaking RF signal. The cylinder is filled with some foam to mechanically fix the coax. The total length (l) of the balun (cylinder length (cl) together with a gap till the antenna board) should be around $\lambda/4$ to show a high impedance at the antenna board position. The gap is required for less deterioration of the antenna radiation pattern. At sub-GHz frequencies, a gap size around 20 mm seems to be proper [7]. The cylinder length is designed accordingly.

The diameter (d) of the cylinder should be large for better blocking, but larger diameter yields stronger influence on the radiation pattern. At the sub-GHz frequencies, diameter values of ~13 to 16 mm seem to be a good compromise [7].

The picture of the 434, 868, and 915 MHz balun is shown in Figure 79, Figure 76, and Figure 80. The dimensions of the realized baluns at the 434, 868 and 915 MHz bands are given in Table 7 on page 96.

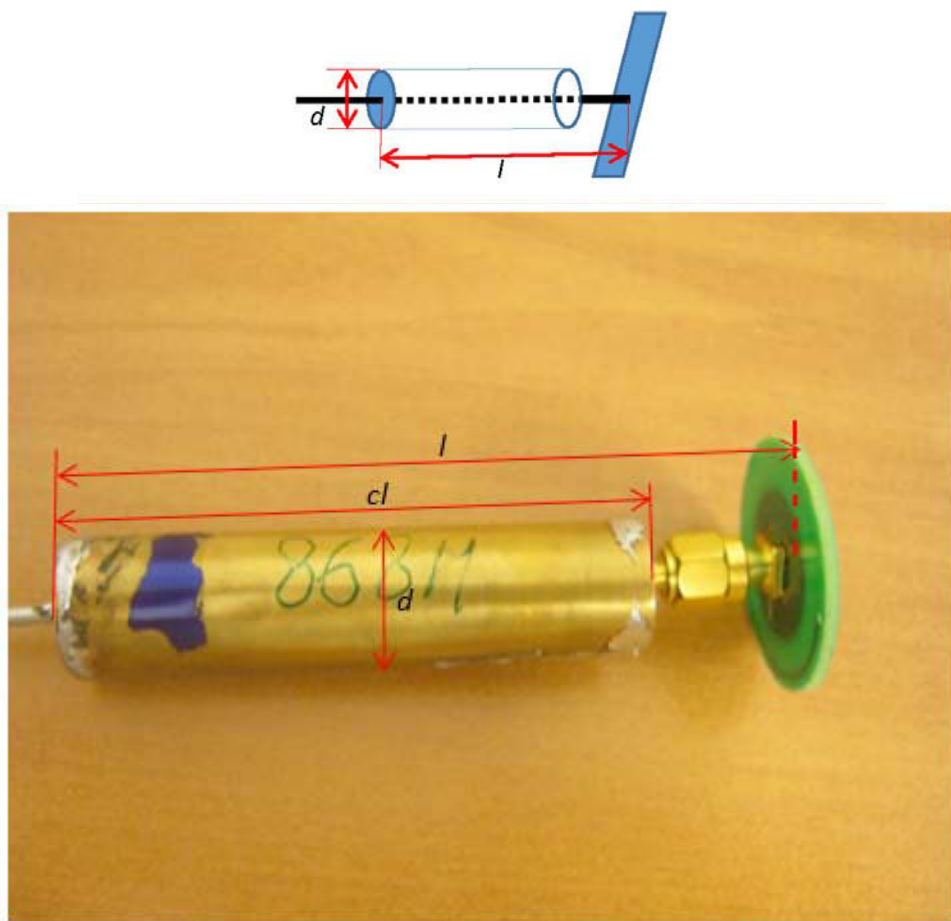


Figure 76. 868 M Bazooka Balun and Dimensions

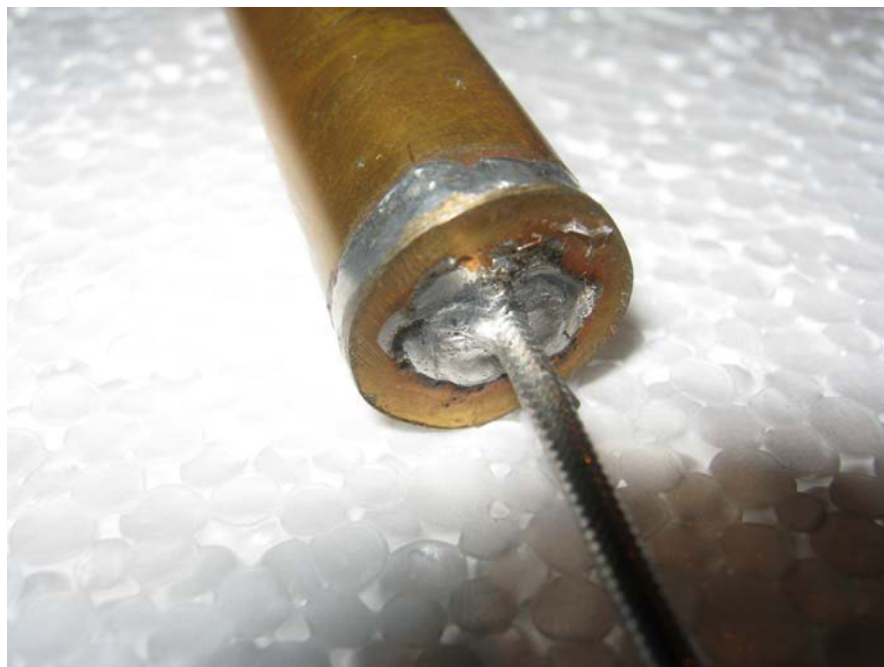


Figure 77. Short End Far from the Antenna

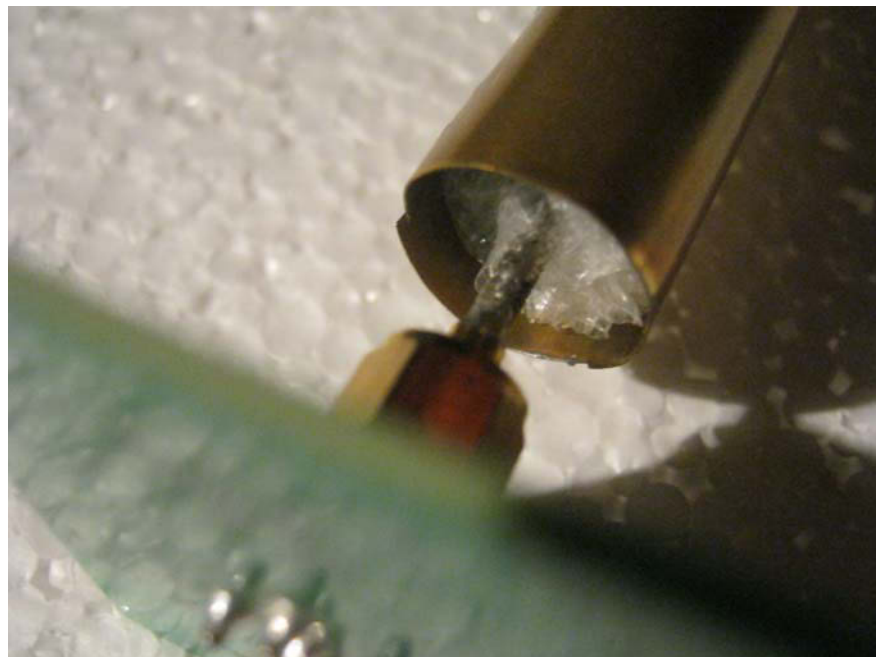


Figure 78. Open End at the Antenna (Cylinder Partly Filled by Foam to Stabilize the Coax)



Figure 79. 434 M Balun with an Additional Pigtail for Impedance Tuning

Note: In Table 79 and 80, the pigtail inner conductor is soldered to the coax outer conductor, while the pigtail outer conductor is soldered to the cylinder.

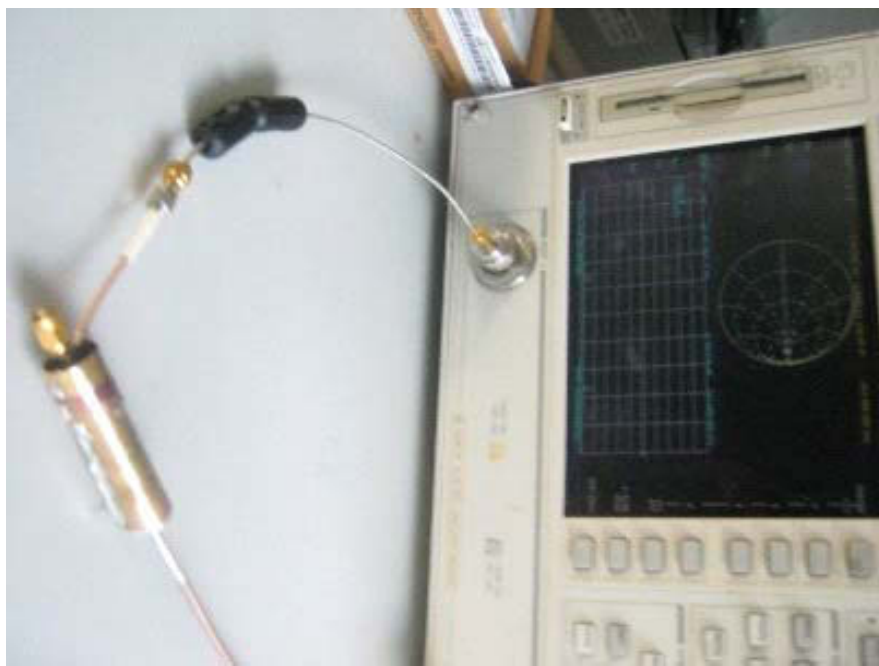


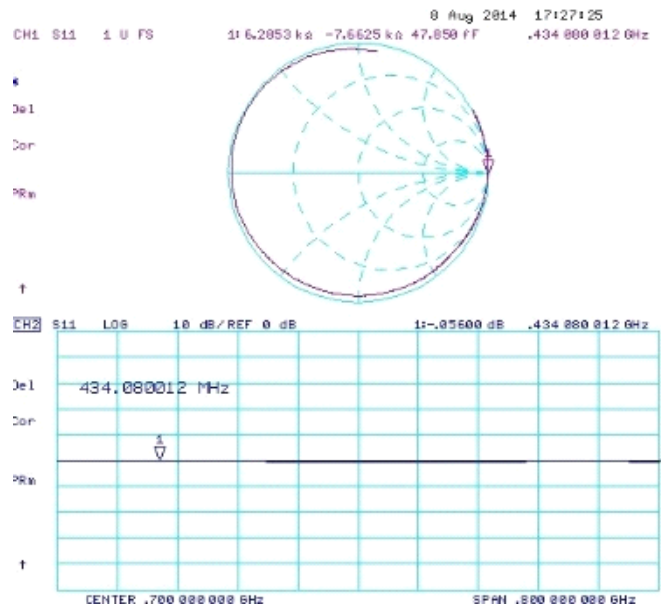
Figure 80. 915 M Balun with an Additional Pigtail for Impedance Tuning

Table 7. Dimensions of the Balun (According to Figure 76)

Frequency [MHz]	Total Length (l) [mm]	Diameter (d) [mm]	Cylinder Length (c_l) [mm]	Gap ($l-c_l$) [mm]
434	164	15.5	142	22
868	82	15.5	64	18
915	74.5	16.5	58	16.5

The measurement and tuning setup is also shown in Figure 79 and Figure 80. The impedance is measured by a pigtail right at the open end of the cylinder (facing the antenna board). The measuring pigtail is soldered between the coax outer conductor and the cylinder. The reference plane is on the pigtail and shifted approximately 20 mm away (virtually in the VNA) from the pigtail solder point. Basically, only the reference plane shift (~20 mm is the starting value) is fine-tuned to get a high impedance at the operating frequency, and this tuned phase shift value is used as gap size ($l-c_l$ in Figure 76.). The proper gap size is physically adjusted by slightly moving the cylinder position on the coax (for this, the short end is continuously resoldered). During this tuning process, the cylinder length (c_l) is fixed. The cylinder length, together with the tuned gap size, results in a high impedance at the antenna board ground connection point (where the SMA outer conductor is connected to the antenna board ground).

The measured impedances of the 434, 868, and 915 MHz balun with the reference phase shifts (from the pigtail solder point) are identical to the gap values given in Table 7 and are shown in Figure 81 for 434 MHz, Figure 82 for 868 MHz, and Figure 83 for 915 MHz. As can be seen, the impedances are very high in all frequencies, which results in ~8 to 10 dB suppression of the leaking RF signal as is reflected in the gain measurements (see Tables 2 and 3 in Section 7.2).

**Figure 81. 434 M Bazooka Balun Impedance with the Dimensions Given in Table 7**

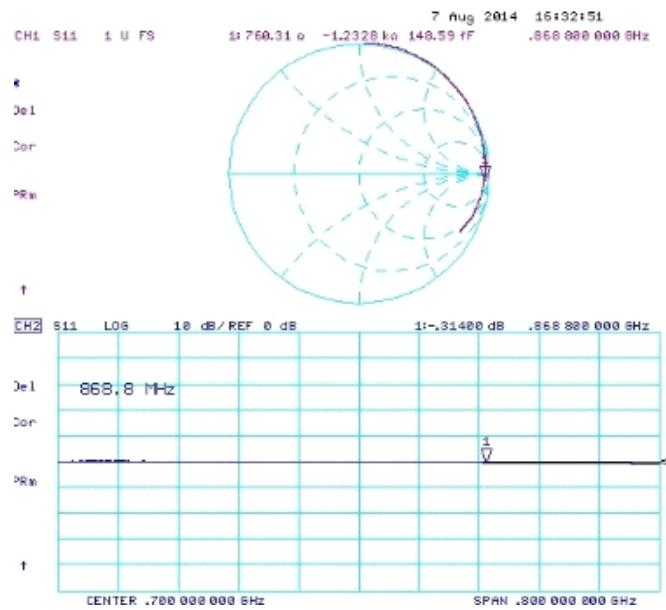


Figure 82. 868 M Bazooka Balun Impedance with the Dimensions Given in Table 7.

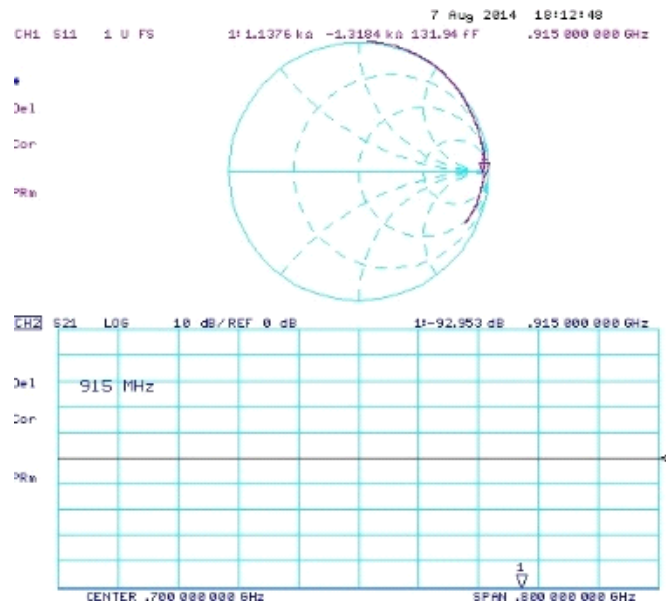


Figure 83. 915 M Bazooka Balun Impedance with the Dimensions Given in Table 7

APPENDIX C—MATCHING CIRCUITS AND MEASURED S11 OF THE ANTENNA BOARDS WITH NAKED COAX, WITH COAX AND BALUN (C&B), AND WITH COAX, BALUN, AND FERRITE (C&B&F) CONFIGURATIONS

The matching networks and the measured S11 of the matrix antennas in Naked Coax (C), Coax and Balun (C&B) and Coax, Balun, Ferrite (C&B&F) configuration is given in Figure 84 for the 434 MHz, Figure 85 for the 868 MHz, and Figure 86 for the 915 MHz bands. The C&B and the C&B&F configurations are matched with the same matching circuit. The reason for this is that the balun isolates the coax from the antenna board and thus, the ferrites have no effect on the impedance and matching.

It should be noted that the C&B&F configuration measures the pure antenna board properties with the best accuracy and, thus, the matching network of the C&B&F configuration should be used with the pure antenna board.

434MHz:	Coax:		Coax+Balun and Coax+Balun+Ferrite	
	S11 [dB]	Matching	S11 [dB]	Matching
WES0071	-13	<p>WES0071_COAX 3.3pF 3.3pF</p>	-13	<p>WES0071_BALUN 6.8pF 12pF 15pF</p>
WES0072	-12.2	<p>WES0072_COAX 6.8pF 47nH</p>	-8.5	0 Ohm
WES0073	-19.2	<p>WES0073_COAX 10pF 39nH</p>	-30	<p>WES0073_BALUN 27nH 3pF</p>
WES0074	-17.1	<p>WES0074_COAX 18nH 18pF</p>	-17	<p>WES0074_BALUN 2.7pF 18nH</p>
WES0075	-17.4	<p>WES0075_COAX 18nH 12pF</p>	-12.6	<p>WES0075_BALUN 3pF 10pF</p>
WES0076	-22.5	<p>WES0076_COAX 9.1nH 9.1pF</p>	-15.1	<p>WES0076_BALUN 39nH 6.2pF</p>
WES0077	-13	<p>WES0077_COAX 2.4pF 33nH</p>	-10	<p>WES0077_BALUN 82nH 0.5pF</p>
WES0078	-21.6	<p>WES0078_COAX 10nH 2.2pF</p>	-11	<p>WES0078_BALUN 27nH 1.8pF</p>

Figure 84. 434 M Antenna Matrix Board Matching Network and S11 Data with Naked Coax (C), Bazooka Balun (C&B), and Bazooka Balun + Ferrite (C&B&F) Configurations

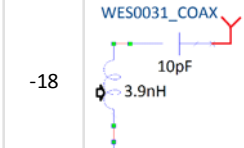
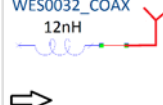
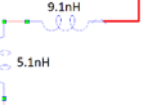
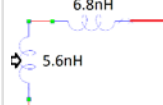
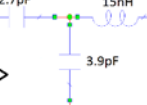
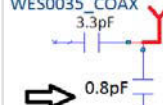
868MHz:	Coax:		Coax+Balun and Coax+Balun+Ferrite	
	S11 [dB]	Matching	S11 [dB]	Matching
WES0031	-18	 WES0031_COAX	-13.5	 WES0031_BALUN
WES0032	-12	 WES0032_COAX	-19.4	 WES0032_BALUN
WES0033	-21.2	 WES0033_COAX	-17.2	 WES0033_BALUN
WES0034	-15	 WES0034_COAX	-16	 WES0034_BALUN
WES0035	-12	 WES0035_COAX	-15	 WES0035_BALUN
WES0036	-18	 WES0036_COAX	-10.6	 WES0036_BALUN
WES0037	-30	 WES0037_COAX	-11.3	 WES0037_BALUN
WES0038	-12.6	 WES0038_COAX	-13.4	 WES0038_BALUN
WES0039	-17.1	 WES0039_COAX	-19	 WES0039_BALUN

Figure 85. 868 M Antenna Matrix Board Matching Network and S11 Data with Naked Coax (C), Bazooka Balun (C&B), and Bazooka Balun + Ferrite (C&B&F) Configurations

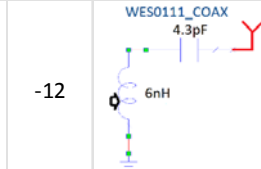
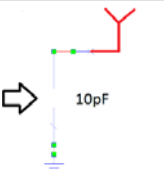
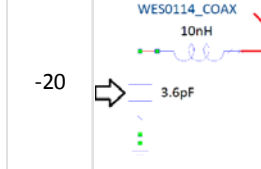
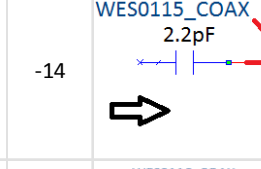
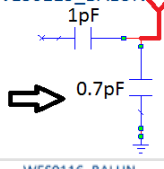
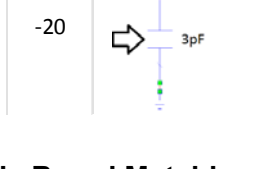
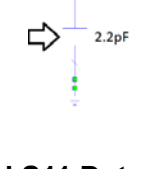
915MHz:	Coax:		Coax+Balun and Coax+Balun+Ferrite	
	S11 [dB]	Matching	S11 [dB]	Matching
WES0111	-12		-19.6	
WES0112	-12	0 Ohm	-19	0 Ohm
WES0113	-11		-20.4	
WES0114	-20		-21.1	
WES0115	-14		-15.7	
WES0116	-19		-20	
WES0117	-15.5		-15	
WES0118	-27		-12.4	
WES0119	-20		-11.6	

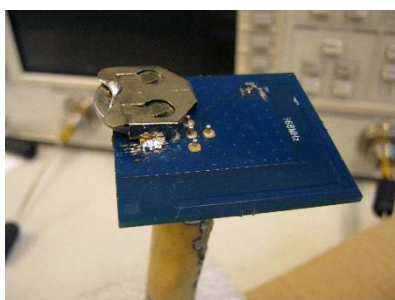
Figure 86. 915 M Antenna Matrix Board Matching Network and S11 Data with Naked Coax (C), Bazooka Balun (C&B), and Bazooka Balun + Ferrite (C&B&F) Configurations

APPENDIX D—MATCHING CIRCUITS AND MEASURED S11 OF THE ANTENNA BOARDS WITH COAX, BALUN, FERRITE, AND BATTERY (C&B&F&BAT) CONFIGURATIONS

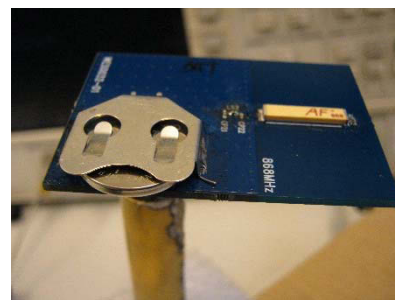
The impedance and the radiation of the antenna boards are tested with 2032 coin cell batteries as well. Some of the boards are detuned by the coin cell, making a matching network change required.

Figure 87 shows pictures of nine basic antenna boards with coin cells. The battery is basically put to the large ground area if it exists or away from the antenna trace around the SMA connector in order to achieve a neutral or positive effect on the radiation.

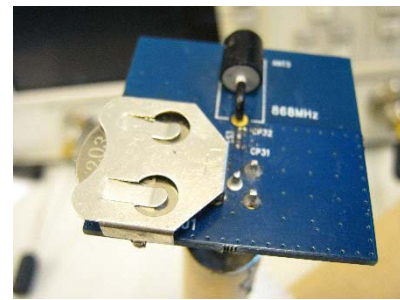
The measured S11 and the matching network topologies for all antenna boards are given in Figure 88 for 434 MHz, Figure 89 for 868 MHz, and Figure 90 for 915 MHz. The reflections are better than -10 dB, so the antennas are perfectly matched with the battery and a bazooka balun.



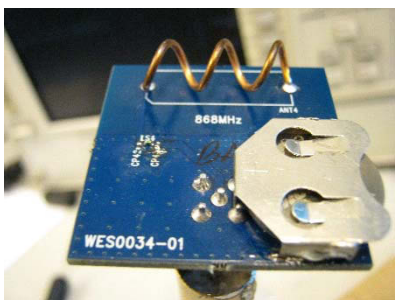
WES0031/0071/0111 types



WES0032/0072/0112 types



WES0033/0113 types



WES0034/0074/0114 types



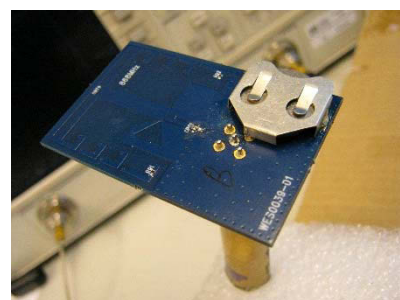
WES0035/0075/0115/0036/0076/0116 types



WES0037/0077/0117 types



WES0038/0078/0118 types



WES0039/0073/0119 types

Figure 87. Matrix Antennas with Coin Batteries Measured with Bazooka Balun

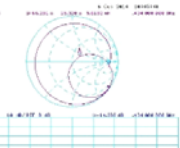
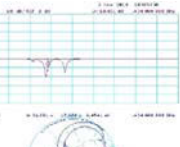
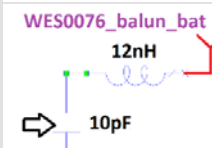
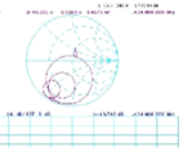
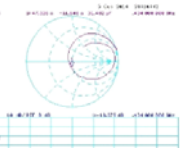
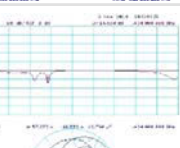
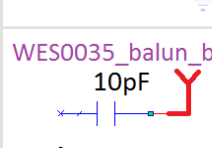
434MHz:	Coax+Balun+Ferrite+Battery		Smith Plot
	S11 [dB]	Matching	
WES0071		same as without battery	
WES0072		same as without battery	
WES0073		same as without battery	
WES0074	-14.3	 WES0074_balun_bat	
WES0075	-10.4	 WES0075_balun_bat	
WES0076	-19.5	 WES0076_balun_bat	
WES0077	-18	 WES0077_balun_bat	
WES0078	-15.7	 WES0078_BALUN_bat	
WES0078_2	-11	 WES0035_balun_bat	

Figure 88. 434 M Antenna Matrix Board Matching Network and S11 Data with Bazooka Balun + Ferrite + Coin Battery (C&B&F&Bat) Configurations

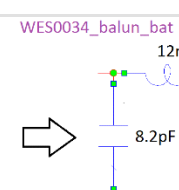
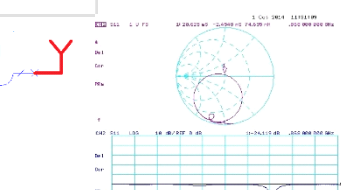
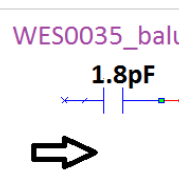
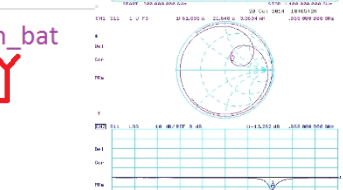
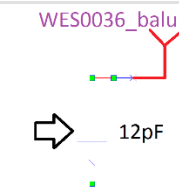
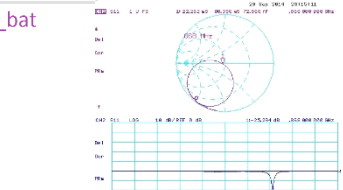
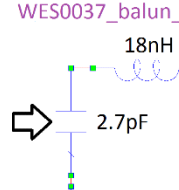
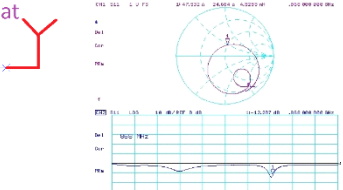
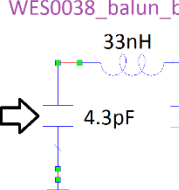
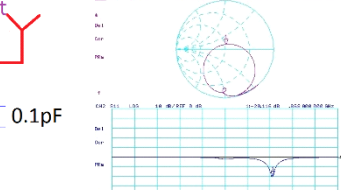
868MHz:	Coax+Balun+Ferrite+Battery		
	S11 [dB]	Matching	
WES0031	same as without battery		
WES0032	same as without battery		
WES0033	same as without battery		
WES0034	-24.1	 	
WES0035	-13.3	 	
WES0036	-25.3	 	
WES0037	-12.4	 	
WES0038	-20.1	 	
WES0039	same as without battery		

Figure 89. 868 M Antenna Matrix Board Matching Network and S11 Data with Bazooka Balun + Ferrite + Coin Battery (C&B&F&Bat) Configurations

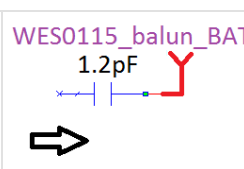
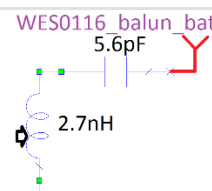
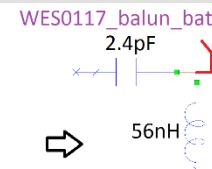
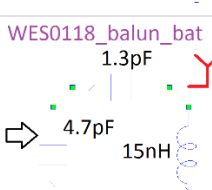
915MHz:	Coax+Balun+Ferrite+Battery	
	S11 [dB]	Matching
WES0111		same as without battery
WES0112		same as without battery
WES0113		same as without battery
WES0114		same as without battery
WES0115	-14.2	 <p>WES0115_balun_BAT 1.2pF</p>
WES0116	-11.2	 <p>WES0116_balun_bat 5.6pF 2.7nH</p>
WES0117	-19.5	 <p>WES0117_balun_bat 2.4pF 56nH</p>
WES0118	-16.3	 <p>WES0118_balun_bat 1.3pF 4.7pF 15nH</p>
WES0119		same as without battery

Figure 90. 915 M Antenna Matrix Board Matching Network and S11 Data with Bazooka Balun + Ferrite + Coin Battery (C&B&F&Bat) Configurations

APPENDIX E—MATCHING CIRCUITS AND MEASURED S11 OF THE ANTENNA BOARDS WITH COAX + BALUN + FERRITE + BATTERY + HAND (C&B&F&BAT&H) CONFIGURATIONS

The impedance and the radiation of some antenna boards typically used in remotes (medium/small ILA, and panic buttons) are tested with hand effect as well. The hand effect strongly detunes the boards, making matching network change required.

In Section "7.5. Hand Effect" on page 79, Figure 68 shows the four antenna PCBs listed above, held by hand (with the Bazooka balun and coin cells). The hand directly touches the PCB and surrounds it in the typical user position.

The measured S11 and the matching network topologies for these configurations are shown in Figure 91 for 434 MHz, Figure 92 for 868 MHz, and Figure 93 for 915 MHz. The reflections are better than -10 dB, so the antennas are perfectly matched with the hand (and with the battery and bazooka balun). These matches are the best starting points for remote application developments. Unfortunately, the plastic effect is not included, so some bench tuning is still required.

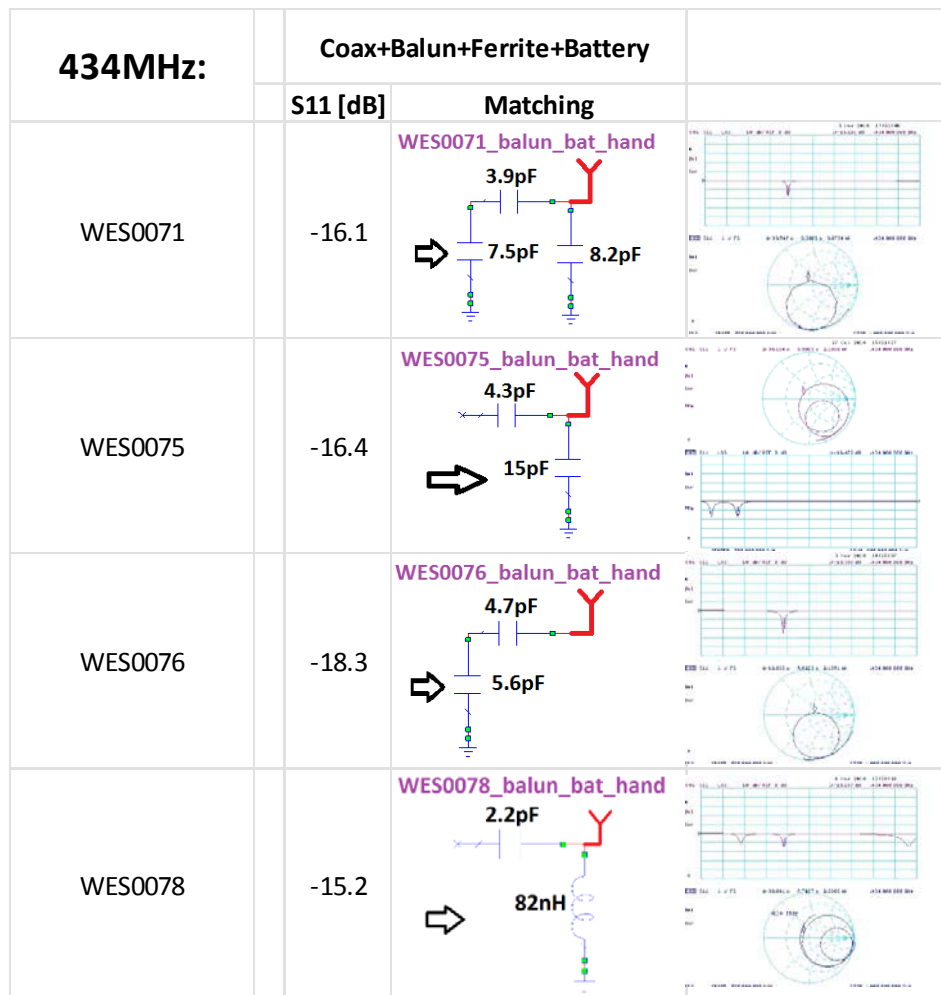


Figure 91. 434 M Antenna Matrix Board Matching Network and S11 Data with Bazooka Balun + Ferrite + Coin + Battery + Hand (C&B&F&Bat&H) Configurations

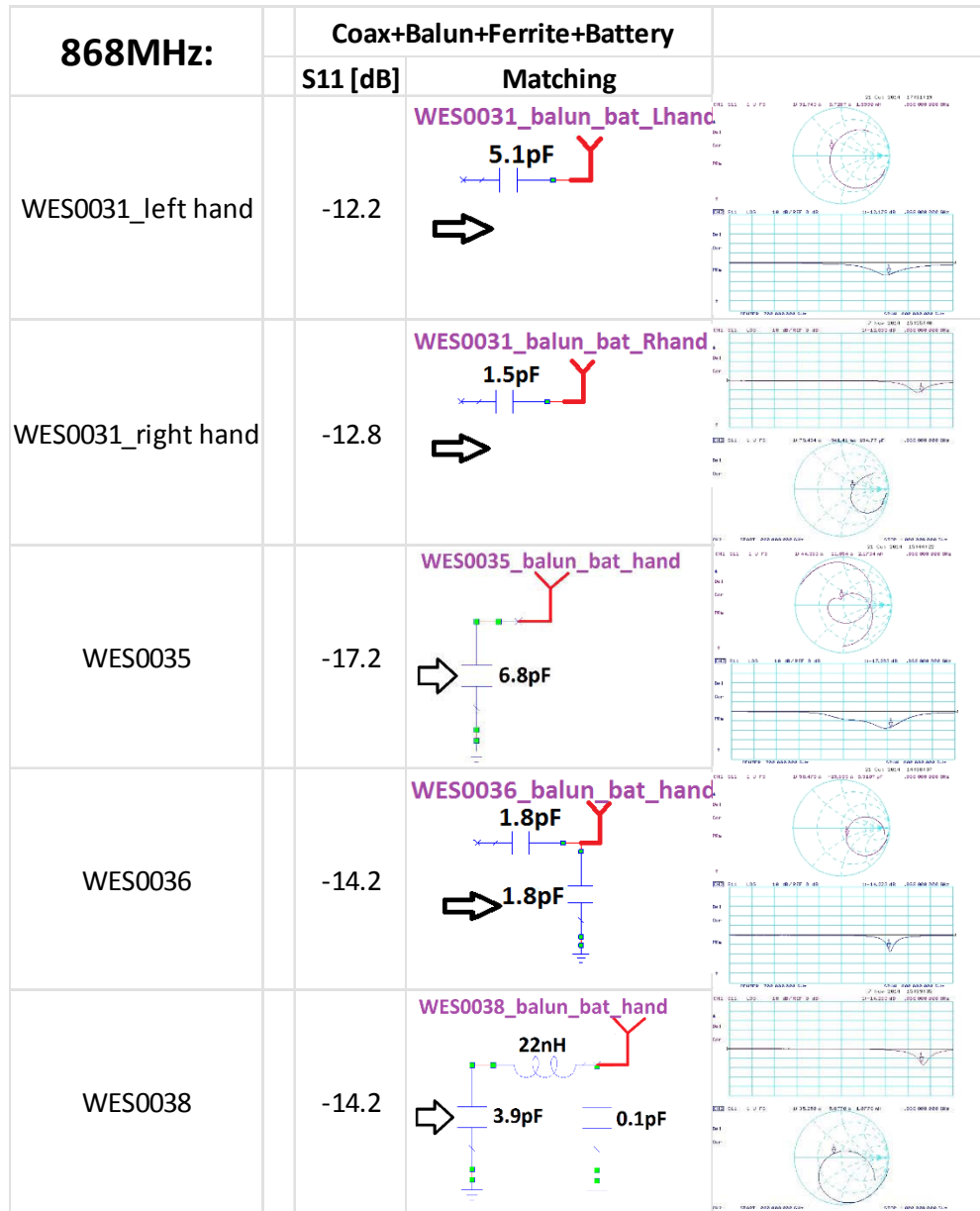


Figure 92. 868 M Antenna Matrix Board Matching Network and S11 Data with Bazooka Balun + Ferrite + Coin + Battery + Hand (C&B&F&Bat&H) Configurations

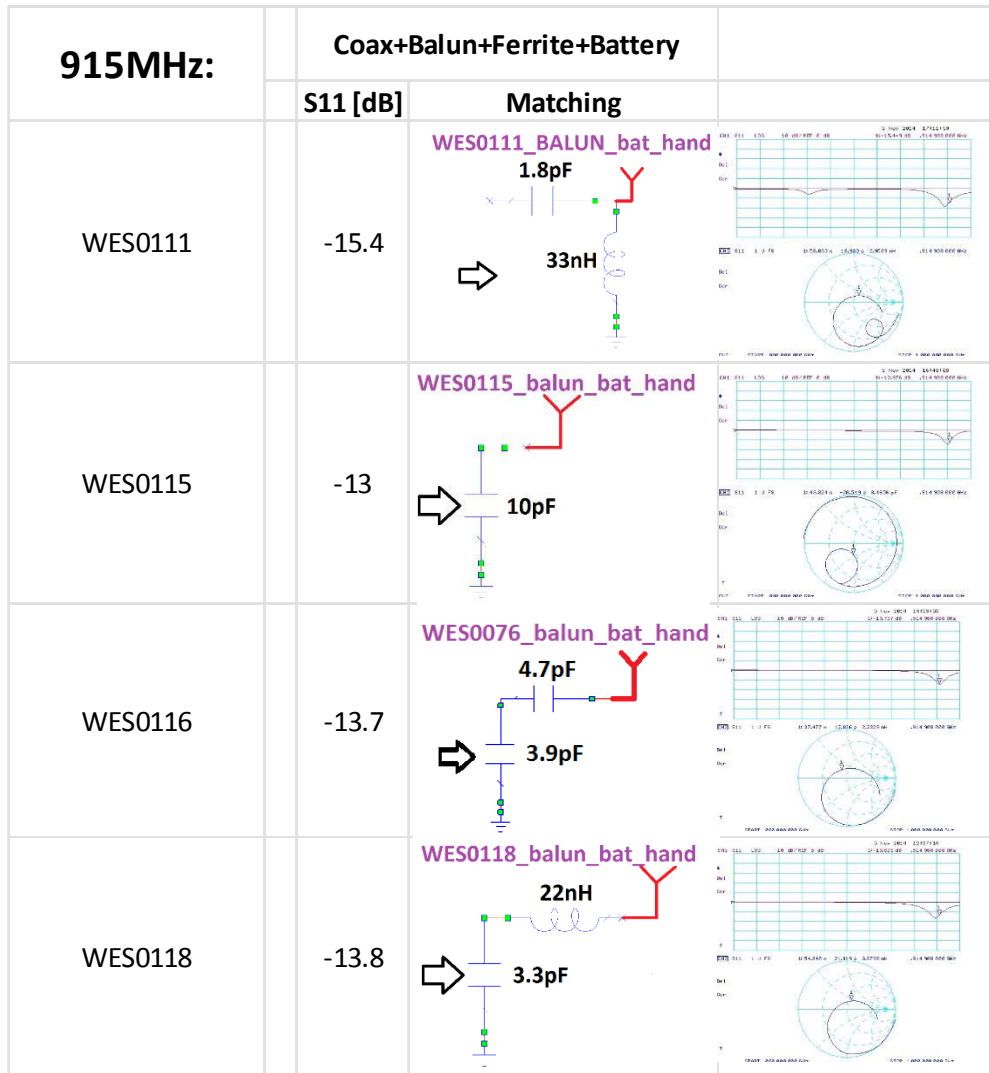
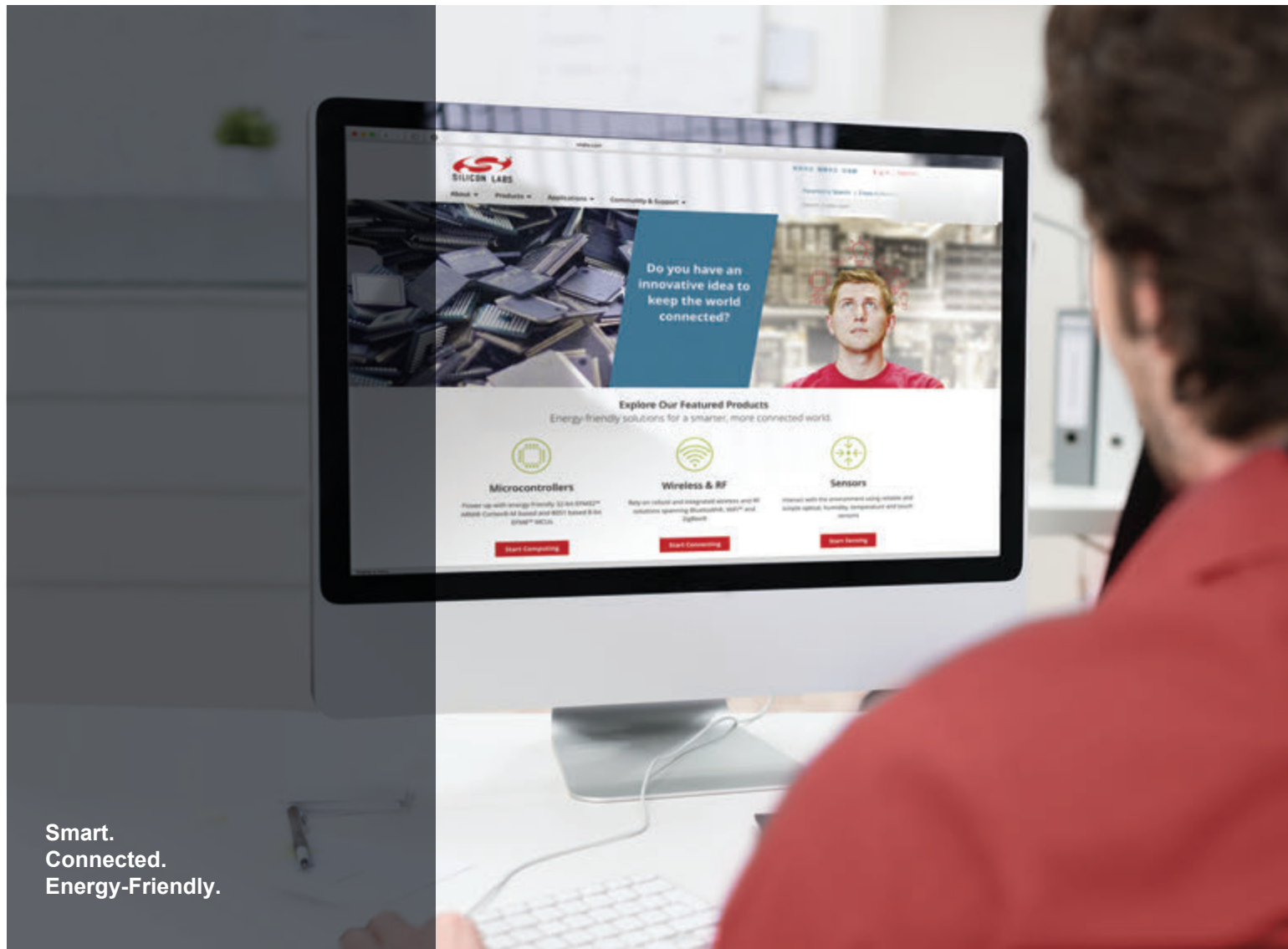


Figure 93. 915 M Antenna Matrix Board Matching Network and S11 Data with Bazooka Balun + Ferrite + Coin + Battery + Hand (C&B&F&Bat&H) Configurations

8. References

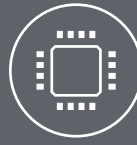
- [1] Melvin M Wiener: "Monopole Antennas", p137, Fig 41, Marcel Dekker Incl. 2003, ISBN 0-8247-0496-7
- [2] A.C. Balanis: "Antenna Theory, Analysis and Design" 2nd Ed., John Wiley and Sons, New York, 1997, ISBN: 0-471-59268-4
- [3] Simon R. Saunders, Alejandro Aragon Zavala: "Antennas and Propagation for Wireless Communication Systems", 2nd Ed., John Wiley and Sons, New York, 2007, ISBN 978-0-470-84879-1
- [4] W.L.Stutzman and G.A.Thiele: "Antenna Theory and Design", John Wiley and Sons, Chichester, 1984, ISBN 0-471-90167-9
- [5] J.D.Kraus and R.Marfehka: "Antennas" 2nd Ed., McRaw Hill education, USA, 2001, ISBN 0-07-232103-2
- [6] K. Fujimoto, A. Henderson, K.Hirasawa and J.R.James: "Small Antennas", John Wiley and Sons, Chichester, 1993, ISBN 0471 91413 4
- [7] Clemens Ichlen, Methods for Measuring RF Radiation Properties of Small Antennas, Helsinki University of Technology, 2001, Espoo
<https://aaltodoc.aalto.fi/bitstream/handle/123456789/2355/isbn9512256886.pdf?sequence=1>
- [8] Christian Gentili: "Microwave Amplifiers and Oscillators", McRaw Hill, USA, 1987, ISBN 10: 0070229953
- [9] C. Gabriel, S Gabriel, E Corthout: "The dielectric properties of biological tissues: I. literature survey", Phys.Med.Biol., Vol 41 (1996), 2231-2249, UK (http://engineering.dartmouth.edu/~d25559k/ENGG168_files/Papers/The%20dielectric%20properties%20of%20biological%20tissues%20.1.%20Literature%20survey.pdf)
- [10] AN768: 868 MHz Single-ended Antenna Matrix Selection Guide, <http://www.silabs.com/Support%20Documents/TechnicalDocs/an768.pdf>
- [11] AN782: 868 MHz Single-ended Antenna Matrix (WES0030-01-AMS868-01) Measurement Report, <http://www.silabs.com/Support%20Documents/TechnicalDocs/AN782.pdf>
- [12] AN847: 915 MHz Single-ended Antenna Matrix Selection Guide, <http://www.silabs.com/Support%20Documents/TechnicalDocs/AN847.pdf>
- [13] AN848: 915 MHz Single-ended Antenna Matrix (WES0110-01-AMS915-01) Measurement Report, <http://www.silabs.com/Support%20Documents/TechnicalDocs/AN848.pdf>
- [14] AN849: 434 MHz Single-ended Antenna Matrix Selection Guide, <http://www.silabs.com/Support%20Documents/TechnicalDocs/AN849.pdf>
- [15] AN850: 434 MHz Single-ended Antenna Matrix (WES0070-01-AMS434-01) Measurement Report, <http://www.silabs.com/Support%20Documents/TechnicalDocs/AN850.pdf>



Smart.
Connected.
Energy-Friendly.



Products
www.silabs.com/products



Quality
www.silabs.com/quality



Support and Community
community.silabs.com

Disclaimer

Silicon Labs intends to provide customers with the latest, accurate, and in-depth documentation of all peripherals and modules available for system and software implementers using or intending to use the Silicon Labs products. Characterization data, available modules and peripherals, memory sizes and memory addresses refer to each specific device, and "Typical" parameters provided can and do vary in different applications. Application examples described herein are for illustrative purposes only. Silicon Labs reserves the right to make changes without further notice and limitation to product information, specifications, and descriptions herein, and does not give warranties as to the accuracy or completeness of the included information. Silicon Labs shall have no liability for the consequences of use of the information supplied herein. This document does not imply or express copyright licenses granted hereunder to design or fabricate any integrated circuits. The products are not designed or authorized to be used within any Life Support System without the specific written consent of Silicon Labs. A "Life Support System" is any product or system intended to support or sustain life and/or health, which, if it fails, can be reasonably expected to result in significant personal injury or death. Silicon Labs products are not designed or authorized for military applications. Silicon Labs products shall under no circumstances be used in weapons of mass destruction including (but not limited to) nuclear, biological or chemical weapons, or missiles capable of delivering such weapons.

Trademark Information

Silicon Laboratories Inc.®, Silicon Laboratories®, Silicon Labs®, SiLabs® and the Silicon Labs logo®, Bluegiga®, Bluegiga Logo®, Clockbuilder®, CMEMS®, DSPLL®, EFM®, EFM32®, EFR®, Ember®, Energy Micro, Energy Micro logo and combinations thereof, "the world's most energy friendly microcontrollers", Ember®, EZLink®, EZRadio®, EZRadioPRO®, Gecko®, ISOmodem®, Precision32®, ProSLIC®, Simplicity Studio®, SiPHY®, Telegesis, the Telegesis Logo®, USBXpress® and others are trademarks or registered trademarks of Silicon Labs. ARM, CORTEX, Cortex-M3 and THUMB are trademarks or registered trademarks of ARM Holdings. Keil is a registered trademark of ARM Limited. All other products or brand names mentioned herein are trademarks of their respective holders.



Silicon Laboratories Inc.
400 West Cesar Chavez
Austin, TX 78701
USA

<http://www.silabs.com>